HOKKAIDO UNIVERSITY

Title	Effects of Thick Clay Layers on Hydrological Processes in Headwater Catchments Underlain by Impermeable and Permeable Bedrock
Author(s)	吉野, 孝彦
Degree Grantor	北海道大学
Degree Name	博士(農学)
Dissertation Number	甲第15304号
Issue Date	2023-03-23
DOI	https://doi.org/10.14943/doctoral.k15304
Doc URL	https://hdl.handle.net/2115/91299
Type	doctoral thesis
File Information	Yoshino_Takahiko.pdf

Effects of Thick Clay Layers on Hydrological Processes in Headwater Catchments Underlain by Impermeable and Permeable Bedrock

Takahiko Yoshino

2023

Effects of Thick Clay Layers on Hydrological Processes in Headwater Catchments Underlain by Impermeable and Permeable Bedrock

Contents

Abstract (in Japanese)

学 位 論 文 内 容 の 要 旨

博士の専攻分野の名称： 博 士（農学）　　　　氏名　　吉 野 孝 彦

学 位 論 文 題 名

Effects of Thick Clay Layers on Hydrological Processes in Headwater Catchments Underlain
by Impermeable and Permeable Bedrock
（厚い粘土層が不透水性・透水性基岩を有する山地源流域における水文プロセスに与
える影響）

　山地源流域にもたらされた降雨は斜面に浸透して斜面内部を移動し，やがて河川へ流出する。この過程で河川の流量や水質が決定され，また斜面崩壊等の土砂災害を発生させることから，防災・減災や社会経済活動の維持，環境保全等の観点から山地源流域における水文プロセスを明らかにすることは極めて重要である。山地源流域は一般に，透水性の低い基岩層の上に透水性の極めて高い土層が載る構造となっている。これまでの研究により，基岩層が実質的に不透水性の場合，基岩層がこれ以深には水がほとんど浸透しない「基盤面」となり，表土層（有機物由来の土層）および風化層（基岩層の風化物で構成される土層）内の水移動が主となる一方，基岩層の透水性が不透水性基岩と比べて高い透水性基岩の場合，表土層・風化層に加えて基岩層にも水が浸透し，各層内を水が移動することでそれぞれ水文プロセスに寄与することが明らかにされてきた。蛇紋岩，凝灰岩，泥岩等の地質を有する流域では，風化層が粘土で構成される場合がある。粘土層は一般に透水性が低いため単に基盤面として働くと考えられ，これまであまり注目されてこなかった。一方，粘土層への水の浸透や粘土層からの流出が水文プロセスに寄与していることを間接的に示唆する研究結果も一部報告されている。粘土層を形成する地質は世界に広く分布しており，また粘土層が斜面崩壊等のすべり面として働くことも考えると，粘土層に着目して直接的かつ詳細な斜面内部の観測等を実施し，水文プロセスに対する粘土層の影響を多角的に解明する必要があるが，これまでそうした研究はほとんど行われていない。そこで本研究では，風化層が厚い粘土で構成される不透水性基岩の蛇紋岩流域（0.068 ha）および透水性基岩の凝灰角礫岩流域（3.3 ha）それぞれで詳細な観測等を実施することにより，粘土層が山地源流域の水文プロセスに与える影響を明らかにすることを目的とした。

　蛇紋岩流域（不透水性基岩の流域）では，表土層・粘土層内の水移動に着目した。本流域の表土層は最大 50 cm 程度と薄く，一方で粘土層は最大 170 cm 程度と厚い。本流域では，表土層・粘土層内の地下水位・圧力水頭の観測および各層の地下水の水質・水温観測を実施した。また，表土層・粘土層からコアサンプルを採取し室内試験を実施することで，水分特性を実測した。室内試験の結果から，表土層は高透水性で大孔隙に富む一方，粘土層は低透水性で大孔隙に乏しいことが明らかになった。また地下水位観測によって，粘土層内に表土層−粘土層境界付近に地下水面を持つ地下水帯が形成されていること，無降雨時でも表土層内に地下水帯が形成されていることが確認された。さらに地下水位・水温観測から，降雨時は粘土層が従来の理解通り基盤面として働き，表土層を通じて雨水を素早く流域外へと流出させることが明らかになった。一方で，無降雨時に表土層内に形成された地下水帯の水質から，この地下水帯の起源は粘土層内に形成された地下水帯であることが明らかになった。粘土層内地下水が表土層へと復帰する経路を探るため，圧力水頭と水分特性から水移動フラックスを計算したところ，降雨時は表土層から粘土層へと鉛直下向きの飽和・不飽和フラックスが

生じるが，無降雨時に表土層と粘土層が乾燥すると，粘土層から表土層への上向きの不飽和フラックスが生じることが明らかになった。観測期間中の上向きの不飽和フラックスの合計は 172.5 mm で，上向きのフラックスが観測された期間に対して観測地下水位から計算した表土層内の地下水流フラックスの合計（9.76 mm）に比べ非常に大きかった。本流域の蒸散量を考慮しても，観測された粘土層から表土層への上向き不飽和フラックスは，無降雨時の表土層内の地下水帯を形成するのに十分な量であった。これらの結果から，不透水性基岩を有する山地源流域において，粘土層は降雨時に基盤面として働きつつも粘土層内に雨水を一部浸透させ，無降雨時は粘土層内に浸透・貯留された水を表土層へと上向き不飽和フラックスとして供給することが示された。

　凝灰角礫岩流域（透水性基岩の流域）では，表土層・粘土層・基岩層内の水移動に着目した。本流域では，厚さ 1 m 程度の表土層の下に，著しく透水性の低い粘土層が非常に厚く（最大 4 m）形成されており，粘土層の下には粘土層より透水性の高い基岩層が分布する。また，流域末端部では表土層内に地下水帯が形成されるとともに，粘土層の上を流れて滲出する湧水が確認されている。本流域では表土層・粘土層・基岩層を対象に，地下水位・圧力水頭，地温・地下水温，水質の観測を実施した。また，湧水を対象に，湧水流量・湧水温・水質の観測を実施した。地下水位・圧力水頭の観測結果から，表土層・粘土層・基岩層内に別個の地下水帯が形成されており，それぞれ降雨に反応して拡大・収縮していた。このことから，粘土層が基盤面として働く一方で，水が粘土層を通過して基岩層へも浸透していることが明らかとなった。圧力水頭から水の移動方向を解析したところ，降雨時・無降雨時に関わらず，表土層から粘土層への鉛直下向きの流れが生じていた一方，斜面末端部の粘土層内地下水帯では恒常的に鉛直上向きの流れが生じていることが確認された。各地下水帯のラグタイム（降雨開始から地下水位・圧力水頭の上昇開始までに要する時間），各地下水帯の拡大・収縮，そして水質・水温の観測結果から，流域末端部に形成される表土層内地下水帯，そして湧水の起源は粘土層内地下水であることが明らかになった。基岩層内地下水位は恒常的に高く，降雨時には度々粘土層−基岩層境界より高い位置まで上昇するものの，基岩層内地下水の表土層内地下水帯や湧水への影響は確認されなかった。これらの結果から，本流域では，著しく透水性の低い粘土層が基岩層内地下水の流出を阻害していることが示唆された。流域末端部で観測された粘土層内地下水帯の上向きの流れは，この地下水流出の阻害によって粘土層深部の圧力が上昇した結果生じたと考えられた。

　最後に，各流域における水文プロセスに粘土層が与える影響に違いが生じる要因について考察を加えた。不透水性基岩の流域では，基岩への水の浸透が生じないため，粘土層内の地下水位が高く維持され，極端に乾燥する表土層との圧力水頭のギャップが大きくなり，表土層への上向きフラックスが生じると考えられた。一方，透水性基岩の流域では，粘土層から基岩層へ水が浸透できるため，粘土層内の地下水位は低下し，表土層への上向きフラックスは生じない一方，著しく透水性の低い粘土層が基岩層内地下水の表土層への流出を阻害していると考えられた。

　以上から，本研究では，山地源流域における水文プロセスにおいて，粘土層が不透水性・透水性基岩いずれの流域においても基盤面として働くのみならず，基岩の透水性に応じていったん粘土層に浸透し貯留された水を表土層に供給したり，基岩層へと浸透した水の表土層への流出を阻害したりするなどの影響を与えており，主要な水移動の場として山地源流域の水文プロセスに大きく関与していることを示した。

Chapter 1

Introduction

1.1. General Background

The headwater catchment is an active site of rainfall runoff, soil development, and landform and forest formation [*Tsukamoto*, 1973; *Benda and Dunne*, 1997; *Gomi et al.*, 2002; *Gannon et al.*, 2014]. An understanding of these processes is important for the achievement of sustainable water resource use. Shallow landslide sites also tend to be concentrated in headwater catchments [*Tsukamoto et al.*, 1978; *Reneau and Dietrich*, 1987; *Sidle and Ochiai*, 2006].

Many researchers have conducted hydrological observations to clarify headwater catchment hydrological processes and examine their effects on stream water volume and chemistry or shallow landslide occurrence; such observations have involved the Maimai catchment in New Zealand [*Mosely*, 1979, 1982; *Pearce et al.*, 1986; *McGlynn et al.*, 2002], the Walker Branch watershed in the USA [*Wilson et al.*, 1991], the LI1 catchment in Llyn Brianne, Wales [*Soulsby*, 1992], the Plastic Lake basin in Canada [*Peters et al.*, 1995], and the Hitachi Ohta experimental watershed in Japan [*Sidle et al.*, 2000]. As a result, the following general conceptual model of the hydrological processes of headwater catchments has been developed. Organic soil layers (OSLs) form mainly through the decomposition of organic matter deposited on the surface, whereas mineral soil layers are solely composed of weathered bedrock material. Because both layers generally have high permeability, rainwater vertically infiltrates the soil (Figure 1.1a), then reaches impeding layers such as bedrock and flows laterally along their surfaces, thus forming a transient groundwater zone in downslope areas (Figure 1.1a). These groundwater zones shrink and eventually disappear as stream water discharges after the cessation of rainfall (Figure 1.1b). The formation of large-volume groundwater storage areas has been in some catchments underlain by permeable bedrock in recent decades [e.g., *Montgomery et al.*, 1997; *Kosugi et al.*, 2006;

1
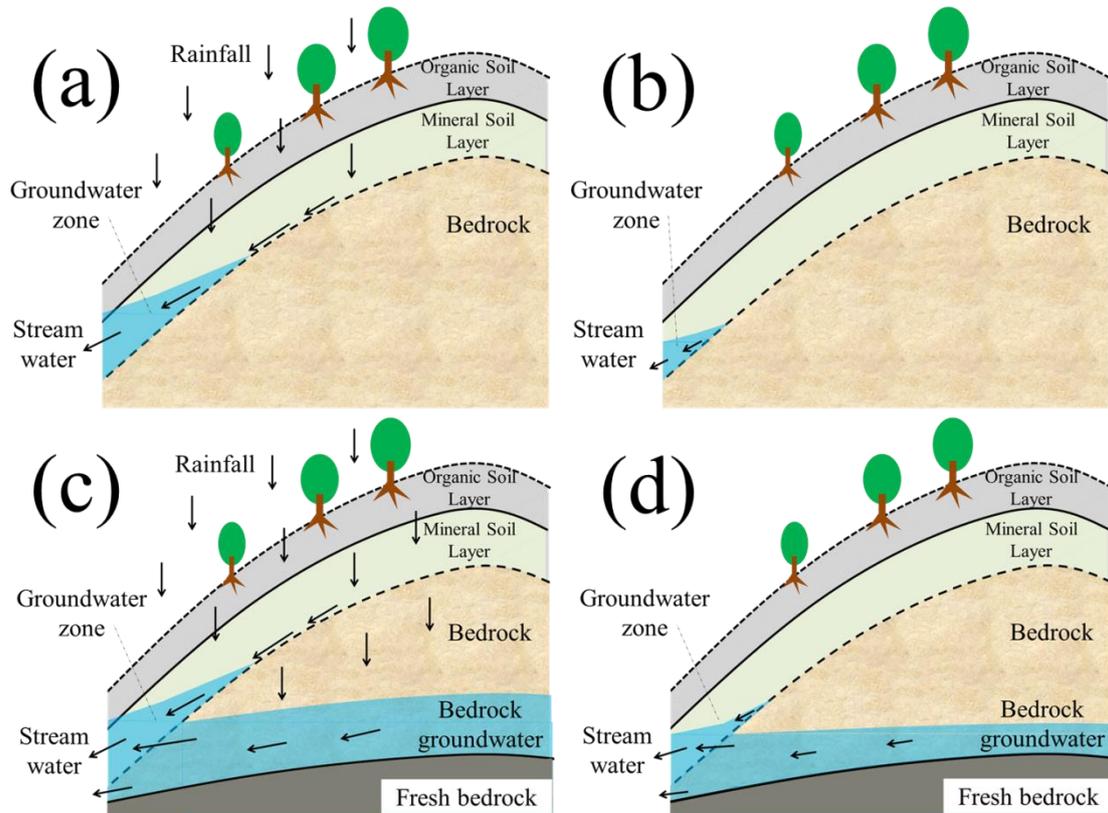
Figure 1.1. Conceptual models of hydrological processes in a catchment underlain by impermeable bedrock (a) during and (b) after rainfall, and in a catchment underlain by permeable bedrock (c) during and (d) after rainfall.

Graham et al., 2010; *Masaoka et al.*, 2016; *Abe et al.*, 2020; *Iwasaki et al.*, 2021]. Bedrock groundwater exfiltrates into a stream channel either directly or through overlying soil layers, influencing the volume and chemistry of the stream, as well as fluctuations in groundwater level (Figure 1.1c, d). Although the depth of impeding layers in catchments with permeable bedrock remain poorly understood, recent studies have indicated that weakly weathered or fresh bedrock with few fractures may function as impeding layers [*Hale et al.*, 2016; *Masaoka et al.*, 2022]. The results of some studies have suggested that bedrock exfiltration is an important factor triggering shallow landslides [*Montgomery et al.*, 2002; *Kosugi et al.*, 2008; *Bogaard and Greco*, 2016]. Based on the findings in these studies, numerous hydrological models have been developed to estimate interflow and streamflow rates using the Richards equation or the Boussinesq and/or kinematic assumptions [e.g., *Trouch et al.*, 2003; *Broda et al.*, 2011, 2014;

Gardner et al., 2020]. For example, *Trouch et al.* [2003] presented a new mathematical formulation of subsurface flow, assuming that bedrock constituted the impeding layers (i.e., no-flow boundaries) during drainage and recharge events. *Gardner et al.* [2020] improved the accuracy of simulated subsurface groundwater fluctuation on hillslopes by assuming that bedrock constituted a permeable layer, then integrating bedrock groundwater exfiltration. Other studies have combined hydrological models with slope stability analyses to create models that forecast the spatial and temporal occurrence of shallow landslides [e.g., *Raia et al.*, 2014]. Therefore, it is important to elucidate the hydrological processes of headwater catchments; this information will facilitate the development of more accurate hydrological models that can improve the accuracy of flood and slope failure predictions.

Mineral soil layers often consist of clayey materials near base rock that is rich in clay minerals (e.g., serpentine, tuff, slate, or mudstone), potentially because of soil particle movement. Such clay mineral layers (CMLs) are typically sandwiched between OSLs and bedrock. Although OSLs can have high permeability regardless of geology [*Hayashi et al.*, 2006], matrices of CMLs generally have low saturated hydraulic conductivity because of the lower porosity associated with fine soil particles. These differences in hydraulic properties between CMLs and OSLs can lead to the formation of a perched groundwater zone on top of the CMLs, which induces rapid groundwater flow in OSLs [e.g., *Todd et al.*, 2006; *Krám et al.*, 2009; *Swarowsky et al.*, 2012]. *Todd et al.* [2006] reported that perched groundwater zones formed above the clay-rich B horizon during storm events; this led to rapid discharge through the A horizon, which had a greater abundance of macropores. In a serpentinite catchment, mineral soil layers comprising clayey materials under the OSL interfered with rainfall infiltration and contributed more water to near-surface flow, producing flash-flood stream responses during rainfall [*Krám et al.*, 2009]. *Swarowsky et al.* [2012] measured the temporal variation in volumetric water content for each soil layer in a headwater catchment, where CMLs had formed under the OSLs; the CMLs restricted

water infiltration in a hydraulic manner, resulting in subsurface flow through the highly permeable organic layers. Thus, CMLs have been widely observed to function as impeding layers because of their low permeability, such that the hydraulic properties of the overlying OSLs control the hydrological processes of subsurface flow. Models have shown that water infiltration into CMLs is negligible on steeper hillslopes with high conductivity contrasts between OSLs and CMLs [*Jackson et al.*, 2014].

However, increasing numbers of hydrological studies in various headwater catchments with CMLs have suggested that CMLs do not function as impeding layers. Based on mixed model analysis and hydrograph separation, *Newman et al.* [1998] showed that a matrix of CMLs (B horizon) functioned as a solute sink that allowed solutes to be transported into a channel under saturated matrix flow. On a hillslope in a tropical headwater catchment, *Sayama et al.* [2021] observed groundwater zone formation in CMLs above bedrock, which constituted a significant response equivalent to the response during a high-intensity rainfall event. In a forested serpentinite catchment with CMLs produced by bedrock weathering, the CMLs prevented rainwater infiltration and promoted rainwater discharge through highly permeable OSLs, thereby increasing the contributions of rainwater and snowmelt to stream water [*Satoh et al.*, 1991, 1993; *Nomura et al.*, 2001]. However, the excessive wetness of OSLs and CMLs above the bedrock hindered deep root penetration [*Satoh et al.*, 1994], suggesting that the rainwater infiltrating CMLs was stored for long periods. On a hillslope in a serpentinite catchment near the catchment studied by *Satoh et al.* [1991, 1994] and *Nomura et al.* [2001], *Yoshino and Katsura* [2018] observed that CMLs functioned as impeding layers; they also used tensiometers to observe rainwater infiltration into the CMLs, revealing that water stored in CMLs contributed to springs at the slope base. These previous findings indicate that rainwater can infiltrate CMLs, and that water stored in these layers affects the hydrology and chemistry of groundwater in OSLs and stream water.

Multiple studies have shown that water can infiltrate bedrock after percolation through CMLs. *McGuire et al.* [2010] conducted hydrological

and chemical observations in a catchment underlain by andesitic tuffs and coarse breccias that contribute to CML formation via weathering. They demonstrated that lateral saturated flow was generated in OSLs above CMLs; vertical unsaturated flow and lateral saturated flow were also generated in CMLs. These flows resulted in the generation of both lateral and vertical saturated flow in fractured bedrock. In the catchment studied by *McGuire et al.* [2010], *Gabrielli et al.* [2012] found that rainwater infiltrated bedrock through CMLs, based on direct measurement of bedrock groundwater levels. *Brönnimann et al.* [2013] examined bedrock groundwater levels in a catchment underlain by conglomerate–sandstone beds and weathered marlstone; although the bedrock was overlain by CMLs with low hydraulic conductivity, they observed rapid fluctuation of bedrock groundwater levels in response to rainfall. *Du et al.* [2016] conducted a hydrological study of OSLs and CMLs on a forested hillslope in a headwater catchment; they found that rainwater flowed within OSLs above the CMLs, although it mainly infiltrated the CMLs through anomalies such as penetrating roots and recharged the deep groundwater zone. *Ishii and Kobayashi* [1995] and *Yamazaki et al.* [2007] conducted hydrological and chemical observations in a forested headwater catchment underlain by tuff breccia and CMLs produced by bedrock weathering. *Ishii and Kobayashi* [1995] demonstrated rainwater infiltration into the CMLs; their data also suggested water movement in the deepest CMLs. *Yamazaki et al.* [2007] examined temporal variation in flow rates, SiO_2 concentrations, and stable isotope ratios in stream and springs. They found evidence of deep water storage with high SiO_2 concentrations that differed from the concentrations in water sampled from CMLs; these high SiO_2 concentrations contributed to streamflow during base flow periods. Because bedrock groundwater typically has high SiO_2 concentrations [e.g., *Uchida et al.*, 2003; *Jung et al.*, 2020], the deep water storage reported by *Yamazaki et al.* [2007] was presumably bedrock groundwater. These previous studies suggested rainwater infiltration into CMLs, along with water movement between the CMLs and bedrock, which resulted in volumetric changes in bedrock groundwater and qualitative changes in stream water.

1.2. Objectives and structure of this study

Previous studies have revealed water movement among OSLs, CMLs, and bedrock, suggesting that the impacts of interactions between hydrological and chemical processes in headwater catchments are non-negligible. A recent study demonstrated the importance of infiltration and exfiltration through CMLs using kinematic modeling; it highlighted the need for process-based hydrological models in accurate modeling [*Bitew et al.*, 2020]. However, water movement between OSLs and CMLs, and between CMLs and bedrock, has received minimal attention because the speed of water movement in CMLs has been considered insufficient to influence hydrological and chemical processes. Most studies thus far have been based on chemical analyses and hydrological separation, rather than detailed observations within OSLs, CMLs, and bedrock. Therefore, it is difficult to accurately model the effects of CMLs on hydrological processes in headwater catchments because of the lack of quantitative and qualitative information regarding changes to water stored within each layer. Considering that geology rich in clay minerals (i.e., serpentine, tuff, slate, and mudstone) is extensively distributed worldwide and that CMLs can function as landslide slip surfaces after the groundwater level has risen [e.g., *Sartohadi et al.*, 2018; *Noviyanto et al.*, 2020], there is a need to measure quantitative and qualitative changes within the water stored in each layer (i.e., OSLs, CMLs, and bedrock) to elucidate the effects of CMLs on hydrological processes in headwater catchments.

The objective of this study was to investigate the effects of CMLs on hydrological and hydrochemical processes in headwater catchments. To better understand the effects of CMLs and their roles in two conventional conceptual models, this thesis performed detailed hydrological, hydrochemical, and hydrothermal observations in two headwater catchments underlain by permeable and impermeable bedrock, respectively, with a focus on the water stored in OSLs, CMLs, and bedrock. The results provide quantitative and qualitative information regarding the water in each of these layers.

Chapter 2 describes the effect of CMLs on hydrological processes in a small, forested headwater catchment underlain by impermeable bedrock, based on intensive hydrological, hydrochemical, and hydrothermal observations. Specifically, we examined the processes of groundwater zone formation in thin OSLs, as a result of interactions between OSLs and CMLs.

Chapter 3 discusses the effect of CMLs on hydrological processes in a forested headwater catchment underlain by permeable bedrock based on intensive hydrological, hydrochemical, and hydrothermal observations.

Chapter 4 summarizes the results presented Chapters 2 and 3 and discusses differences in the effects of CMLs between the two types of catchments; it also presents a general conclusion.

References

Abe, Y., Y. Uchiyama, M. Saito, M. Ohira, and T. Yokoyama (2020), Effects of bedrock groundwater dynamics on runoff generation: a case study on granodiorite headwater catchments, western Tanzawa Mountains, Japan. *Hydrological Research Letters*, 14(1), 62–67.

Benda, L., and T. Dunne (1997), Stochastic forcing of sediment supply to channel networks from landsliding and debris flows. *Water Resources Research*, 33, 2849–2863.

Bitew, M. M., C. R. Jackson, D. C. Goodrich, S. E. Younger, N. A. Griffiths, K. B. Vaché, B. Rau (2020), Dynamics domain kinematic modeling for predicting interflow over leaky impeding layers. *Hydrological Processes*, 34, 2895–2910.

Bogaard, T. A., and R. Greco (2016), Landslide hydrology: from hydrology to pore pressure. *Wires Water*, 3, 439–459.

Broda, S., C. Paniconi, M. Larocque (2011), Numerical investigation of leakage in sloping aquifers. *Journal of Hydrology*, 409, 49–61.

Broda, S., M. Larocque, C. Paniconi (2014), Simulation of distributed base

flow contributions to streamflow using a hillslope-based catchment model coupled to a regional-scale groundwater model. *Journal of Hydrologic Engineering*, 19(5),

http://doi.org/10.1061/(ASCE)HE.1043-5584.000877

Brönnimann, C., M. Stähli, P. Schneider, L. Seward, and S. M. Springman (2013), Bedrock exfiltration as a triggering mechanism for shallow landslides. *Water Resources Research*, 49, 5155–5167.

Du, E., C. R. Jackson, J. Klaus, J. J. McDonnell, N. A. Griffiths, M. F. Williamson, J. L. Greco, and M. Bitew (2016), Interflow dynamics on a low relief forested hillslope: Lots of fill, little spill. *Journal of Hydrology*, 534, 648–658.

Gabrielli, C. P., J. J. McDonnell, and W. T. Jarvis (2012), The role of bedrock groundwater in rainfall-runoff response at hillslope and catchment scales. *Journal of Hydrology*, 450–451, 117–133.

Gannon, J. P., S. B. Bailey, and K. McGuire (2014), Organizing groundwater regimes and response thresholds by soils: A framework for understanding runoff generation in a headwater catchment. *Water Resources Research*, 50, 8403–8419.

Gardner, W. P., K. Jensco, Z. H. Hoylman, R. Livesay, M. P. Maneta (2020), A numerical investigation of bedrock groundwater recharge and exfiltration on soil mantled hillslopes. *Hydrological Processes*, 34, 3311–3330.

Gomi, T., R. C. Sidle, and J. S. Richardson (2002), Understanding processes and downstream linkages of headwater systems. *BioScience*, 52, 905–916.

Graham, C. B., van Verseveld, M., Barnard, H. R., and McDonnell, J. J. (2010), Estimating the deep seepage component of the hillslope and catchment water balance within a measurement uncertainty framework. *Hydrological Processes*, 24, 3631–3647.

Hale, V. C., J. J. McDonnell, M. K. Stewart, D. K. Solomon, J. Doolitte, G. G. Ice, and R. T. Pack (2016), Effects of bedrock permeability on stream base flow mean transit time scaling relationships: 2. Process study of storage and release. *Water Resources Research*, 52(2), 1375–1397.

Hayashi, Y., K. Kosugi, and T. Mizuyama (2006), Changes in pore size distribution and hydraulic properties of forest soil resulting from structural development. *Journal of Hydrology*, 331, 85–102.

Ishii, Y., and D. Kobayashi (1995), Movement of subsurface water on a forested hillslope in the Moshiri experimental basin I; Observation of the pressure head using tensiometer nest (in Japanese with English abstract). *Low Temperature Science. Series A*, *Physical sciences*, 53, 23–24.

Iwasaki, K., Y. Nagasaka, and A. Nagasaka (2021), Geological effects on the scaling relationships of groundwater contributions in forested watersheds. *Water Resources Research*, 57, doi: 10.1029/2021WR029641.

Jackson, C. R., M. Bitew, E. Du (2014), When interflow also percolates: downslope travel distances and hillslope process zone. *Hydrological Processes*, 28, 3195–3200.

Jung, Y. Y., D. C. Koh, J. Lee, M. Tsujimura, S. T. Yun, and K. S. Lee (2020), Mean transit time and subsurface flow paths in a humid temperate headwater catchment with granitic bedrock. *Journal of Hydrology*, 587, 124942.

Kosugi, K., S. Katsura, M. Katsuyama, and T. Mizuyama (2006), Water flow processes in weathered granitic bedrock and their effects on runoff generation in a small headwater catchment. *Water Resources Research*, 42, W02414, doi:10.1029/2005WR004275.

Kosugi, K., S. Katsura, T. Mizuyama, S. Okumura, and T. Mizutani (2008), Anomalous behavior of soil mantle groundwater demonstrates the major effects of bedrock groundwater on surface hydrological processes. *Water Resources Research*, 44, W01407, doi:10.1029/2006WR005859.

Krám, P., F. Oulehle, V. Štědrá, J. Hruška, J. B. Shanley, R. Minocha, and E. Trainster (2009), Geoecology of a forest watershed underlain by Serpentine in central Europe. *Northeastern Naturalist*, 16(Special Issue 5), 309–328.

Masaoka, N., K. Kosugi, Y. Yamakawa, and D. Tsutsumi (2016), Processes of bedrock groundwater seepage and their effects on soil water fluxes in

a foot slope area.   *Journal of Hydrology*, 535, 160–172.

Masaoka, N., K. Kosugi, and M. Fujimoto (2021), Bedrock groundwater catchment area unveils rainfall-runoff processes in headwater basins. *Water Resources Research*, 57, doi:10.1029/2021WR029888.

McGlynn, B.L., J. J. McDonnell, and D. D. Brammer (2002), A review of the evolving perceptual model of hillslope flowpaths at the Maimai catchments, New Zealand.   *Journal of Hydrology*, 257, 1–26.

McGuire, K. J., and J. J. McDonnell (2010), Hydrological connectivity of hillslopes and streams: Characteristic time scales and nonlinearities. *Water Resources Research*, 46, W10543, doi:10.1029/2010WR009341.

Montgomery, D. R., W. E. Dietrich, R. Torres, S. P. Anderson, J. T. Heffner, and K. Loague (1997), Hydrologic response of a steep, unchanneled valley to natural and applied rainfall.   *Water Resources Research*, 33(1), 91–109.

Montgomery, D. R., W. E. Dietrich, and J. T. Heffner (2002), Piezometric response in shallow bedrock at CB1: Implications for runoff generation and landsliding.   *Water Resources Research*, 38(12), 1274, doi:10.1029/2002WR001429.

Mosely, M. P. (1979), Streamflow generation in a forested watershed, New Zealand.   *Water Resources Research*, 15, 795–806.

Mosely, M. P. (1982), Subsurface flow velocities through selected frost soils South Island, New Zealand.   *Journal of Hydrology*, 55, 65–92.

Newman, B. D., A. R. Campbell, and B. P. Wilcox (1998), Lateral subsurface flow pathways in a semiarid ponderosa pine hillslope. *Water Resources Research*, 34(12), 3485–3496.

Nomura, M., K. Yazaki, K. Sasa, F. Satoh, D. Ashiya, and S. Sugata (2001), Comparison of snowmelt runoff in Tertiary with in serpentine basin (in Japanese).   *Research bulletin of the Hokkaido University Forests*, 58(2), 1–9.

Noviyanto, A., J. Sartohadi, B. H. Purwanto (2020), The distribution of soil morphological characteristics for landslides-impacted Sumbing volcano, central Java –Indonesia.   *Geoenvironmental Disasters*, 9, 23, https://doi.org/10.1155/2018/2648185.

Pearce, A. J., M. K. Stewart, and M. G. Sklash (1986), Storm runoff generation in humid headwater catchments. 1. Where does the water come from? *Water Resources Research*, 22, 1263–1272.

Peters, D. L., J. M. Buttle, C. H. Taylor, and B. D. LaZerte (1995), Runoff production in a forested, shallow soil, Canadian Shield. *Water Resources Research*, 31(5), 1291–1304.

Raia, S., M. Alvioli, M. Rossi, R. L. Baum, J. W. Godt, F. Guzzetti (2014), Improving predictive power of physically based rainfall-induced shallow landslide models: a probabilistic approach. *Geoscientific Model Development*, 7, 495–514.

Reneau, S., and W. Dietrich (1987), Size and location of colluvial landslides in a steep forested landslides. *International Association of Hydrological Sciences Publications*, 165, 39–48.

Sartohadi, J., N. A. H. J. Pulungan, M. Nurudin, W. Wahyudi (2018), The ecological perspective of landslides at soils with high clay content in the middle Bogowonto watershed, central Java, Indonesia. *Hindawi Applied and Environmental Soil Science*, http://doi.org/10.1155/2018/2648185.

Satoh, F., K. Masumoto, and H. Ichikawa (1991), Effects of forests on streamwater runoff and water quality from serpentinite mountain (in Japanese*). *Annual test report of Hokkaido University Forests*, 9, 16–17.

Satoh, F., F. Mochida, K. Sasa, H. Ichikawa, and D. Ashiya (1994), Forest and geological effects on runoff during rainfall (in Japanese*). *Annual test report of Hokkaido University Forests*, 12, 41–42.

Sayama, T., R. Araki, K. Yamamoto, and Apip (2021), Characteristics of soil and hillslope responses in humid tropical forests in Sumatra, Indonesia. *Hydrological Research Letters*, 15(2), 23–30.

Sidle, R.C., T. Tsuboyama, S. Noguchi, I. Hosoda, M. Fujieda, and T. Shimizu (2000), Stormflow generation in steep forested headwaters: A linked hydrogeomorphic paradigm. *Hydrological Processes*, 14, 369–385.

Sidle, R., and H. Ochiai (2006), *Lnadslides: Processses, Prediction, and*

LandUse. Water Resources Monograph 18, American Geophysical Union: Washington, D.C.

Soulsby, C (1992), Hydrological controls on acid runoff generation in an afforested headwater catchment at Llyn Brianne, Mid-Wales. *Journal of Hydrology*, 138, 431–448.

Swarowsky, A., R. A. Dahlgren, and A. T. O'Green (2012), Linking subsurface lateral flowpath activity with streamflow characteristics in a semiarid headwater catchment. *Soil Science Society of America Journal*, 76, 532–547.

Todd, A. K., J. M. Buttle, and C. H. Taylor (2006), Hydrologic dynamics and linkages in a wetland-dominated basin. *Journal of Hydrology*, 319, 15–35.

Troch, P. A., C. Paniconi, E. E. van Loon (2003), Hillslope-storage Boussinesq model for subsurface flow and variable source areas along complex hillslopes: 1. Formulation and characteristic response. *Water Resources Research*, 39(11), 1316, doi: 10.1029/2002WR001728.

Tsukamoto, Y. (1973), Characteristics of a couple of torrential rainfall type landslides (in Japanese*). *Proceedings of the 13th Annual Symposium on Natural Disaster Science*, 303–306.

Tsukamoto, Y., M. Matsuoka, and K. Kurihara (1978), Study on the growth of stream channel (VI) –Landslides as the process of erosional development of basin morphology– (in Japanese). *Journal of the Japan Society of Erosion Control Engineering*, 30(4), 25–32.

Uchida, T., Y. Asano, Y. Ohte, and T. Mizuyama (2003), Seepage area and rate of bedrock groundwater discharge at a granitic unchanneled hillslope. *Water Resources Research*, 39(1), 1008, doi: 10.1029/2002WR001298.

Wilson, G.V., P. M. Jardine, R. J. Luxmoore, L. W. Zelazny, D. E. Todd, and D. A. Lietzke (1991), Hydrogeochemical processes controlling subsurface transport from an upper subcatchment of walker branch watershed during storm events. 2. Solute transport processes. *Journal of Hydrology*, 123, 317–336.

Yamazaki, M., Y. Ishii, and N. Ishikawa (2007), Hydrochemical processes

during snowmelt season in a nival mountainous watershed (in Japanese with English abstract). *Journal of Japanese Association of Hydrological Sciences*, 37(3), 123–135.

Yoshino, T., and S. Katsura (2018), Rainfall-runoff processes of rotational secondary slide in weathered serpentinite region (in Japanese*). *Proceeding of 67th annual conference of the Japan Society of Erosion Control Engineering*, 535–536.

* The title or source is a tentative translation by the authors from the original.

Chapter 2

Effects of Clay Layers on Hydrological Processes in a Headwater Catchment Underlain by Impermeable Bedrock

2.1. Introduction

In a headwater catchment underlain by impermeable bedrock, as noted in **Chapter 1**, it has been considered that groundwater flow dominantly occurs within soil layers above bedrock. In this hydrological process, groundwater zone formed on impeding layers shrinks through the discharge of water into stream after rainfall has ceased; it generally disappears (especially in small catchments) during dry periods because of the low capacity of a small headwater catchment to store water, combined with high permeability of soil layers. In a headwater catchment underlain by impermeable bedrock rich in clayey minerals, mineral soil layers can form clay layers sandwiched between organic soil layers and bedrock. In this case, dominant groundwater flow has been thought to occur within organic soil layers above clay layers because clay layers act as impeding layers. However, some studies have suggested that clay layers may not simply function as impeding layers and rainwater also infiltrates to clay layers [e.g., *Satoh et al.*, 1991, 1994; *Newman et al.*, 1998; *Nomura et al.*, 2001; *Sayama et al.*, 2021]. Some studies suggested that organic soil layers and clay layers were too wet for roots relatively long-term to penetrate deeply into them and water stored into clay layers contributed to spring [*Satoh et al.*, 1994; *Yoshino and Katsura*, 2018].

In this chapter, we observed groundwater dynamics in a small headwater catchment (0.068 ha) with gentle topography underlain by impermeable serpentine in the same region as *Yoshino and Katsura* [2018]. In this catchment, a semi-perennial to perennial groundwater zone, which would have disappeared during dry periods under the aforementioned process, forms in thin, high-permeability organic soil layers (OSLs) in an unchanneled hollow; it remains present during dry periods. The aforementioned hydrological processes, which were based on observations

in catchments with no thick clay mineral layers, cannot explain the semi-perennial to perennial groundwater zone observed in this catchment. Another hydrological process appeared to occur and contribute to groundwater zone in this catchment. Using hydrometric, hydrochemical, and thermal observations, this study explored the effects of clay layers on hydrological processes in this catchment while focusing on the formation process of the semi-perennial to perennial groundwater zone observed in the OSLs.

2.2. Material and Methods

2.2.1 Study Site

The study was conducted in a very small forested headwater catchment (0.068 ha; 44°52′ N, 142°4′ E) on Kunneshiri Mountain in Nakagawa Experimental Forest, which is managed by Hokkaido University and located in Hokkaido, northern Japan (Figure 2.1). The elevation of the catchment ranges from 241 to 257 m above sea level (Figure 2.1c), and a spring is present at the catchment outlet. The region has a mean annual temperature of 5.9 °C (1989–2019) and precipitation of 1240 mm (1989–2019) according to data from the nearest weather station (the Japan Meteorological Agency Automated Meteorological Data Acquisition System (AMeDAS) Nakagawa observation station, located approximately 5 km south-southwest of the catchment). The snowfall season in Nakagawa Experimental Forest is from late November through late April or early May [*Hiura et al.*, 1998], and the maximum snow depth during this season is about 1.7 ± 0.5 m [*Kobayashi et al.*, 2022]. The dominant tree species in Nakagawa Experimental Forest are *Abies sachalinensis*, *Picea glehnii*, *Picea jezoensis*, *Sorbus commixta*, *Quercus crispula*, and *Acer pictum* [*Hiura et al.*, 2019]; the understory is densely covered with *Sasa kurilensis* and *Sasa senanensis* [*Hiura e al.*, 1999].
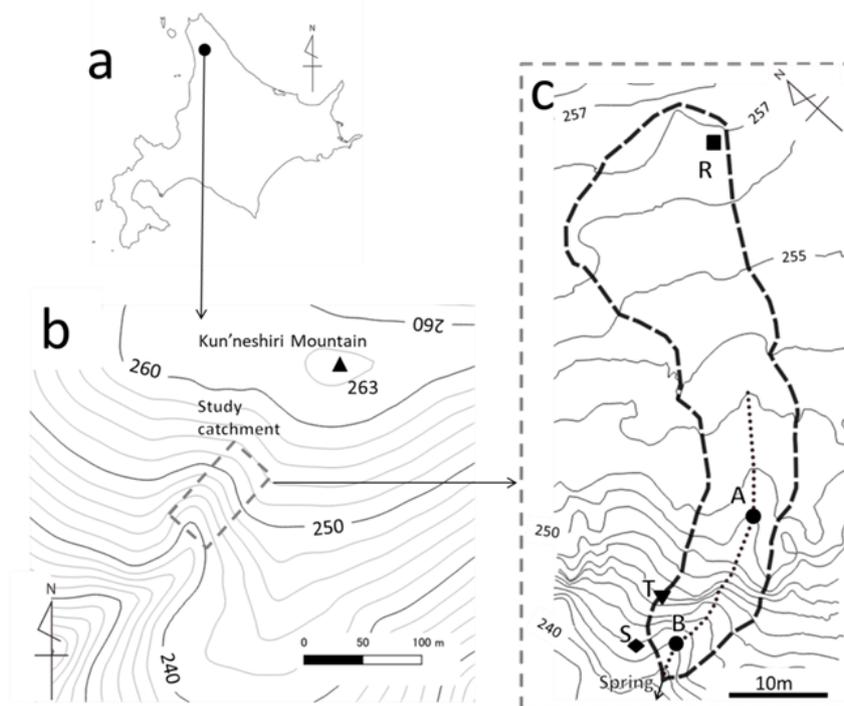
Figure 2.1. Maps of (**a**) Hokkaido, (**b**) the Kunneshiri Mountain area in Nakagawa Experimental Forest, and (**c**) the study catchment. In panel (**b**), black and gray contours represent intervals of 10 and 2 m, respectively. In panel (**c**), the contour interval is 1 m. Dotted and dashed lines in panel (**c**) indicate an unchanneled hollow in the study catchment and the catchment boundary, respectively.

The study catchment is underlain by serpentinite bedrock and features low elevation, gentle hillslopes, and a rounded ridge with a mean gradient of 14°. These topographic characteristics are consistent with the characteristics of other serpentinite catchments in Japan [*Suzuki*, 2006]. The surface soil type of the area underlain by serpentine is "Wet Iron Podzol" [*Nakata et al.*, 1987]. In this catchment, OSLs are very thin, with thickness ranging from 10 to 50 cm. Mineral soil layers derived from weathering of the serpentinite bedrock consist of clayey materials (referred to as CMLs in this study), with thickness ranging from 30 to 170 cm. Each layer is thicker in the middle of the slope and thinner in the upper and lower parts. Whereas macropores and pipes can form within CMLs and contribute to preferential flow in catchments with geological settings other than serpentinite [*Tani*,

1997; *Newman et al.*, 1998], they are not observed in the study catchment because the CMLs consist of stiff clayey materials and the high concentration of nickel in serpentine soils inhibits root growth into the CMLs [*Gabbrielli et al.*, 1990].

2.2.2 Laboratory Measurement

Figure 2.2 shows a flowchart of the methodology used to explore the formation process of the semi-perennial to perennial groundwater zone observed in the OSLs of this catchment. First, to measure the hydraulic properties of OSLs, CMLs, and the boundary layers between them, we collected undisturbed core samples (100 cc in volume) from a trench (Figure 2.3) excavated at Point S in Figure 2.1c. The thicknesses of the OSL and CML at this point are 10 and 33 cm, respectively. In total, three, one, and four samples were collected from the OSL, boundary layer, and CML, respectively. We confirmed that the soil and bedrock structure at this point is almost the same as the structure at other points (e.g., Points A, B, and T; mentioned later). Moreover, the area of the study catchment is very small (0.068 ha). Hence, we assumed that the collected samples were representative of each layer in the catchment.
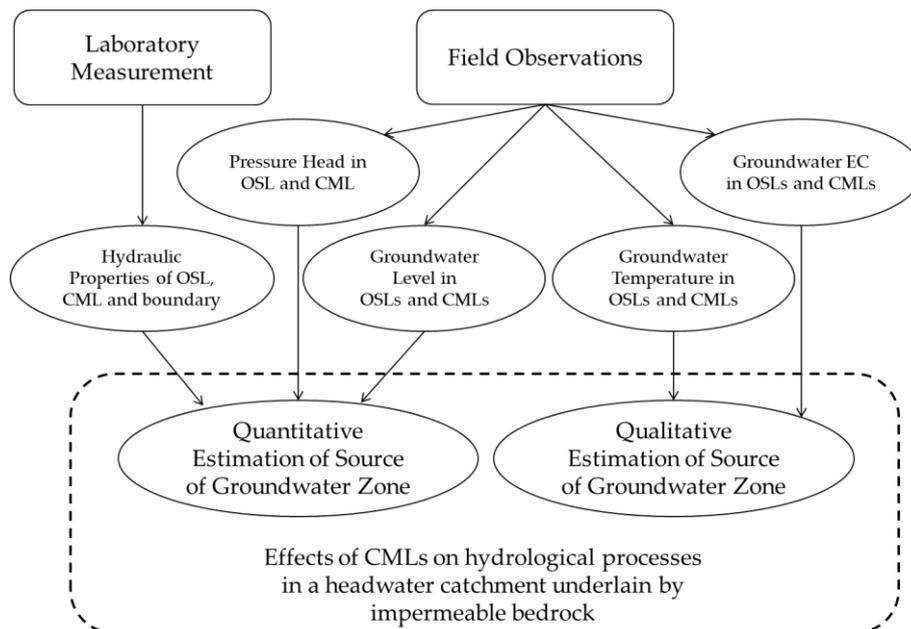
Figure 2.2. Flowchart of methodology of this study.
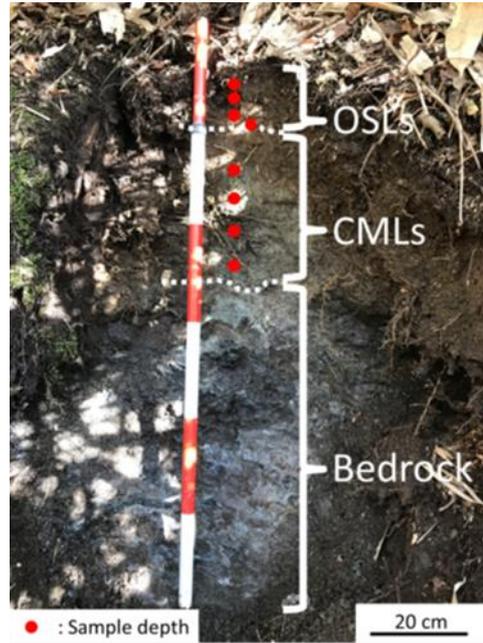
Figure 2.3. Photograph of the trench at Point S. White dotted lines indicate boundaries between the OSLs and CMLs and between the CMLs and bedrock. Solid red circles indicate the depths at which undisturbed core samples were collected.

We conducted water retention tests on all core samples in the laboratory. To obtain and characterize water retention curves for each sample, we fitted a lognormal model [*Kosugi*, 1996] to the observed relationship between volumetric water content, θ, and pressure head, ψ (cm). The lognormal model was derived by applying the lognormal distribution law to the soil pore radius distribution function, and the water retention curve is expressed as follows:

$$S_e = \frac{\theta - \theta_r}{\theta_s - \theta_r} = Q\left(\frac{ln(\psi/\psi_m)}{\sigma}\right) \qquad (2-1)$$

where S_e represents the effective saturation; θ_s and θ_r are the saturated and residual volumetric water contents, respectively; ψ_m is the pressure head at $S_e = 0.5$; σ is a dimensionless parameter characterizing the width of the pore-size distribution; and Q is the complementary normal distribution function:

$$Q(x) = \int_x^\infty \frac{1}{\sqrt{2x}} \exp\left(-\frac{u^2}{2}\right) du \qquad (2-2)$$

We determined the values of θ_r, ψ_m, and σ for each sample through minimization of the residual sum of squares, which was obtained from the measured and calculated values of θ at the applied ψ, with θ_s fixed at the measured value. Finally, the mean water retention curves of OSLs and CMLs were obtained using the mean parameter values of core samples collected from each layer (arithmetic means of θ_s, θ_r, and σ; geometric mean of ψ_m). The water retention curve for the OSL–CML boundary zone was obtained using parameter values determined from the OSL–CML boundary core sample.

We also measured the saturated hydraulic conductivity, K_s, for all core samples in the laboratory. The hydraulic conductivity curve was obtained using the model proposed by *Kosugi* [1996]. The following functional relationship between hydraulic conductivity, K, and ψ was obtained by combining Equation (1) with *Mualem*'s [1976] model:

$$K(\psi) = K_s S_e^{1/2} \left[Q \left(\frac{ln(\psi/\psi_m)}{\sigma} + \sigma \right) \right]^2 \qquad (2-3)$$

Mean hydraulic conductivity curves for OSLs and CMLs were obtained using the geometric mean value of K_s for core samples collected from each layer with the mean parameter values of ψ_m and σ, which were determined as described above. The hydraulic conductivity curve for the OSL–CML boundary was obtained using the measured value of K_s and the parameter values of ψ_m and σ.

2.2.3. Field Observations

Temporal variations of ψ were measured at Point T (Figure 2.1c) at 60 min intervals from 15 May to 1 November 2019 using tensiometers. We selected this point because it is located at the catchment boundary in the downslope area and therefore roughly represents the average degree of wetness for the whole catchment. The OSL depth is 31 cm at this location. The tensiometer installation depths were 30 (in the OSLs), 50, and 80 cm (in the CMLs).

To separately monitor groundwater levels and temperature in the OSLs and CMLs, two pairs of observation wells (for OSLs and CMLs) were

manually excavated at Points A and B along an unchanneled hollow in the study catchment (Figure 2.1c). All wells were constructed using 6 cm diameter polyvinyl chloride pipes perforated with numerous 5 mm diameter holes. The depths of the wells for observation of the OSLs at Points A and B (equivalent to the depths to the CML surfaces at each point) were 41 and 38.5 cm, respectively. The depths of the wells for the CMLs at Points A and B were 209 and 164 cm (equivalent to the depths of the bedrock surfaces at each point), respectively. To prevent groundwater in the OSLs from directly infiltrating into the CML wells, the upper sections of the CML wells were unperforated. The depth of the unperforated section was 60 cm at Point A and 43 cm at Point B; it was greater than the OSL depth at each point. A water-level gauge with a temperature recorder was installed at the bottom of each observation well, where it measured the groundwater level and temperature simultaneously at 60 min intervals from 15 May to 1 November 2019.

For analysis of electrical conductivity (EC; μS cm^{-1}), water samples were collected at intervals of approximately 4–5 weeks from mid-May through early November 2019. Samples of groundwater in the OSLs and CMLs were collected directly from the wells. Rainwater samples were collected using a plastic bottle equipped with a mesh-covered 21-cm-diameter funnel located at Point R in a clearing in the study catchment (Figure 2.1c). The measured EC values were converted to values at a standard temperature of 25 °C.

All rainfall and air temperature data were obtained from the Japan Meteorological Agency AMeDAS Nakagawa observation station.

2.3. Results
2.3.1 Hydraulic Properties

Figure 2.4 shows the water retention and hydraulic conductivity curves of the OSLs, CMLs, and boundary layer. The parameter values are listed in Table 1. The θ value of the OSLs is large at $\psi = 0$ cm (i.e., $\theta_s = 0.707$); it shows a sharp and continuous decrease (approximately 0.204) as ψ decreases to -200 cm (Figure 2.4a). The decrease in θ is most

21
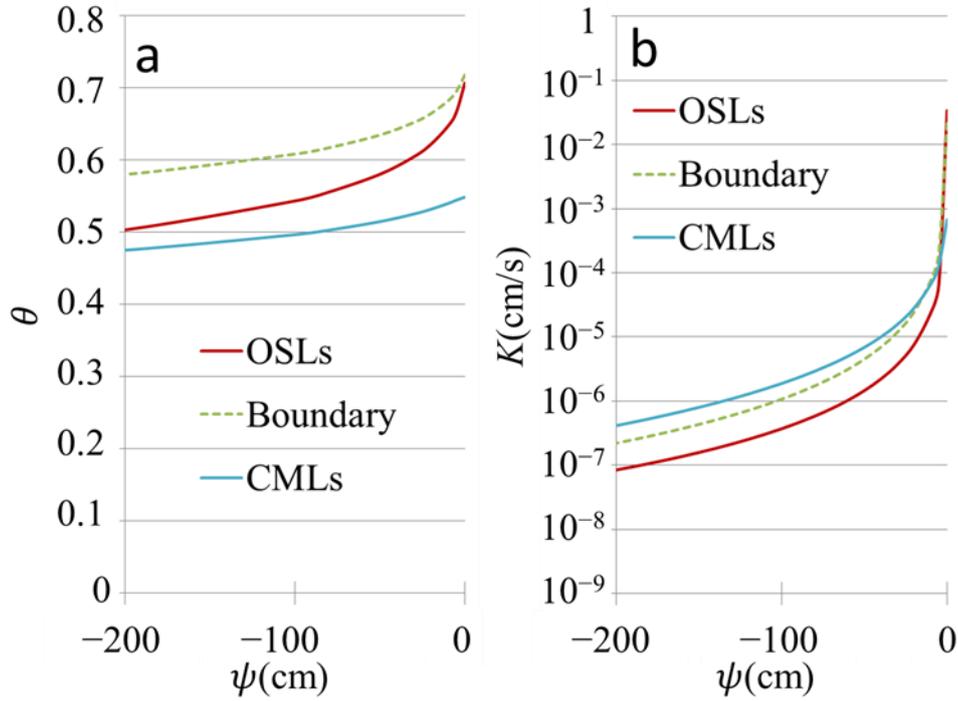
Figure 2.4. a) Water retention curves and (**b**) hydraulic conductivity curves of the OSLs, CMLs, and boundary zone between the OSLs and CMLs.

Table 2.1. Parameter values for hydraulic properties.

	K_s cm s^{-1}	θ_s	θ_r	ψ_m cm	σ
OSLs	3.38×10^{-2} [a]	0.707 [b]	0.250 [b]	−303.4 [a]	3.05 [b]
CMLs	6.76×10^{-4} [a]	0.549 [b]	0.374 [b]	−303.2 [a]	2.10 [b]
Boundary	2.14×10^{-2}	0.718	0.442	−200.3	2.67

Note(s): [a] Geometric mean. [b] Arithmetic mean.

prominent in the wet range of $\psi > -10$ cm (0.060). In contrast, θ in the CMLs is smaller at $\psi = 0$ cm ($\theta_s = 0.549$) than in the OSLs; it decreases less sharply (0.074) from θ_s as ψ decreases to -200 cm, with no prominent decrease in the wet range. Because θ_s is equivalent to the total volume of soil pores and water drains earlier from larger pores than from smaller pores as ψ decreases, these water retention curves suggest that the OSLs contain many pores of various sizes from very large (as indicated by the prominent change in θ in the wet range) to small, whereas the CMLs have only a few large pores. The θ value of the OSL–CML boundary is similar to the θ value of OSLs at $\psi = 0$ cm ($\theta_s = 0.718$), and it shows an

22

intermediate rate of decrease (0.138) as ψ decreases to -200 cm.

The measured K_s values of the OSLs ranged from 1.07×10^{-2} to 6.06×10^{-2} cm s^{-1}, with a geometric mean of 3.38×10^{-2} cm s^{-1}; these values were larger than the K_s of CMLs, which ranged from 2.37×10^{-4} to 6.08×10^{-3} cm s^{-1}, with a geometric mean of 6.76×10^{-4} cm s^{-1} (Table 1). Figure 2.4b depicts hydraulic conductivity curves for the OSLs, CMLs, and OSL–CML boundary; it shows that the K of the OSLs rapidly decreases from 3.38×10^{-2} cm s^{-1} to 2.34×10^{-5} cm s^{-1} as ψ decreases from 0 to -10 cm. In contrast, the reduction in the K values of CMLs across the same ψ range is smaller (6.76×10^{-4} cm s^{-1} to 6.58×10^{-5} cm s^{-1}). Therefore, although OSLs have a larger K_s (K at $\psi = 0$ cm) than CMLs, OSLs have a smaller K than CMLs in the range of $\psi < -1.5$ cm ($K < 3.00 \times 10^{-4}$ cm s^{-1}). At the OSL–CML boundary, K decreases from 2.14×10^{-2} to 7.50×10^{-5} cm s^{-1} as ψ decreases from 0 to -10 cm. In the range of $\psi < -10$ cm, OSLs, CMLs, and the OSL–CML boundary all show gentler changes in K than in the range of $\psi > -10$ cm.

2.3.2 Pressure Head

Figure 2.5 shows hourly rainfall and ψ in the OSL (30 cm depth) and CMLs (50 and 80 cm depths) at Point T. Total precipitation during the study period was 468.5 mm. Positive and negative ψ values indicate saturated and unsaturated conditions, respectively. The OSLs showed a rapid increase in ψ and often reached saturation in response to rainfall, whereas periods without rainfall resulted in ψ decreases and severe drying. Careful examination of Figure 2.5b demonstrates that ψ in the OSL displayed a rapid decrease from saturation to approximately -10 cm, followed by a gentler decrease as ψ decreased further. This tendency can be attributed to the water retention curve of OSLs (Figure 2.4a). The observed rapid decrease in ψ from saturation to $\psi = -10$ cm presumably reflects rapid drainage of water through very large pores. Based on the tendencies described here, we defined wet and dry periods in this study as periods with OSL ψ of > -10 cm and < -10 cm, respectively. The variations of ψ are shown in Figure 2.5b, c for wet and dry periods,
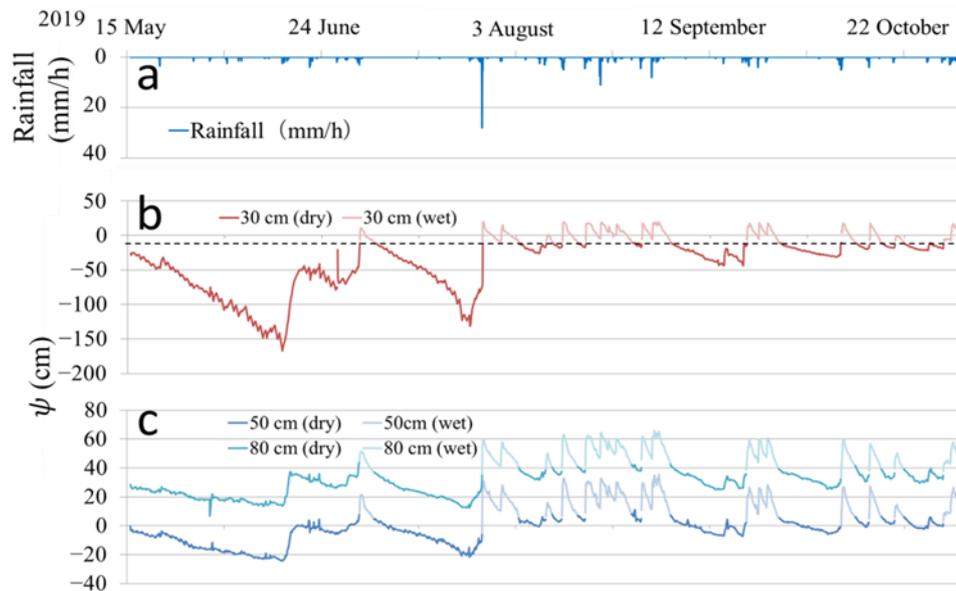
Figure 2.5. (a) Rainfall and ψ in the (b) OSLs (30 cm) and (c) CMLs (50 and 80 cm). Dashed line in panel (b) represents ψ = −10 cm.

respectively. The 80 cm sampling depth in the CMLs showed smaller ψ responses to rainfall and was constantly saturated in both wet and dry periods. The 50 cm sampling depth in the CMLs became saturated in response to rainfall and gradually returned to unsaturation after rainfall ceased. The ψ fluctuated less at 50 cm than at 30 cm (in the OSLs); it remained close to saturation even when ψ values at depths upward of 20 cm indicated severely dry conditions. These ψ dynamics indicate wetter conditions in the CMLs than in the OSLs, especially during dry periods.

2.3.3 Groundwater Level and Temperature

Figure 2.6 shows hourly rainfall and the groundwater level in the OSLs and CMLs at Points A and B. The groundwater level is presented as the depth below the ground surface, and the OSL–CML boundary is denoted with a dashed line. In the study catchment, we observed two distinct groundwater levels, in OSLs and CMLs (OSL groundwater and CML groundwater, respectively). Observation data for OSL groundwater at Point
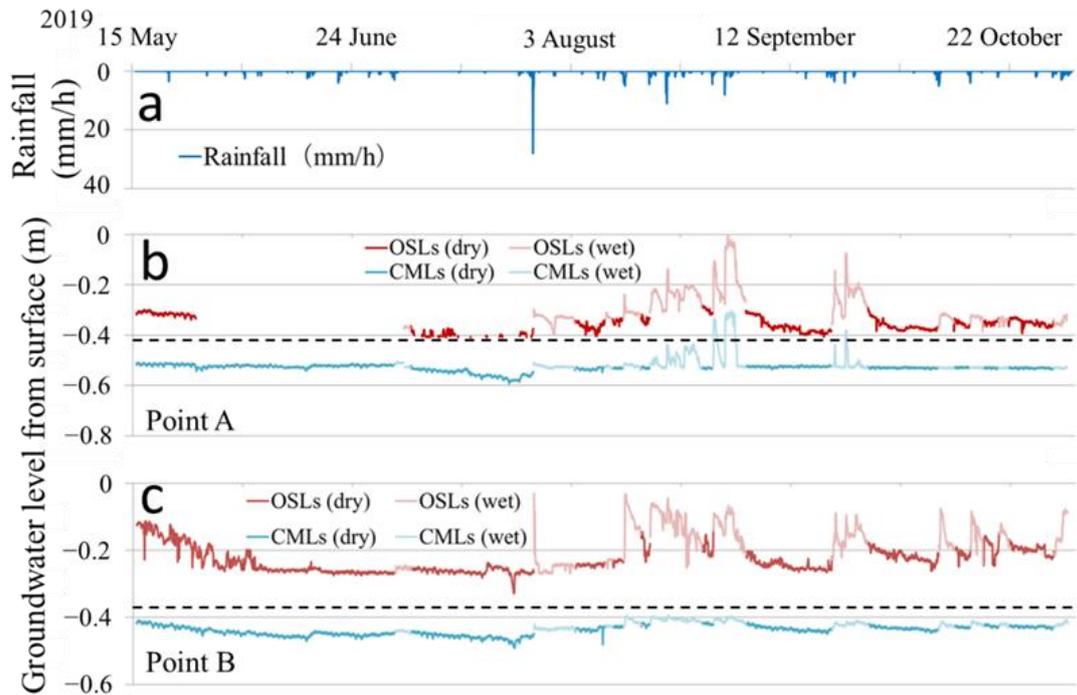
Figure 2.6. a) Rainfall and groundwater levels at (b) Point A and (c) Point B. The groundwater level is presented as depth below the ground surface. Dashed lines in panels (b,c) indicate the boundary between the OSLs and CMLs.

A are missing because of equipment failure from 26 May at 13:00 through 3 July at 10:00.

At Point A, the OSL groundwater showed rapid fluctuations in response to rainfall; it was present throughout the observation period except in July, when low precipitation and high evapotranspiration during the summer drought period in Hokkaido [*Ishii et al.*, 2004] caused the groundwater level to intermittently decrease to zero (Figure 2.6b). Notably, OSL groundwater was sustained from 2 September through 17 September despite extremely low rainfall (5.0 mm) during this period. In contrast, the CML groundwater level was less responsive to rainfall. The CML groundwater level generally did not reach the OSL–CML boundary, although a few rainfall events increased the CML groundwater level above the OSL–CML boundary. Even during such periods, the CML groundwater level did not match the OSL groundwater level, suggesting distinct groundwater zones in the OSLs and CMLs. The minimum groundwater level

25

in the CMLs was −0.593 m, which was observed on 22 July at 16:00 during the drought period; this level was 0.183 m below the boundary.

At Point B, the groundwater level in the OSLs was observed continuously; it showed steep increases and decreases in response to rainfall (Figure 2.6c). Excluding the rapid decrease and recovery of the groundwater level within the OSLs from 23 July at 1:00 to 14:00 during the summer drought period, the minimum groundwater level was −0.282 m on 17 July at 16:00 (in a dry period), which was 0.103 m above the boundary; this finding indicated that groundwater was permanently present at approximately 10 cm above the OSL–CML boundary, even during dry periods. Conversely, the CML groundwater response to rainfall was gentle and small. The CML groundwater level did not reach the OSL–CML boundary throughout the observation period. The minimum groundwater level in the CMLs was −0.492 m, which was observed on 23 July at 14:00 (in a dry period) and was 0.107 m below the boundary. Note that the groundwater level dynamics at Points A and B were similar to the pressure head dynamics at Point T (Figure 2.5), except that Points A and B, located in the hollow, were wetter.

Figure 2.7 shows rainfall, air temperature, and the temperature measured at the bottom of each observation well. Because groundwater was nearly always present in all wells, we hereafter refer to the temperature in the wells as the groundwater temperature. The groundwater temperature in the OSLs at Points A and B showed diurnal variations that can be attributed to changes in air or rainwater temperature, as well as a seasonal trend with a peak in early August. In contrast, the groundwater temperature in the CMLs at each point was minimally affected by diurnal air temperature changes or rainwater; it showed gentle seasonal variations with a peak in mid-September. The dynamics of groundwater temperature did not differ between dry and wet periods.
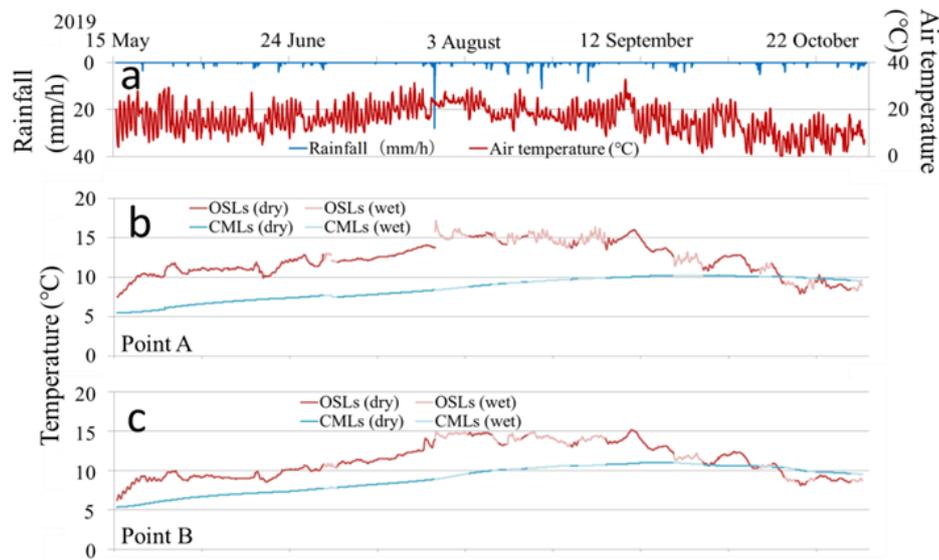
Figure 2.7. (a) Rainfall and air temperature and groundwater temperature at (b) Point A and (c) Point B.

2.3.4 Electrical Conductivity

Figure 2.8 shows the EC values of water samples. Rainwater EC (ranging from 29 to 34 µS cm^{-1}) was significantly lower than the values of other samples based on the two-tailed t-test ($p < 0.05$). Two water samples from the OSLs at Point A showed EC of 147 and 180 µS cm^{-1}. The EC of OSL groundwater at Point B ranged from 162 to 279 µS cm^{-1}; this overlapped the values of CML groundwater. Greater variation in groundwater EC in the CML was observed at Point B than at Point A (from 221 to 379 µS cm^{-1} and from 377 to 426 µS cm^{-1}, respectively). Overall, the OSL groundwater had significantly lower values than the CML groundwater ($p < 0.05$). Figure 2.8 also shows that the EC values of OSL groundwater tended to be higher during dry periods than during wet periods. No such tendency was recognized for CML groundwater.

Figure 2.8. EC of collected water samples.

2.4. Discussion

2.4.1 Sources of Groundwater

While semi-perennial to perennial groundwater zones were present in both OSLs and CMLs within the unchanneled hollow, their fluctuation characteristics differed. 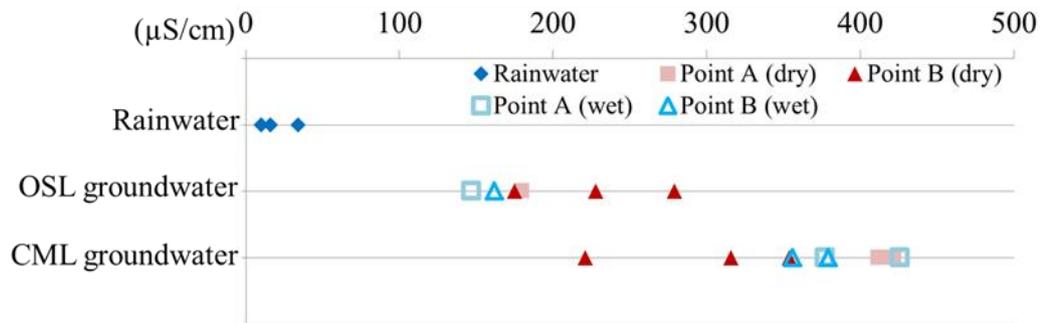The responses of CML groundwater to rainfall were small and gentle (Figure 2.6), presumably because of the hydraulic properties of CMLs, which have low permeability even under saturated conditions and contain small numbers of large pores (Figure 2.4). Additionally, ψ in the CMLs at Point T was consistently high, even during dry periods (Figure 2.5c), because the large number of small pores in the CMLs prevents drainage of water stored in the pores during dry periods. In contrast, the OSL groundwater level in the hollow and ψ at Point T showed rapid fluctuations in response to rainfall (Figures 2.5b and 2.6). These fluctuations during wet periods suggest rapid rainwater infiltration into and drainage from large pores, reflecting the hydraulic properties of OSLs (Figure 2.4). The process of groundwater generation in OSLs in the hollow during wet periods can be explained by the conventional conceptual model described in the Introduction section: rainwater vertically infiltrates into the highly permeable OSLs until it reaches the less permeable CMLs. Water then laterally flows along the CML surface, forming a groundwater zone above CMLs in the downslope area. The EC of OSL groundwater tended to be lower during wet periods than during dry periods (Figure 2.8), suggesting that the infiltration of rainwater with low EC (Figure 2.8) affected the OSL groundwater during wet periods.

Surprisingly, the groundwater zone remained present for a long period of time in the OSLs in the hollow during dry periods (Figure 2.6). The high permeability of the OSLs does not allow groundwater in the OSLs to be maintained consistently during dry periods. Previous studies indicated that groundwater zone in soil layers can maintain during dry periods due to hillslope topography such as depression or highly convergent topography [e.g., *Frisbee et al.*, 2007; *Fujimoto et al.*, 2008]. However, because the study catchment is small, with gentle hillslopes and thin OSLs, no large depression or convergent topography is available to provide water storage. The EC values of OSL groundwater collected from a depth of several tens of centimeters during dry periods were high (175 to 279 μS cm^{-1}; Figure 2.8). In Japan, reported EC values in soil layers at a few centimeters directly below leaf litter were high (> 300 μS cm^{-1}), especially in autumn when many broadleaf trees drop their leaves; these values decreased with infiltration into OSLs [*Sakuma et al.*, 1978; *Hayakawa et al.*, 2021]. *Sakuma and Sato* [1978] showed that the EC values of water collected from OSLs overlying pyroclastic fall deposits in Hokkaido, Japan, were in the range of approximately 30–70 μS cm^{-1}. *Miyata et al.* [2003] reported that, in OSLs at the depth of 20 cm in a granitic catchment in Gifu Prefecture, Japan, the mean EC value of stored water was 17.36 μS cm^{-1}. In a catchment consisting of volcanic rock and sedimentary rock in Akita, Japan, the EC of water stored at approximately 20–40-cm depth in an OSL was 51 μS cm^{-1} [*Hayakawa et al.*, 2021]. Compared with the EC values measured in these previous studies, the OSL groundwater EC values observed in the present study during dry periods were surprisingly high. This comparison suggests that the high values of OSL groundwater EC during dry periods are influenced by CML groundwater, which has high EC values (Figure 2.8); moreover, CML groundwater is an important source of groundwater present in the OSLs during dry periods.

One possible explanation for the contribution of CML groundwater to the groundwater zone in the OSLs involves runoff of CML groundwater into the OSLs via macropores or pipes within the CMLs. However, no such structures were observed in the study catchment. The results of temperature

29

observations (Figure 2.7) suggested that such runoff of CML groundwater into the OSLs was unlikely; the groundwater temperature in the CMLs showed moderate seasonal variations and minimal impact from diurnal air or rainwater temperature, whereas water in the OSLs was sensitive to air and rainwater temperature. If macropores or pipes had contributed to water flow, the CML groundwater temperature would be affected by air or rainwater temperature, such that it would show sensitive fluctuation during wet periods; during dry periods, the OSL groundwater temperature would show moderate fluctuations driven by runoff of CML groundwater. The EC values of CML groundwater showed no clear difference between dry and wet periods (Figure 2.8), which is consistent with these inferences.

These findings suggest that CML groundwater contributed to maintenance of the groundwater zone in OSLs in the hollow during dry periods through a mechanism that did not involve runoff of CML groundwater into the OSLs via macropores or pipes.

2.4.2 Water Flow Direction and Flux Analysis across OSL-CML Boundary

2.4.2.1 Flow Direction Analysis

To examine the contribution of CML groundwater to the OSL groundwater zone in the hollow during dry periods, we analyzed the water flow direction between OSLs and CMLs using the ψ values recorded at Point T. We focused on the flow direction between the 30 and 50 cm tensiometers, which were located immediately above and below the OSL– CML boundary (depth: 31 cm). Figure 2.9 shows the temporal variations in the difference in total head, H, defined as the sum of ψ and the elevation head, between 30 and 50 cm. We used the ground surface as the reference level for calculating elevation head. A positive value of H indicates upward flow from the CMLs into the OSLs, whereas a negative value indicates downward flow from the OSLs into the CMLs. Figure 9 demonstrates that the main flow direction during wet periods was downward.

Figure 2.10 shows the relationship between simultaneous ψ
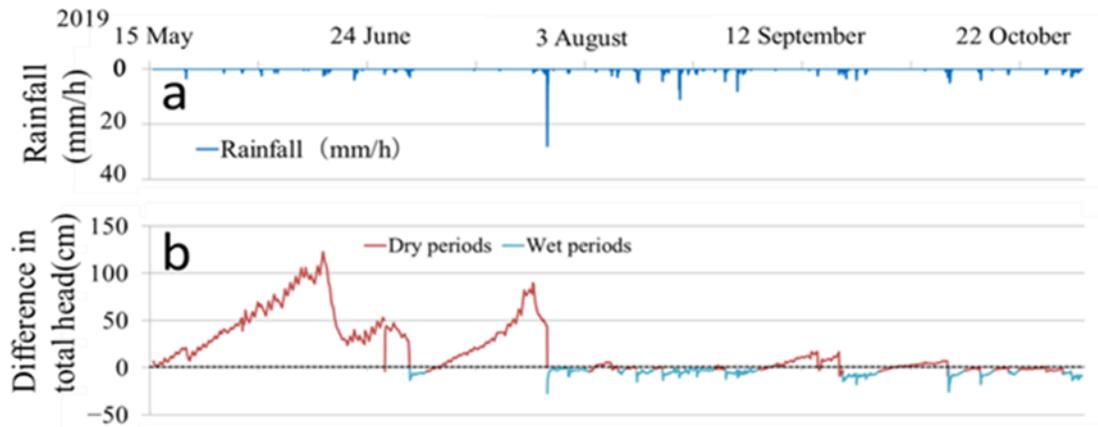
Figure 2.9. (a) Rainfall and (b) the difference in total head between the depths of 30 and 50 cm at Point T.
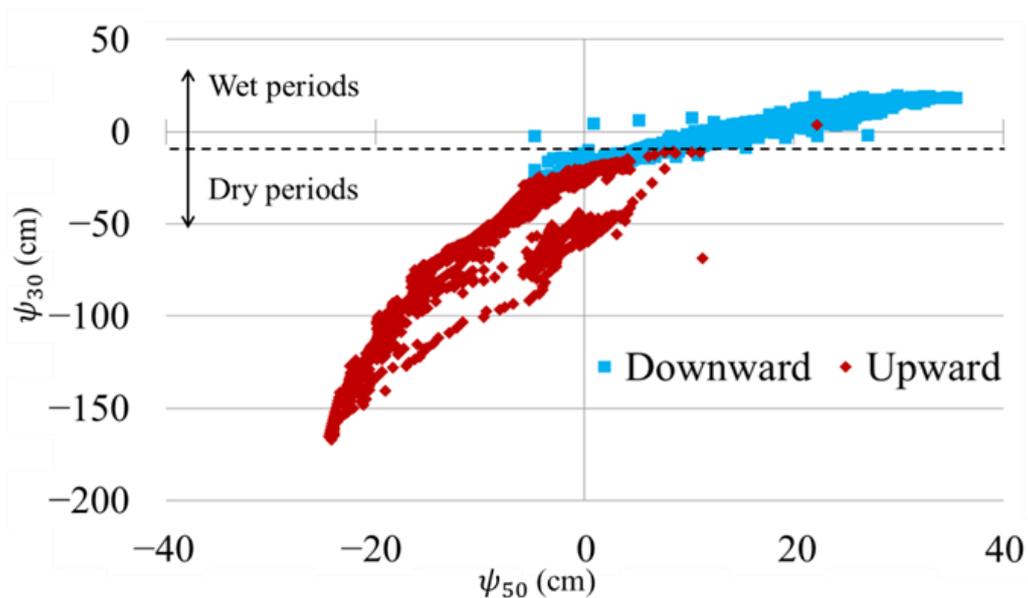
Figure 2.10. Relationship between simultaneous ψ_30 and ψ_50 observations. Dashed line represents ψ = −10 cm.

measurements from the 30 and 50 cm tensiometers (ψ_{30} and ψ_{50}, respectively); in this plot, two groups are distinguished according to the flow direction (upward or downward). During wet periods, downward flow was observed for 1104 h, whereas upward flow was observed for only 1 h. Thus, downward flow from the OSLs to the CMLs occurred mainly during wet periods including rainfall periods, indicating that a portion of the rainwater infiltrated into the CMLs and recharged the CML groundwater.

Conversely, after the cessation of rainfall, downward flow decreased and the flow direction switched from downward to upward; upward flow was observed during dry periods (Figure 2.9). Upward and downward flows were observed during a dry period at 2296 and 662 h, respectively (Figure 2.10). Thus, upward flow consistently occurred during dry periods. The OSLs, with high permeability under saturated conditions and a large number of large pores, became unsaturated and dried up during dry periods. The CMLs, with low permeability under saturated conditions and no large pores, remained nearly saturated even during dry periods. The frequent and long-term occurrence of upward flow can be attributed to these differences in hydraulic properties between OSLs and CMLs.

2.4.2.2 Upward Flux Analysis during Dry Periods

Next, we analyzed the vertical water flux across the OSL–CML boundary at Point T using H. According to Darcy's Law, water flux, q, at the boundary can be calculated as follows:

$$q = -K_{bo}(\psi_{31})\frac{H}{s} \qquad (2-4)$$

where K_{bo} is the hydraulic conductivity of the OSL–CML boundary, ψ_{31} is ψ at the boundary (at 31 cm depth), and s is the distance in the direction of flow (20 cm). We computed ψ_{31} as follows:

$$\psi_{31} = \frac{\psi_{50}s_{30} + \psi_{30}s_{50}}{s} \qquad (2-5)$$

where s_{30} and s_{50} are the vertical distances from the boundary to the 30 and 50 cm tensiometers (i.e., 1 and 19 cm), respectively. $K_{bo}(\psi_{31})$ was calculated using the hydraulic conductivity curve of the OSL–CML boundary shown in Figure 2.4b.

Figure 2.11b, c shows the temporal variations in upward and downward q, respectively. Note that downward q in Figure 2.11c is plotted on a logarithmic scale. The maximum upward flux during dry periods was 0.36 mm h^{-1}, observed on 1 July at 17:00, which was extremely small compared to the maximum downward flux during wet periods of 983 mm h^{-1}, which was observed on 9 October at 0:00. However, the upward flux during
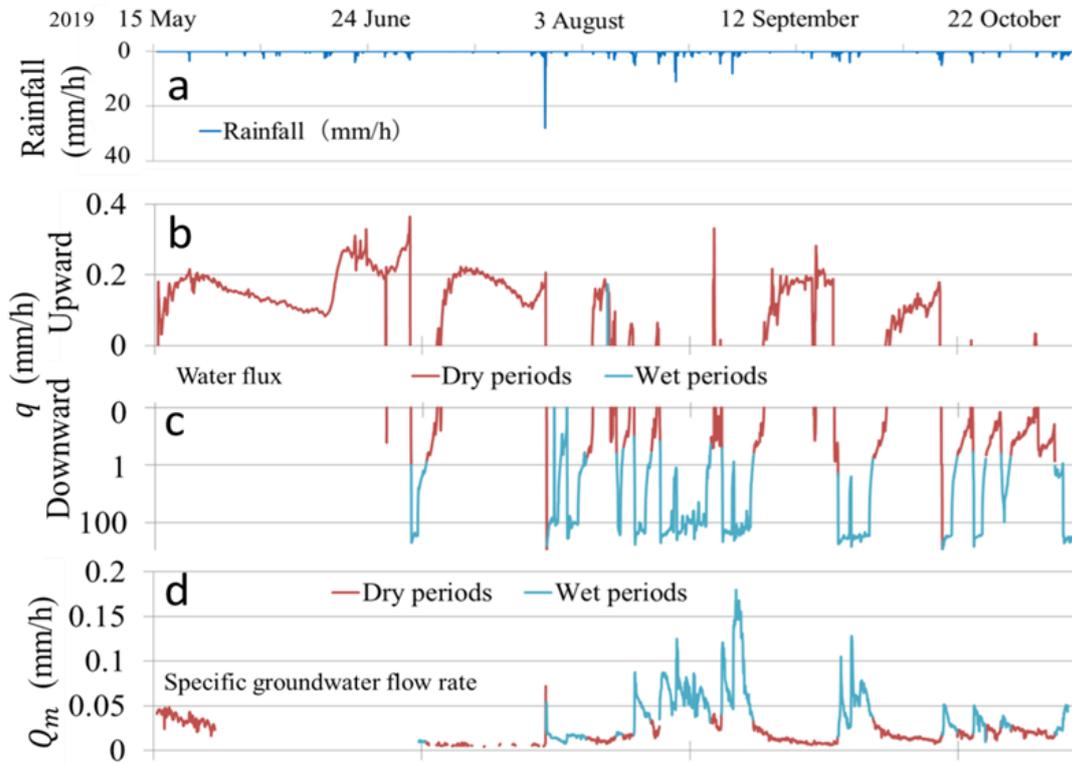
Figure 2.11. (a) Rainfall, (b) upward and (c) downward water flux at Point T, and (d) rate of specific groundwater flow at the midpoint between Points A and B.

dry periods averaged 0.16 mm h^{-1} and totaled 360 mm, equivalent to three-quarters of the total precipitation (468.5 mm). This similarity suggests that the accumulation of water that moved upward from the CMLs into the OSLs in areas where the OSLs were dry ($\psi < -10$ cm; Figure 2.10) contributed to the maintenance of the groundwater zone in the OSLs along the hollow (including Points A and B) during dry periods.

　　To determine whether the calculated upward q can explain the observed groundwater level in the OSLs in the hollow during dry periods, we conducted a crude calculation of the specific groundwater flow rate in the OSLs at the midpoint between Points A and B. The rate of specific groundwater flow in the OSLs at the midway point, Q_m, can be approximated as follows:

$$Q_m = \frac{q_m A_C}{A_m} \tag{2-6}$$

33

where q_m is groundwater flux at the midway point, A_C is the cross-sectional area of the groundwater zone at the midway point calculated assuming a triangular area, and A_m is the catchment area at the midway point (0.056 ha). By applying Darcy's law to saturated groundwater flow in the OSLs between Points A and B, q_m can be approximated as follows:

$$q_m = K_{s\_OSLs} \frac{H_{AB}}{S_s} \qquad (2-7)$$

where K_{s_OSLs} is the mean saturated hydraulic conductivity of OSLs (3.38×10^{-2} cm s^{-1}), H_{AB} is the difference in elevation of the groundwater table in the OSLs between Points A and B, and S_s is the slope length from Points A to B (19.0 m).

Figure 2.11d shows the temporal variations of Q_m (data are missing from 26 May at 13:00 though 3 July at 10:00 due to the lack of the groundwater level data at Point A). The maximum Q_m was 0.18 mm h^{-1}, observed on 31 August at 14:00 during a wet period. During dry periods, Q_m reached its maximum (0.072 mm h^{-1}) on 27 July at 3:00 and averaged 0.018 mm h^{-1}. The findings in Figure 2.11b,d indicate that upward q was larger than Q_m for nearly the entire observation period when upward flux was generated. The sums of upward q and Q_m during dry periods with upward flux from 1 July to 31 October were 172.5 and 9.76 mm, respectively. *Kondo et al.* [1992] estimated that mean transpiration in July through October in this region (including the study catchment) was 172 mm. Comparison of these values suggests that most of the upward q is consumed by transpiration (some water that flowed only through the OSLs was presumably also consumed by transpiration), whereas the remaining q could generate the observed saturated groundwater flow in the OSL in the hollow. Thus, water supplied from the CMLs to OSLs as upward flux accumulated and contributed to the groundwater zone in the OSLs in the hollow during dry periods.

2.4.3 Conceptual Model of Hydrological Processes in a Headwater Catchment with Thick CMLs Underlain by Impermeable Bedrock

Based on the discussion above, Figure 2.12 illustrates the

hydrological processes in the study catchment. During wet periods including rainfall periods (Figure 2.12a), rainwater vertically infiltrates into the highly permeable OSLs until it reaches the less permeable CMLs; it then becomes perched groundwater above the OSL–CML boundary. The perched groundwater flows downslope along the OSL–CML boundary as saturated
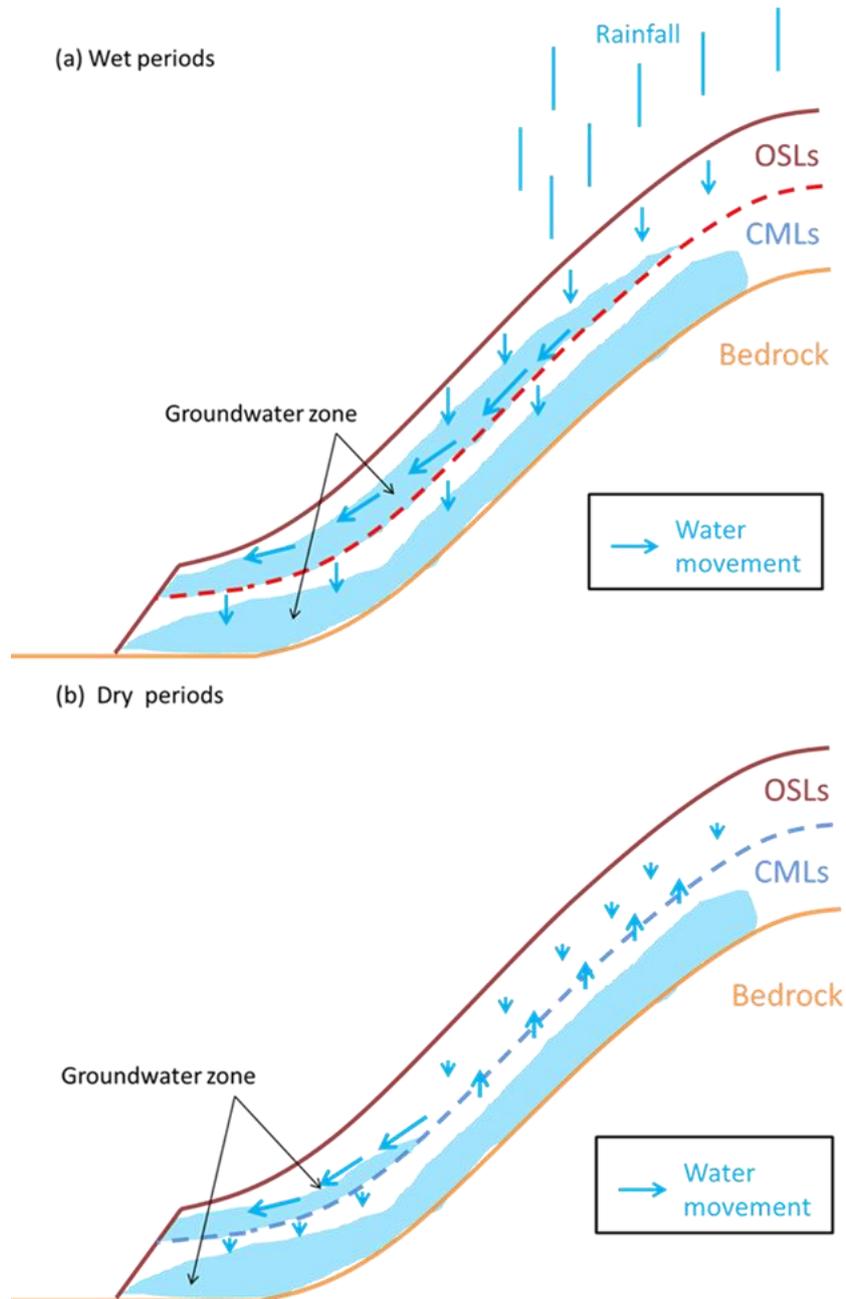

Figure 2.12. Hydrological processes in the study catchment during (a) wet periods and (b) dry periods.

lateral flow, thereby expanding or increasing the depth of the groundwater zone in the OSLs in the hollow. In areas where the OSLs are wet ($\psi > -10$ cm), a portion of this water infiltrates into the CMLs as downward flux (Figure 2.10) and slowly recharges the CML groundwater.

In contrast, during dry periods (Figure 2.12b), the contribution of rainwater to the OSL groundwater zone decreases and upward flow from the CMLs occurs mainly in areas where the OSLs are dry ($\psi < -10$ cm) (Figure 2.10). This water then flows downslope along the OSL–CML boundary as unsaturated or saturated lateral flow, forming the groundwater zone in the OSLs in the hollow of the downslope area.

2.4.4 Importance of Water Supply from CMLs to OSLs as Upward Flux during Dry Periods

Groundwater zone within the soil layers of a headwater catchment has been recognized as one of the most important factors controlling volumetric [*Katsuyama et al.*, 2002; *Detty et al.*, 2010; *Martínez-Carreras et al.*, 2016] and chemical [*Bishop et al.*, 2004; *Gannon et al.*, 2015] changes in streamflow and in the induction of shallow landslides [*van Ash et al.*, 2005; *Sidle et al.*, 2016]. Therefore, upward flux that contributes to the formation of groundwater zone in soil layers has long been focused. Upward flux in a headwater catchment has been reported previously [*McGlynn et al.*, 1999; *Harria et al.*, 2006], and two mechanisms of upward flux generation have been proposed. One mechanism is unsaturated upward flux resulting from the balance of the matrix potential of soil layers (i.e., unsaturated matrix flow), as observed in this study, which occurs as soil layers become dry and the groundwater level decreases [*Tsujimura*, 1992; *Tsurita et al,*, 2009; *Gannon et al.* 2016]. The other mechanism is saturated upward flux, which occurs in association with the local exfiltration of bedrock groundwater into soil layers through fissures and cracks in the bedrock [*Montgomery et al.*, 1997; *Haga et al.*, 2005; *Masaoka et al.*, 2016]. In catchments underlain by permeable bedrock specifically, this local exfiltration of bedrock groundwater are recognized as important contributor to groundwater zone in soil layers during dry periods [*Uchida et al.*, 2003;

Katsura et al., 2008] and stream discharge and quality during baseflow periods [*Uhlenbrook et al.*, 2002; *Gabrielli et al.*, 2012; *Zhao et al.*, 2019]. Although saturated upward flux is often considered as an important water supply process for soil layers, unsaturated upward flux caused by matrix flow has attracted minimal attention because of the small fluxes involved relative to saturated upward fluxes. *Frisbee et al.* [2007] reported large-volume groundwater storage in a depression located near the base of the slope in a 0.60 ha catchment during periods of low water table position. In this case, the soil thickness of the depression was as much as approximately 4 m. From the results of this study, unsaturated upward flux may be an important process that sustains wet soil layers during dry periods in still smaller, impermeable bedrock headwater catchments with thinner soil layers.

At Point T in the study catchment, upward flux from the CMLs to the OSLs generally occurred as unsaturated flow during dry periods. Although the maximum upward flux was small (0.36 mm h^{-1}), the total upward flux over the entire observation period was large (360 mm). This continuous upward flux contributed to the maintenance of the groundwater zone in the OSLs in the hollow of the downslope area during dry periods, which presumably caused subsequent volumetric and chemical changes in streamflow. Moreover, in a serpentinite catchment in Hokkaido, Japan, *Aipassa* [46] described the occurrence of surface slides (a type of slope failure) with the slip surface located at the OSL–CML boundary; such slides were reported to occur on steep slopes when rainfall is sufficiently heavy to saturate the slip surface. Although no traces of such slides were found in the study catchment, presumably because of the low gradient, continuous unsaturated upward flux can influence such slides by raising the groundwater level or expanding the groundwater zone in the OSLs of hollows during rainfall periods through the generation of a small groundwater zone before the rainfall, which reduces the stability of the OSLs. Thus, the present findings emphasize the important role of water supply from CMLs to OSLs during dry periods in the formation of a groundwater zone in OSLs in hollows, in addition to its effects on

streamflow and shallow landslides.

2.5. Conclusions

Detailed hydrological, hydrochemical, and thermal observations in a forested serpentinite headwater catchment containing mineral soil layers composed of thick clayey materials produced by weathering of impermeable bedrock (i.e., CMLs), along with hydraulic property measurements in the laboratory, were conducted to elucidate the effects of CMLs on hydrological processes in the study catchment. The groundwater temperature and chemistry suggested that runoff of the CML groundwater into the OSLs via macropores or pipes is unlikely. Instead, water flux analysis across the OSL–CML boundary revealed that unsaturated upward flow from the CMLs into OSLs occurs in areas where the OSLs are dry (pressure head < −10 cm). Accumulation of this upward flux can explain the groundwater zone observed in the OSLs of the hollow during dry periods. We conclude that water infiltrates from the OSLs into CMLs during wet periods (including rainfall periods) and then is supplied into the OSLs as upward flux during dry periods; this upward flux contributes to the generation of a semi-perennial to perennial groundwater zone in the OSLs in the hollow.

This study has clarified the effects of clay layers on hydrological processes, specifically that CMLs act not only as impeding layers during wet periods but also as water supplier by unsaturated upward flux to OSLs during dry periods. Land users and management organizations of catchments underlain by thick CMLs should pay attention to volumetric and chemical changes in streamflow and the surface slides that could be caused by the semi-perennial to perennial groundwater zone formed by upward flux. In future research, detailed observations of other serpentinite catchments and catchments underlain by other bedrock types with thick CMLs (e.g., mudstone and slate catchments) are needed to determine the generalizability of the present findings.

References

Aipassa, M. I. (1991), Landslide debris movement and its effects on slope and river channel in mountainous watershed. *Res. Bull. Coll. Exp. For.*, 48, 375–418.

Bishop, K., J. Seibert, S. Köhler, amd H. Laudon (2004), Resolving the double paradox of rapidly mobilized old water with highly variable responses in runoff chemistry. *Hydrol. Process.* 18, 185–189.

Detty, J. M, and K. J. McGuire (2010), Threshold changes in storm runoff generation at a till-mantled headwater catchment. *Water Resour. Res.*, *46*, W07525.

Frisbee, M. D., C. J. Allan, M. J. Thomasson, and R. Mackereth (2007), Hillslope hydrology and wetland response of two small zero-order boreal catchments on the Precambrian Shield. *Hydrol. Process.*, 21, 2979–2997.

Fujimoto, M., N. Ohte, and M. Tani (2008), Effects of hillslope topography on hydrological responses in a weathered granite mountain, Japan: Comparison of the runoff response between the valley-head and the side slope. *Hydrol. Process.*, 22, 2581–2594.

Gabbrielli, R., T. Pandolfini, O, Vergnano, and M. R. Palandri (1990), Comparison of two serpentine species with different nickel tolerance strategies. *Plant Soil*, 122, 271–277.

Gabrielli, C. P., J. J. McDonnell, and W. T. Jarvis (2012), The role of bedrock groundwater in rainfall-runoff response at hillslope and catchment scales. *J. Hydrol.*, *450–451*, 117–133.

Gannon, J. P., S. W. Bailey, K. J. Mcguire, and J. B. Shanley (2015), Flushing of distal hillslopes as an alternative source of stream dissolved organic carbon in a headwater catchment. *Water Resour. Res.*, 51, 8114–8128.

Gannon, J. P., K. J. McGuire, S. W. Bailey, R. R. Bourgault, and D. S. Ross (2016), Lateral water flux in the unsaturated zone: A mechanism for the formation of spatial soil heterogeneity in a headwater catchment. *Hydrol. Process.* 31, 3568–3579.

Haga, H., Y. Matsumoto, J. Matsutani, M. Fujita, K. Nishida, and Y.

Sakamoto (2005), Flow paths, rainfall properties, and antecedent soil moisture controlling lags to peak discharge in a granitic unchanneled catchment. *Water Resour. Res.*, *41*, W12410. https://doi.org/10.1029/2005WR004236.

Harria, A. H., and P. Shand (2006), Near-stream soil water-groundwater coupling in the headwaters of the Afon Hafren, Wales: Implications for surface water quality. *J. Hydrol.*, 331, 567–579.

Hayakawa, A., H. Ota, R. Asano, H. Murano, Y. Ishikawa, and T. Takahashi (2021), Sulfur-based denitrification in streambank subsoils in a headwater catchment underlain by marine sedimentary rock in Akita, Japan. *Front. Environ. Sci. 9*, 664488.

Hiura, T., N. Uejima, A. Okuda, H. Hojo, T. Ishida, and S. Okuyama (1998), Crowding effects on diameter growth for *Abies sachalinensis*, *Quercus crispula* and *Acer mono* trees in a northern mixed forest, Nakagawa Experimental Forest. *Res. Bull. Hokkaido Univ. For.*, *55*, 255–261. (In Japanese with English Summary)

Hiura, T., and K. Fujiwara (1999), Density-dependence and co-existence of conifer and broad-leaved trees in a Japanese northern mixed forest. *J. Veg. Sci.*, 10, 843–850.

Hiura, T., G. Sato, and I. Hayashi (2019), Long-term forest dynamics in response to climate change in northern mixed forests in Japan: A 38-year individual-based approach. *For. Ecol. Manag.*, *449*, 117469.

Ishii, Y. Y. Kodama, R. Nakamura, and N. Ishikawa (2004), Water balance of a snowy watershed in Hokkaido, Japan. In *Northern Research Basins Water Balance (Proceedings of a Workshop Held at Victoria, Canada, March 2004);* IAHS Publication: Oxfordshire, UK, Volume 290, pp. 13–27.

Katsura, S., K. Kosugi, T. Mizutani, S. Okumura, and T. Mizuyama (2008), Effects of bedrock groundwater on spatial and temporal variations in soil mantle groundwater in a steep granitic headwater catchment. *Water Resour. Res.*, *44*, W09430. https://doi.org/10.1029/2007WR006610.

Katsuyama, M., and N. Ohte (2002), Determining the sources of stormflow

from the fluorescence properties of dissolved organic carbon in a forested headwater catchment. *J. Hydrol.*, 268, 192–202.

Kobayashi, M., P. H. Templer, A. Katayama, O. Seki, and K. Takagi (2022), Early snowmelt by an extreme warming event affects understory more than overstory trees in Japanese temperate forest. *Ecosphere*, *13*, e4182.

Kondo, J., M. Nakazono, T. Watanabe, and T. Kuwagata (1992),. Hydrological climate in Japan (3) Evapotranspiration from forest. J. Jpn. Soc. Hydrol. Water Resour., 5, 8–18.

Kosugi, K. (1996), Lognormal distribution model for unsaturated soil hydraulic properties. *Water Resour. Res.,* 32, 2697–2703.

Martínez-Carreras, N., C. Hissler, L. Gourdol, J. Klaus, and J. Juilleret (2016), Storage controls on the generation of double peak hydrographs in a forested headwater catchment. *J. Hydrol.* **2016**, 543, 255–269.

Masaoka, N, K. Kosugi, Y. Yamakawa, and D. Tsutsumi (2016), Processes of bedrock groundwater seepage and their effects on soil water fluxes in a foot slope area. *J. Hydrol.***,** 535, 160–172.

McGlynn, B. L. J. J. McDonnell, J. B. Shanley, and C. Kendall (1999), Riparian zone flowpath dynamics during snowmelt in a small headwater catchment. *J. Hydrol.*, 222, 75–92.

McGlynn, B. L., J. J. McDonnell, and D. D. Brammer (2002), A review of the evolving perceptual model of hillslope flowpaths at the Maimai catchments, New Zealand. *J. Hydrol.*, 257, 1–26.

Miyata, S., T. Uchida, Y. Asano, H. Ando, and T. Mizuyama (2003), Effects of bedrock groundwater seepage on runoff generation at a granitic first order stream. *J. Jpn. Soc. Eros. Control. Eng.*, 56, 13–19. (In Japanese with English Abstract)

Montgomery, D. R., W. E. Dietrich, and R. Torres (1997), Anderson, S.P.; Heffner, J.T.; Loague, K. Hydrologic response of a steep, unchanneled valley to natural and applied rainfall. *Water Resour. Res.*, 33, 91–109.

Mosley, M.P. (1979), Streamflow generation in a forested watershed, New

Zealand. *Water Resour. Res.*, 15, 795–806.

Mosley, M. P. (1982), Subsurface flow velocities through selected forest soils South Island, New Zealand. *J. Hydrol*, 55, 65–92.

Mualem, Y. (1976), A new model for predicting the hydraulic conductivity of unsaturated porous media. *Water Resour. Res*, 12, 513–522.

Nakata, N., and S. Kojima (1987), Effects of serpentine substrate on vegetation and soil development with special reference to Picea Glehnii forest in Teshio District, Hokkaido, Japan. For. Ecol. Manag. 1987, 20, 265–290.

Newman, B. D., A. R. Campbell, and B. P. Wilcox (1998), Lateral subsurface flow pathways in a semiarid ponderosa pine hillslope. *Water Resour. Res.*, 34, 3485–3496.

Nomura, M., K. Yazaki, K. Sasa, F. Satoh, D. Ashiya, and S. Sugata (2001), Comparison of snowmelt runoff in Tertiary with in serpentine basin (in Japanese). *Research bulletin of the Hokkaido University Forests*, 58(2), 1–9.

Pearce, A. J., M. K. Stewart, and M. G. Sklash (1986), Storm runoff generation in humid headwater catchments. 1. Where does the water come from? Water Resour. Res. 1986, 22, 1263–1272.

Sakuma, T., and F. Satoh (1978), Dynamics of inorganic elements in soils under deciduous forest (Part 1). Res. Bull. Coll. Exp. For., 44, 537–552. (In Japanese with English Summary)

Satoh, F., K. Masumoto, and H. Ichikawa (1991), Effects of forests on streamwater runoff and water quality from serpentinite mountain (in Japanese*). *Annual test report of Hokkaido University Forests*, 9, 16–17.

Satoh, F., F. Mochida, K. Sasa, H. Ichikawa, and D. Ashiya (1994), Forest and geological effects on runoff during rainfall (in Japanese*). *Annual test report of Hokkaido University Forests*, 12, 41–42.

Sayama, T., R. Araki, K. Yamamoto, and Apip (2021), Characteristics of soil and hillslope responses in humid tropical forests in Sumatra, Indonesia. *Hydrological Research Letters*, 15(2), 23–30.

Suzuki, T. (2006), Formative processes of specific features of serpentinite

mountains. Trans. Jpn. Geomorphol. Union, 27, 417–460.

Sidle, R. C., T. Tsuboyama, S. Noguchi, I. Hosoda, M. Fujieda, and T. Shimizu (2000), Stormflow generation in steep forested headwaters: A linked hydrogeomorphic paradigm. Hydrol. Process., 14, 369–385.

Sidle, R. C., and T. A. Bogaard (2016), Dynamic earth system and ecological controls of rainfall-initiated landslides. Earth-Sci. Rev., 159, 275–291.

Soulsby, C. (1992), Hydrological controls on acid runoff generation in an afforested headwater catchment at Llyn Brianne, Mid-Wales. J. Hydrol., 138, 431–448

Tani, M. (1997), Runoff generation processes estimated from hydrological observations on a steep forested hillslope with a thin soil layer. J. Hydrol., 200, 84–109.

Tsujimura, M. (1993), Behavior of subsurface water in a steep forested slope covered with a thick soil layer. J. Jpn. Assoc. Hydrol. Sci., 23, 3–18. (In Japanese with English Abstract)

Tsurita, T., S. Yoshinaga, and T. Abe (2009), Estimation of vertical water flux through forest subsoil using Buckingham-Darcy Equation. J. Jpn. For. Soc. 91, 151–158. (In Japanese with English Abstract)

Uchida, T., Y. Asano, N. Ohte, and T. Mizuyama (2003), Analysis of flowpath dynamics in a steep unchannelled hollow in the Tanakami Mountains of Japan. Hydrol. Process., 17, 417–430.

Uhlenbrook, S., M. Frey, C. Leibundgut, and P. Maloszewski (2002), Hydrograph separations in a mesoscale mountainous basin at event and seasonal timescales. Water Resour. Res., 38, 1096. https://doi.org/10.1029/2001WR000938.

van Asch, T., T. Buma, and L. VanBreek (2005), A view on some hydrological triggering systems in landslides. Geomorphology 2005, 30, 25–32.

Wilson, G.V., P. M. Jardine, R. J. Luxmoore, L. W. Zelazny, D. E. Todd, and D. A. Lietzke (1991), Hydrogeochemical processes controlling subsurface transport from an upper subcatchment of walker branch watershed during storm events. 2. Solute transport pro-cesses. J.

Hydrol., 123, 317–336.

Zhao, S., H. Hu, C. J. Harman, F. Tian, Q. Tie, Y. Liu, and Z. Peng (2019), Understanding of storm runoff generation in a weathered, fractured granitoid headwater catchment in northern China. Water, 11, 123. https://doi.org/10.3390/w11010123.

* The title or source is a tentative translation by the authors from the original.

Chapter 3

Effects of Clay Layers on Hydrological Processes in a Headwater Catchment Underlain by Permeable Bedrock

3.1. Introduction

The effects of subsurface flow through bedrock on hydrological processes in headwater catchments underlain by permeable bedrock have been the focus of several studies [e.g., *Montgomery et al.*, 1997; *Kosugi et al.*, 2006, 2008; *Graham et al.*, 2010; *Masaoka et al.*, 2016; *Abe et al.*, 2020; *Iwasaki et al.*, 2021]. *Kosugi et al.* [2006] demonstrated a large potential for bedrock infiltration and exfiltration based on a water balance calculation and hydraulic observations in granitic catchments. *Abe et al.* [2020] calculated the rate of rainwater infiltration into bedrock and the exfiltration of bedrock groundwater in two granodiorite catchments using the hydrological cycle model. Their results suggested that the rate of deep infiltration into bedrock influenced both the runoff rate and base flow generation.

In a study of catchments underlain by permeable bedrock with clay layers, *McGuire et al.* [2010] found deep infiltration into bedrock and a contribution of subsurface flow through bedrock to streamflow in a catchment underlain by andesitic tuffs and coarse breccias, which form clay layers as a result of weathering. *Brönnimann et al.* [2013] measured the fluctuation of the bedrock groundwater level in a catchment underlain by conglomerate-sandstone beds and weathered marlstone overlain by clayey soil layers. They proposed that clayey layers inhibit bedrock groundwater exfiltration, increase the water pressure at the soil-bedrock interface, and reduce the stability of the soil layers, thus triggering shallow landslides. Those studies therefore demonstrated that clay layers influence hydrological processes in headwater catchments underlain by permeable bedrock and have the potential to cause landslides. However, because the rate of deep infiltration into bedrock through clay layers is assumed to be small, due to the low permeability of clay layers, the hydrological processes

45

in headwater catchments, where clay layers are formed, have received scant attention. In addition, most studies that have suggested water movement between clay layers and bedrock have been based on chemical analyses and hydrological separation, not on detailed observations. The lack of information on quantitative and qualitative changes in water stored within clay layers and bedrock has hindered the understanding of the effects of clay layers on hydrological processes. In this chapter, the effect of clay layers on hydrological processes is discussed based on the knowledge gained in hydrological, hydrochemical, and hydrothermal observations.

3.2. Methods

3.2.1 Site Description

The experiments described in this chapter were conducted in the Kanai catchment, a headwater catchment of the Moshiri Experimental Watershed in the Uryu Experimental Forest (Figure 3.1).
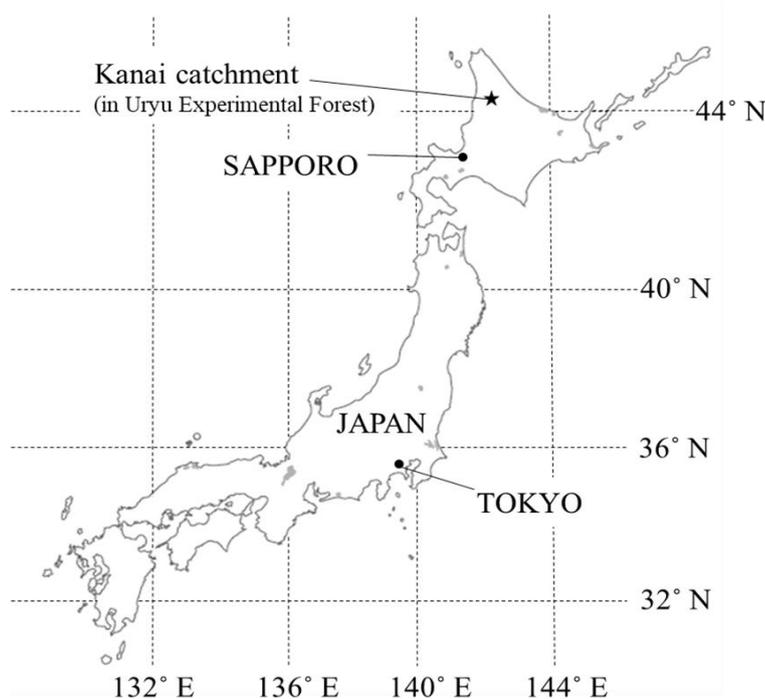

Figure 3.1. Location of the study site.

3.2.1.1 The Uryu Experimental Forest and the Moshiri Experimental Watershed

The Uryu Experimental Forest is a natural, cool-temperate, mixed broadleaved and conifer forest managed by Hokkaido University. The dominant tree species are *Abies sachalinensis*, *Quercus crispula*, *Tilla japonica*, *Betula ermanii*, and *Aver pictum*, and the dominant understory is dwarf bamboo (*Sasa senanensis* and *S. kurilensis*) [*Fukuzawa et al.*, 2020]. The annual mean temperature and precipitation from 1956 to 2014 were 3.1℃ and 1390 mm, respectively. Approximately 50% of the precipitation falls as snow, which covers the ground from November to May [*Akitsu et al.*, 2020]. Weather observations have been ongoing since 1993.

The Moshiri Experimental Watershed is a 120 ha forested watershed located at 44°22'N, 142°17'E, with an elevation ranging from 290 m to 545 m. The entire watershed is underlain by tuff breccia and clay layers produced by bedrock weathering. A topographical map of the Moshiri Experimental Watershed is shown in Figure 3.2a. Detailed hydrological observations together with determinations of the water balance of the watershed were conducted from 1988 to 1998 (Figure 3.3) [*Ishii et al.*, 2004]. The dominant trees species are *Picea jezoensis*, *Abies sachalinensis*,
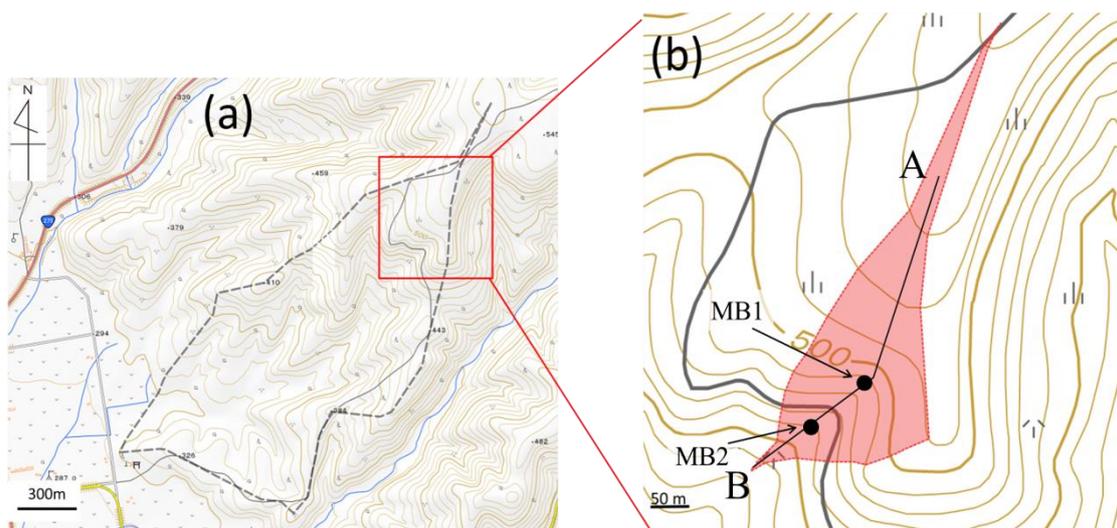
Figure 3.2. Topography of (a) the Moshiri Experimental Watershed and (b) Kanai catchment. The solid line between A and B in (b) indicates an unchanneled hollow.

Quercus cirspula, and *Betula ermanii*, and the understory is *S. kurilensis* [*Yamazaki et al.*, 2007]. *Ishii and Kobayashi* [1995] described the soil layer structure in the Moshiri Experimental Watershed as organic at a depth of 10–20 cm below the ground surface, with clay layers formed by bedrock weathering at a thickness of 3–6 m below the soil layers. Other parameters identified in that study were a saturated hydraulic conductivity (Ks) at depths of 70 and 170 cm of 6.48×10^{-6} and 3.72×10^{-6} cm s^{-1}, respectively. Their study also included water retention curves (Figure 3.4) using soil samples obtained from a slope in the Moshiri Experimental Watershed.

Figure 3.3. Mean annual water balance from 1988 to 1998 [*Ishii et al.*, 2004]. P, Q, E, and dS are precipitation, discharge, evapotranspiration, and storage change, respectively.

Figure 3.4. Water retention curves at depths of 70 cm and 170 cm below ground surface, measured by *Ishii and Kobayashi* (1995).

48

3.2.1.2 Kanai Catchment

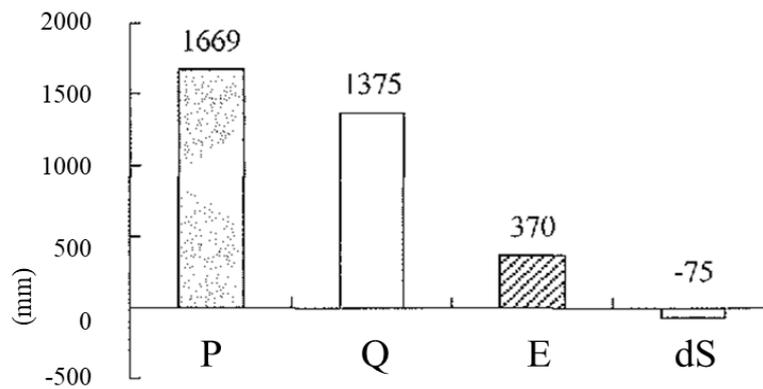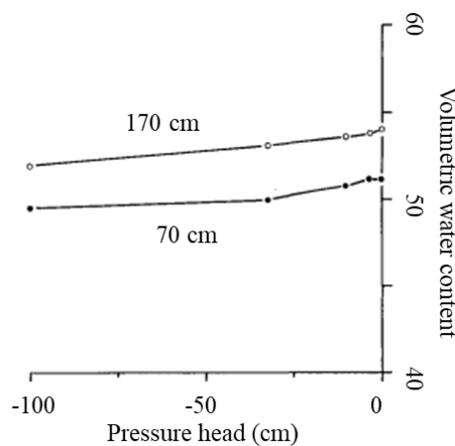The Kanai catchment is a 3.3 ha forested headwater and zero-order catchment of the Moshiri Experimental Watershed, with an elevation ranging from 440 m to 545 m (Figure 3.2b). The gradient of Kanai catchment becomes gradual at around 510 m elevation. The average gradient between 440 m and 510 m elevation is 18° and that from 510 m elevation to the top is 6°. The vegetation, geology, and meteorology are almost the same as in the Moshiri Experimental Watershed. Soil thicknesses to bedrock, confirmed by two boreholes (MB1 and MB2, described below), are 4.0 m and 5.1 m, respectively, and thus generally consistent with those of the Moshiri Experimental Watershed reported by *Ishii and Kobayashi* [1995]. A spring outflow point is present at the base of the catchment, at 437 m elevation. This spring flows on clay layers and finally, at an elevation of 423 m, on bedrock. A ~4 m deep trench was excavated at 460 m elevation in 2020. Based on the soil profile of the trench, the boundaries between the organic soil layers and clay layers are not distinct when viewed with the naked eye but the soil layers form clay layers at a depth of least 150 cm below the surface. Soil layers in Kanai catchment can be divided into organic soil layers (OSLs), which extend from the ground surface to a depth of 150 cm below the surface, and clay mineral layers (CMLs), beginning at a depth of 150 cm. The deeper the CML, the greater its content of gravels, which may be as large as 30 cm in diameter. The CMLs in Kanai catchment are highly compacted and hardened, thus far preventing the trench's collapse.

From late September to mid October 2020, two boreholes, MB1 and MB2, were drilled in the Kanai catchment (Figure 3.2b), with total depths of 35 and 25 m, respectively, and each with a diameter of 6.6 cm. Undisturbed bedrock cores 5.0 cm in diameter were obtained by drilling through the total depth of the boreholes (Figure 3.5) and were classified according to weathering class as D, CL, and CM, defined as highly, moderately, and weakly weathered bedrock, respectively [*Yoshinaka et al.*, 1989]. Table 3.1 summarizes the characteristic of each weathering class. Figure 3.6 shows the weathering profile of the MB1 and MB2 cores. The
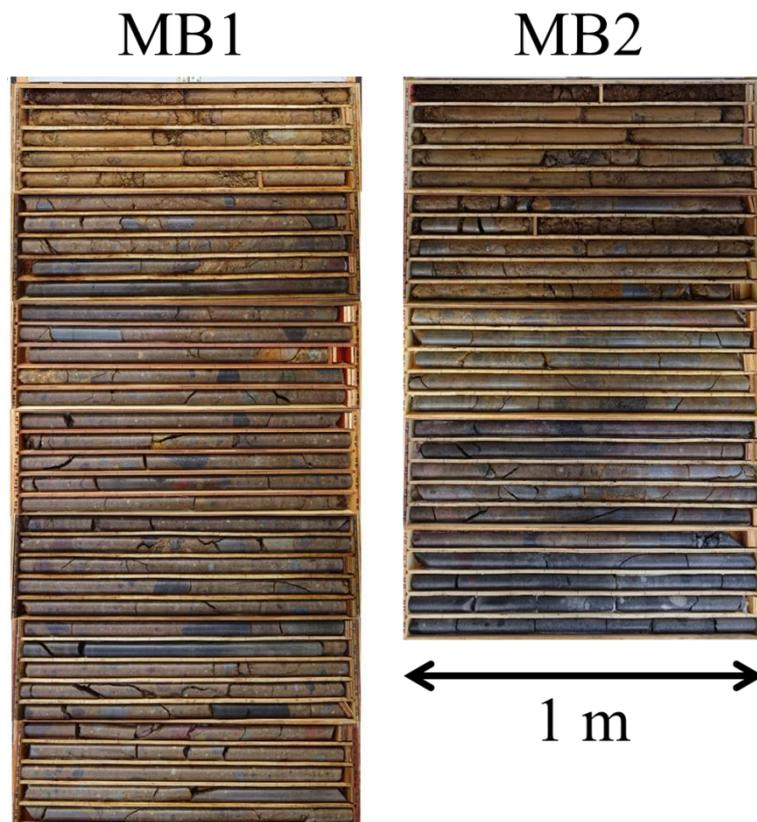
Figure 3.5. Photographs of the core samples obtained from boreholes MB1 and MB2 at Kanai catchment.

Table 3.1. Characteristics of each weathering class [*Yoshinaka et al.*, 1989].

Weathering class	Degree of weathering
A	• Significantly fresh • Rock nodules are rarely distributed • Very hard
B	• Fresh • Distribution of rock nodules is sparse • Hard
C_H	• Generally fresh and hard • Rock nodules are fairly well distributed • Nodular surface are often discolored and contaminated by weathering, but are generally adhere well
C_M	• Generally somewhat weathering • Rock nodules are open, often interspersed with clay or weathered material
C_L	• Significantly weathering • Rock nodules are open, with significant interbedding of clay and weathered material
D	• Significantly weathering with sandy and clayey potions • Distribution of rock nodules rather indistinct
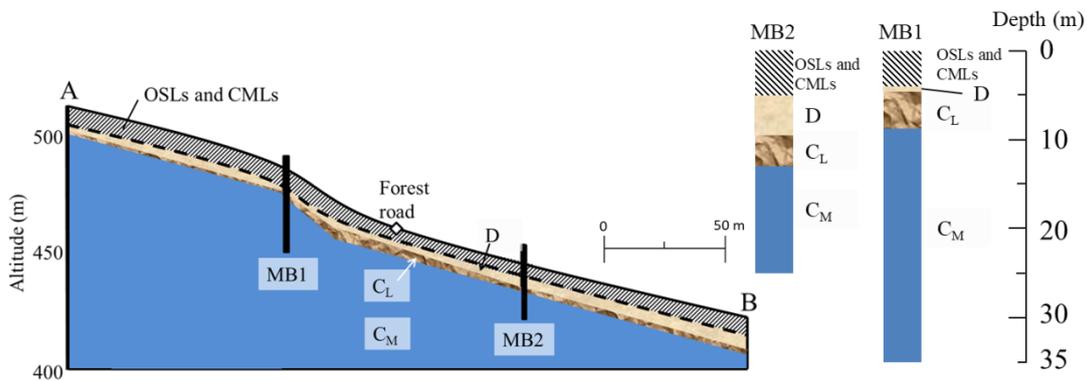
Figure 3.6. Weathering degree profile at boreholes MB1 and MB2 and estimated for Kanai catchment. The catchment drawing range is corresponds to the unchanneled hollow shown in Figure 3.2b.

matrix of the highly weathered bedrock had turned partially to sediment and to clay, thus obscuring any cracks, but it remained brittle because it did not become compacted like the clay layers situated above. At MB2, highly weathered bedrock was located 5.1 m below the surface and its thickness was 4.5 m, whereas at MB1, located upslope in the Kanai catchment, the highly weathered bedrock was shallower (4.0 m below the surface) and thinner (0.7 m thickness). The moderately weathered bedrock was hard, with well-defined cracks due to the limited, non-clayed sedimentation of the surrounding matrix. The thickness of the matrix at boreholes MB1 and MB2 did not significantly differ (4.2 and 3.4 m, respectively). The weakly weathered bedrock was located just beneath the moderately weathered bedrock and extended to the lowest depth of the boreholes (35 and 25 m, respectively). It was generally hard with little sedimentation.

Suzuki [2022] conducted water retention tests and measured the K_s values of the soil layers and bedrock matrix in Kanai catchment using core samples collected from the trench and undisturbed bedrock cores. The water retention and hydraulic conductivity curves are shown in Figure 3.7, and the K_s values of the soil layers and bedrock matrix in Table 3.2. The in situ K_s values of moderately and weakly weathered bedrock from the boreholes are also presented in Table 3.2. *Suzuki* [2022] showed that the hydraulic properties of OSLs and CMLs greatly differ. The relatively high K_s value

(9.79 $\times 10^{-3}$ cm s^{-1}) of the OSLs indicates a rapid θ decrease in the water retention curve as ψ decreases to -100 cm. For the CMLs, the saturated hydraulic conductivities and water retention curves result in a low K_s value (7.81 $\times$ 10^{-6} cm s^{-1}) and a flat water-retention curve as ψ decreased to -100 cm. Thus, while OSLs have a high permeability and pore sizes ranging from very large to small, CMLs have a low permeability and few large pores.
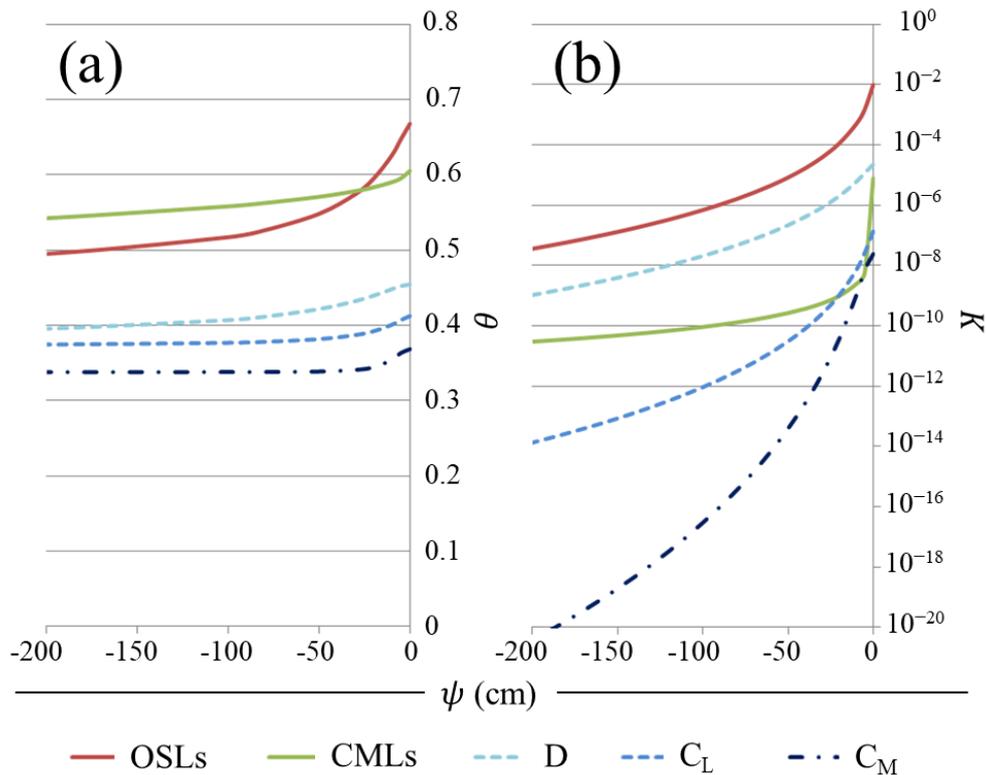
Figure 3.7. (a) Water retention curves and (b) hydraulic conductivity curves of organic soil layers (OSLs), clay mineral layers (CMLs), and bedrock divided by degree of weathering (D, C$_L$ and C$_M$).

Table 3.2. K_s of each layer and the *in situ* K_s measured in the boreholes.

	K_s of matrix (cm s^{-1})	In situ K_s (cm s^{-1})
OSLs	9.79 $\times$ 10^{-3}	
CMLs	7.81 $\times$ 10^{-6}	
D	2.29 $\times$ 10^{-5}	
C$_L$	1.34 $\times$ 10^{-7}	1.04 $\times$ 10^{-6}
C$_M$	2.39 $\times$ 10^{-8}	2.90 $\times$ 10^{-5}

The characteristics of the matrix of highly weathered bedrock are similar to those of CMLs, with a low K_s value (2.29 $\times10^{-5}$ cm s^{-1}) and a flat water-retention curve. *Suzuki* [2022] also found no significant difference between the hydraulic conductivity of the CMLs and that of the matrix of highly weathered bedrock (P > 0.05, two-tailed t-test). These similarities were consistent with the characteristics of the clayed matrix of the highly weathered bedrock. The lack of clear cracks due to clayey matrix filling accounts for a low permeability, as in the CMLs. The hydraulic properties of the matrices of moderately and weakly weathered bedrock were similar, with significantly low K_s values (1.34 $\times10^{-7}$ cm s^{-1} and 2.39 $\times10^{-8}$ cm s^{-1}, respectively) and flat water-retention curves. Based on these characteristics and a comparison with the in situ K_s values determined from the boreholes, *Suzuki* [2022] concluded that, in moderately and weakly weathered bedrock, water flow is mostly through crack and fissure rather than through the matrix. As a result, the permeability of moderately and weakly weathered bedrock is higher than that of either CMLs or highly weathered bedrock. Kanai catchment can thus be hydrologically described as a headwater catchment underlain by impermeable soil layers situated above relatively permeable bedrock.

3.2.2 Hydrological, Hydrochemical and Hydrothermal Observations

A flowchart of the methodology used to explore the effects of clay layers on the hydrological processes in Kanai catchment is shown in Figure 3.8, and the instrumentation used in the study is illustrated in Figure 3.9. The pressure head, ψ, in the OSLs and CMLs was measured at points T0, T1, T2, T3, and T4 along the main hollow (Figure 3.9). T1 and T2 neighbor MB1 and MB2, respectively. The depths of the tensiometer installation are listed in Table 3.3. The ψ was recorded automatically at 10 min intervals from 1 November 2021 to 7 June 2022.
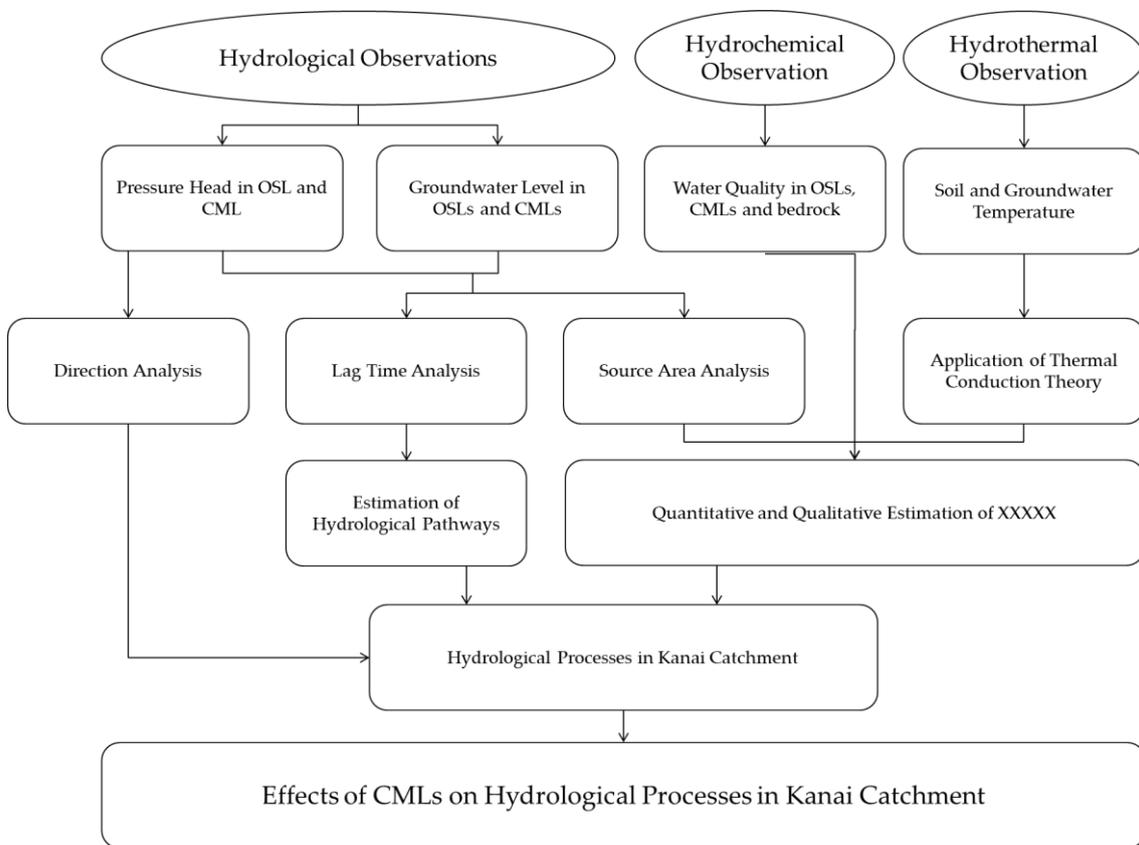
Figure 3.8. Flowchart of the methodology.
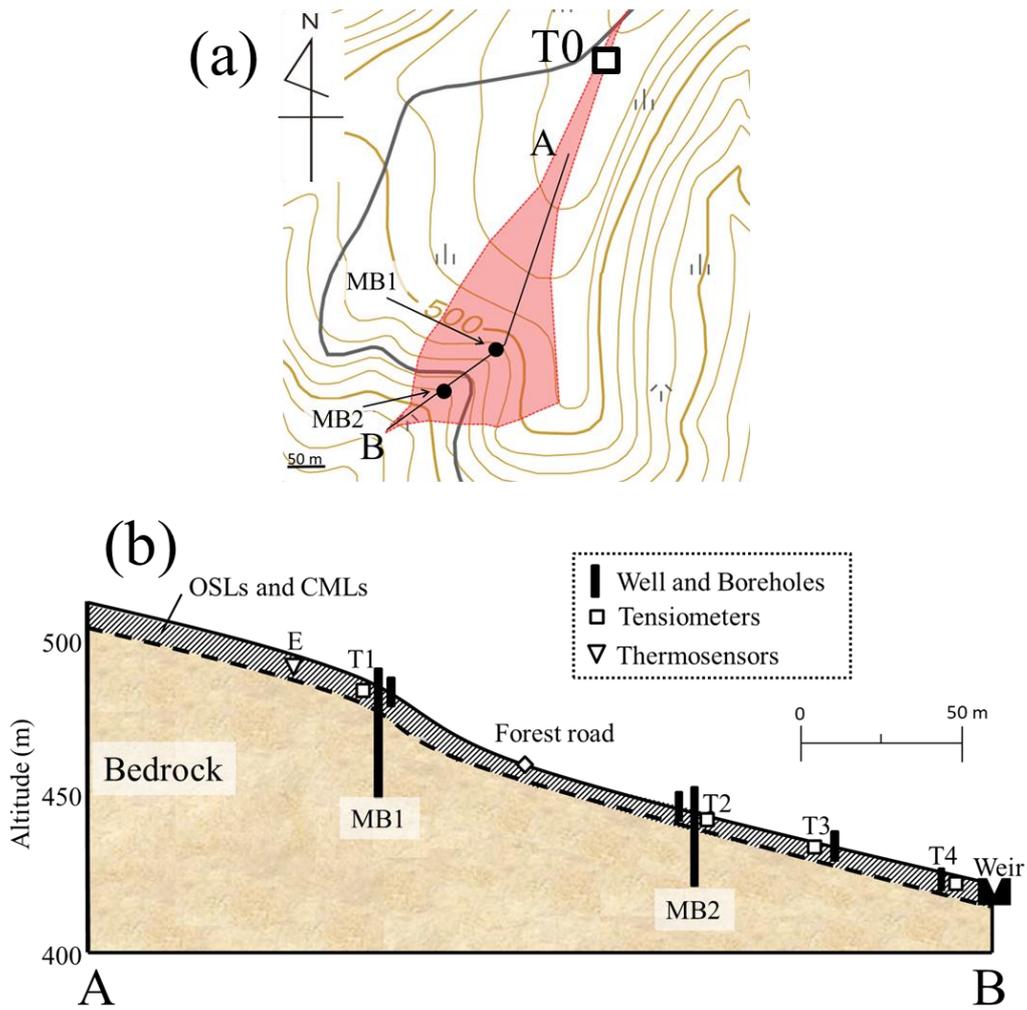
Figure 3.9. Instrumentation used at Kanai catchment. A and B are the same as in Figure 3.2b.

Table 3.3. Depth of tensiometer installation

Point	Layer	Depth of tensiometer installation from ground surface (cm)
T0	OSL	37
	CML	223.5
T1	OSLs	35, 87
	CML	227.5
T2	OSLs	36, 90
	CML	227.5
T3	OSLs	37, 86
	CML	227.5
T4	CMLs	86, 228.5

The locations of the observation facilities are also shown in Figure 3.9. To sustain boreholes MB1 and MB2, steel gas pipes, with strainer sections at the bottom 30 m (MB1) and 18.9 m (MB2), were inserted. The groundwater level and groundwater temperature in the boreholes were monitored using water-level gauges fitted with temperature recorders. Measurements were obtained at 10 min intervals from 1 November 2020 to 7 June 2022. Observation wells were manually excavated at T1, T2, T3, and T4 (Figure 3.9b) using a 6 cm diameter polyvinyl chloride pipe perforated with numerous 5 mm diameter holes. At T4 (30 cm), the well depth corresponded to the boundary between the OSLs and CMLs. At T1, T2, and T3 (29.5, 39.5, 37 cm, respectively), the well depths were within the OSLs. The groundwater level and groundwater temperature at the four wells were monitored using the same equipment and observation interval. At T4, the monitoring duration was the same as that of bedrock groundwater at MB1 and MB2. At T1, T2, and T3, monitoring was conducted from 16 October 2021 to 7 June 2022. When groundwater was generated in the well, the temperature in the well represented that of the groundwater; otherwise, it represented that of the soil at the bottom of the well. The rate of spring flow, determined using a V-notch weir with an angle of 30°, and the spring temperature were measured simultaneously at 10 min intervals, with the same equipment, observation interval, and monitoring duration as applied to the bedrock groundwater at MB1 and MB2 (Figure 3.9b). The weir was installed to collect only the spring water flowing above the CML surface.

For chemical analysis, groundwater samples were collected once or twice every few months. Bedrock groundwater samples of MB1 and MB2 were collected directly from the wells, and groundwater and spring water samples were collected directly from T4 and the weir, respectively. Unsaturated water stored in the OSLs and CMLs was sampled by applying suction pressure (50 kg cm^{-2}) at depths almost the same as those of tensiometer installation in the vicinity of T2. Collected samples were sealed in 100 mL polyethylene bottles and refrigerated until analyzed for inorganic solutes. Solute concentrations were analyzed in a laboratory at Hokkaido University. The samples were filtered through 0.45 μm cellulose acetate

filters and their ion (Al^{3+}, Ba^{2+}, Ca^{2+}, K^+, Li^+, Mg^{2+} and Na^+) concentrations were measured using an inductively coupled plasma (ICP) emission spectrometer (PerkinElmer, Waltham, Massachusetts, United States, ELAN DRC-e).

For thermal analyses, the soil temperature profile at point E in Figure 3.9b was measured at 60 min intervals, using thermosensors, from 20 October 2020 to 7 June 2022. Measurement depths were 10, 30, 60, 100, and 200 cm.

All precipitation and air temperature data were obtained from the Uryu Experimental Forest. Micrometeorology data were drawn from front yard measurements at the Uryu Experimental Forest Office, located at 44°22'N, 142°15'E, with an elevation of 288 m. To account for the effect of snowmelt, the amount of water that ultimately reached the ground surface (i.e., meltwater and/or rainwater; MR) was calculated as follows. First, precipitation on a day with a daily mean temperature > 2℃ was defined as rainfall; otherwise, it was considered snowfall. Rainfall was assumed to reach the ground surface immediately, and snowfall was assumed to form or accumulate as snow cover. The snow cover was assumed to melt in response to rising temperatures and to reach the ground surface immediately thereafter. Snowmelt was calculated based on the degree-day method, by multiplying the positive daily mean temperature by the snowmelt coefficient of 6 mm $℃^{-1}$ day^{-1}. For days with a negative daily mean temperature, the snowmelt coefficient was assumed to be 0 mm $℃^{-1}$ day^{-1}. Finally, MR was calculated by adding rainfall to snowmelt.

Snowfall and snowmelt periods were defined based on calculated snow water equivalents and snowmelt volume, respectively. A snowfall period was defined as one in which the calculated snow water equivalent was positive, and a snowmelt period was define as one in which the calculated snowmelt volume was positive. Precipitation outside of snowfall and snowmelt periods delimited different rainfall events. A new rainfall event was defined if the rainfall began after 24 h without rainfall and if the rainfall began after the end of the snowmelt period. The end of a rainfall period was defined as if a rainless period lasted 24 h or the snowfall period

began.

3.3. Results

Snowfall and snowmelt periods occurred intermittently from November to December. The main snowfall periods were from 21 November 2020 to 22 March 2021 and from 13 December 2021 to 24 March 2022. The main snowmelt periods were from 23 March to 15 May 2021 and from 25 March to 22 April 2022. Table 3.4a shows the rainfall events during the observation periods, as well as the total precipitation and strongest rainfall intensity of those events. There were 35 rainfall events in total. During those events, the maximum total rainfall was 84 mm and the maximum rainfall intensity was 35 mm h^{-1}. Total precipitation during the hydrological year (i.e., from 1 November 2020 to 31 October 2021) was 1923.8 mm and that during the observation periods was 2373.5 mm.

Table 3.4. (a) Rainfall and (b) snowmelt events during the observation periods. (a) Total precipitation and the strongest rainfall intensity during each event. (b) Total volume of MR during each event.

(a)

No.	Event Initiation	Total Precipitation (mm)	Strongest Rainfall Intensity (mm h⁻¹)
1	2020/11/1	34.5	7.5
2	2020/11/6	36.5	5.5
3	2021/5/16	41.5	2.5
4	2021/5/19	1	0.5
5	2021/5/21	0.5	0.5
6	2021/5/23	58.5	2.5
7	2021/6/4	43.5	3.5
8	2021/6/8	4	1
9	2021/6/20	18.5	6.5
10	2021/7/5	32.5	5
11	2021/8/5	20.5	5
12	2021/8/7	35.5	35
13	2021/8/9	34	3.5
14	2021/8/18	4	1
15	2021/8/25	17.5	5.5
16	2021/8/31	16	4.5
17	2021/9/12	41.5	12.5
18	2021/9/17	0.5	0.5
19	2021/9/23	25	6.5
20	2021/9/30	33	11
21	2021/10/4	84	18
22	2021/10/8	1.5	1
23	2021/10/10	51.5	14.5
24	2021/10/12	0.5	0.5
25	2021/10/15	0.5	0.5
26	2021/10/24	0.5	0.5
27	2021/10/25	2.5	2
28	2021/11/28	13	1
29	2021/11/10	1	0.5
30	2021/11/13	5.5	1
31	2022/5/3	45	5.5
32	2022/5/7	25	7.5
33	2022/5/13	11.5	2
34	2022/5/22	30	4
35	2022/5/28	20.5	1

(b)

No.	Event Initiation	Total MR (mm)	Strongest MR (mm day⁻¹)
1	2021/3/23	26.3	16.3
2	2021/3/28	62.6	20.2
3	2021/4/3	32.3	21.1
4	2021/4/7	4.6	4.6
5	2021/4/11	49.1	83.2
6	2021/4/16	34.1	174.7
7	2021/4/27	141	43
8	2021/5/3	506.8	72
9	2022/3/25	47.1	17.3
10	2022/4/3	53	17.1
11	2022/4/9	110.8	32.7
12	2022/4/19	79.8	39.5

3.3.1 Results of Hydrological Observations

3.3.1.1 Pressure Head in OSLs and CMLs

Figure 3.10 shows the hourly rainfall and ψ in the OSLs (~35 and ~90 cm depth) and the CMLs (~230 cm) and the groundwater level in the OSLs at T0, T1, T2, T3, and T4.

At T0 (Figure 3.10b), data on ψ were obtained only during the snowfall and snowmelt periods from 2021 to 2022. ψ in the OSL at a depth of 37 cm increased at a faster rate in response to rainfall and snowmelt water than in the CML at a depth of 223.5 cm. The OSL ψ indicated almost saturated conditions (about -10 cm) before snowfall periods, but it decreased slowly, to approximately -40 cm, during snowfall periods. During snowmelt periods, the OSL ψ fluctuated rapidly while sustaining nearly saturated conditions. CML ψ increased rapidly following the increase in OSL ψ, but its fluctuations were larger than those in the OSL. The maximum values of ψ in the OSL and CML during the snowmelt period in 2022 were 10.1 cm, recorded on 27 March, and 22.0 cm, recorded on 13 April, respectively. Larger values for ψ were recorded at the peak in the CML than in the OSL.

At T1 (Figure 3.10c), the ψ in the shallower OSL at 35 cm depth underwent a conspicuous decrease in July 2021. In 2022, after 8 July, there was no rainfall until 5 August, resulting in a decrease in ψ in the shallower OSL to -285.1 cm and to drought. In the deeper OSL, at 87 cm depth, the response of ψ was similar to that in the shallower OSL but its fluctuations were smaller in the former. During snowfall periods, ψ in the shallower and deeper OSLs decreased to approximately -50 cm and -40 cm, respectively. As the snowmelt period began, ψ in both OSLs increased and indicated almost saturated conditions. Although higher values of ψ were recorded at the deeper than the shallower OSL throughout the observation periods, during rainfall but not during snowmelt periods the ψ in the shallower OSL occasionally exceeded that in the deeper OSL. In response to rainfall and snowmelt water, the CML at 227.5 cm depth was characterized by both sharp and gentle fluctuations in ψ. Sharp increases in ψ resulted in higher values in the CML than in the OSL. Sharp decreases in ψ in the
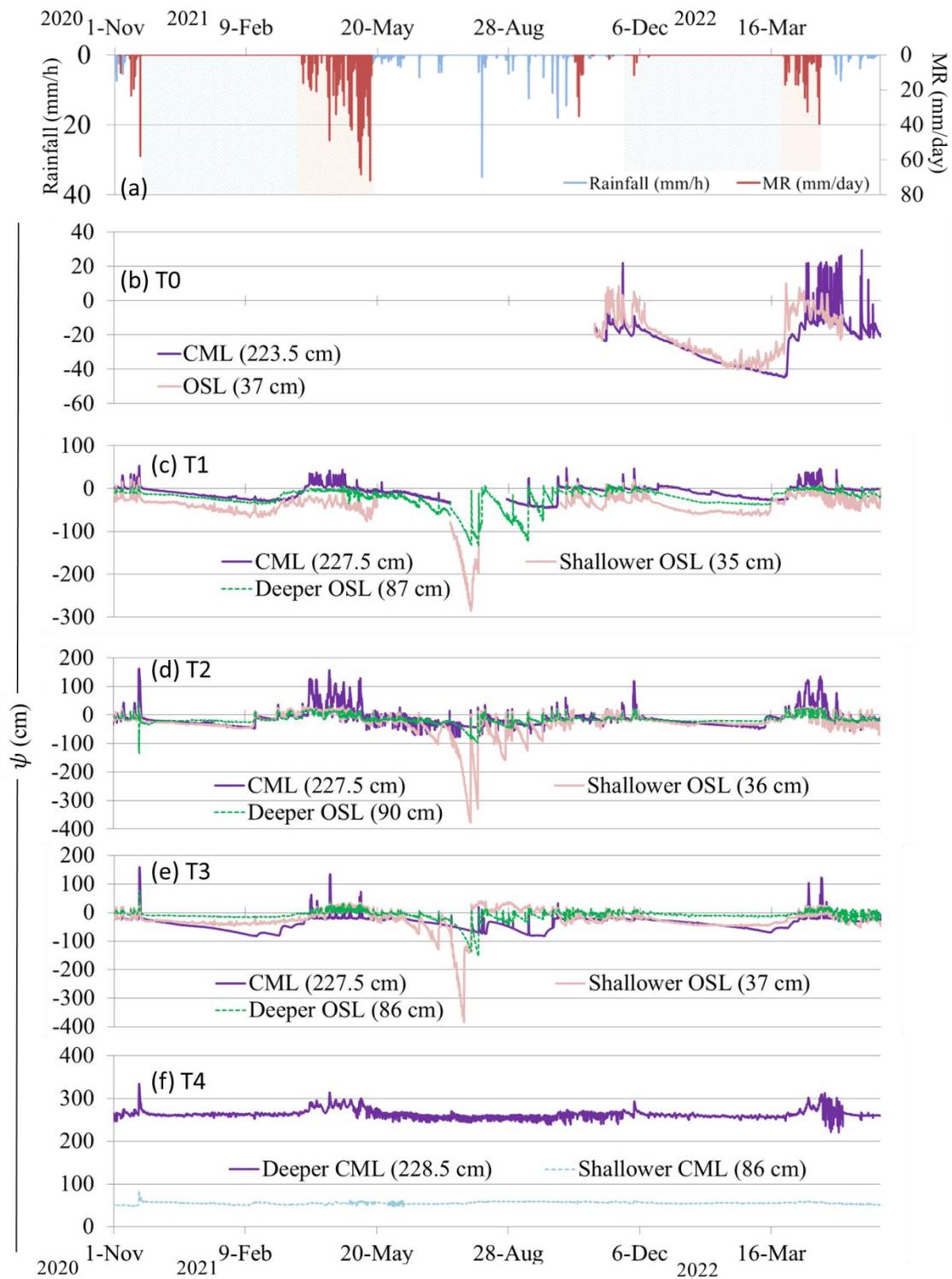
Figure 3.10. (a) Rainfall and combined meltwater and/or rainwater (MR) and the pressure head at the OSLs and CMLs determined at (b) T0, (c) T1, (d) T2, (e) T3 and (f) T4. Blue and red shaded areas in (a) are the main snowfall and snowmelt periods, respectively.

61

CML were followed by gentle decreases and the maintenance of wetter conditions than in the OSL. The shallower depths of T1 were drier for almost all observation periods.

At T2 (Figure 3.10d), ψ values in response to rainfall and snowmelt were higher in the shallower OSL (depth of 36 cm) than in the deeper OSL (depth of 90 cm). Hence, saturated conditions more often occurred in the shallower OSL at T2 than in the shallower OSL at T1. The ψ values recorded in the shallower OSL were lower than those recorded in the deeper OSL, both immediately after rainfall and during snowfall periods. The shallower OSL tended to respond immediately and to become saturated faster than the CML. Fluctuations in ψ in the CML (227.5 cm depth) were sharper and larger than those at T1. Although T2 was located downslope from T1, the CML ψ at T2 more often indicated dryer conditions than at T1. This tendency was significant during snowfall periods, when ψ at T2 decreased to approximately −50 cm, compared to approximately −25 cm at T1. Therefore, the wettest conditions were at the deeper OSL during snowfall periods but the driest condition were also detected at the deeper OSL, due to the sharper and larger increases in ψ in both the shallower OSL and the CML during snowmelt periods and large rainfall events.

At T3 (Figure 3.10e), gentler increases in ψ at the CML (227.5 cm depth) characterized the period from early August 2021 to early September 2021, but each sharp increase and decrease in ψ was more distinct than in the CML at T0, T1, and T2. However, during drought and snowfall periods, the CML was drier at T3 than at the other observation points. In the shallower OSL, ψ increased sharply and became saturated in response to rainfall and snowmelt water. In the deeper OSL (86 cm depth), conditions were wetter than at either the shallower OSL or the CML during all observation periods except the drought period.

At T4 (Figure 3.10f), the recorded ψ values were in the CML, at depths of 86 cm and 228.5 cm. Because the groundwater level was several cm below the surface (see Section 3.3.1.3), both ψ indicated perennial saturation. Larger fluctuations were detected at the deeper than the shallower CML.

Table 3.5 shows the number of hours of saturation at T0, T1, T2, and T3 during the observation periods as well as the number of hours in which all layers were saturated at the same time. At T0, the OSL and CML were saturated for 315 and 224 h, respectively, but the two layers were simultaneously saturated for only 35 h, suggesting that the groundwater level was often located in the OSLs, above the unsaturated CMLs, when the OSL was saturated. The wetter condition in the CML at T1 was well reflected by the large number of saturation hours (3656 h) but all layers were simultaneously saturated for only 97 h: 42 h during the snowfall and snowmelt periods and 55 h during other periods. At T2, the deeper OSL indicated relatively wetter conditions during snowfall periods, but the number of hours of saturation at the deeper OSL of T2 was the shortest, given the sharper rise of ψ in its shallower OSL and CML. Although all layers were saturated for 1257 h, the majority (1066 h) occurred during the snowfall and snowmelt periods. A comparison of the time in which all layers were saturated with the duration of saturation in each layer showed that in half, the shallower OSL likely formed over the unsaturated zone in the deeper OSL or CML. At T3, the CML had the fewest saturation hours, reflecting the distinct, sharp, and instantaneous increases and decreases in ψ. The differences in the number of hours of saturation between the OSL

Table 3.5. Number of hours of saturation of the OSLs and CMLs at T0, T1, T2, and T3 during the observation periods. The number of hours that all layers were simultaneously saturated is also shown, distinguishing between snowfall and snowmelt periods and other periods.

	Shallower OSL		Deeper OSL		CML		All layer saturated	
	Saturated	Unsaturated	Saturated	Unsaturated	Saturated	Unsaturated	Rainfall periods	Snowmelt periods
T0	315	4521			224	5217	27	8
T1	167	11198	563	13969	3656	12935	55	42
T2	2505	13599	1542	13990	2207	13990	191	1066
T3	2932	13991	3182	13991	379	13991	102	180

and CML suggested that the groundwater level formed above the unsaturated CML.

Compared to other observation points, more hours of saturation occurred at the shallower and deeper OSL in the lower point of the study catchment and at nearly the same depth. The opposite was determined for the CML, as more hours of saturation occurred at the higher point of the catchment. In addition, at T3 the saturated zone in the OSL often formed above the unsaturated CMLs. Thus, saturation zones formed separately in the OSLs and CMLs. At T4, due to the sustained saturation of the OSL and CML, the two saturation zones merged to form a single saturation zone.

3.3.1.2 Direction Analysis of Water Movement

The direction of water movement between the OSLs and CMLs and in the CMLs was analyzed by calculating the differences in the total head, H, defined as the sum of ψ and the elevation head between the deeper OSLs and CMLs. Figure 3.11 shows the temporal variation in H between the deeper OSLs and CMLs at T1, T2, and T3, and between the shallower CML and deeper CML at T4. A positive value indicated upward flow from the CMLs into the deeper OSLs or from the deeper CML into the shallower CML, whereas a negative value indicated downward flow from the deeper OSLs into the CMLs or from the shallower CML to the deeper CML. With the exception of the upward flow observed instantaneously at T2 on 20 November 2021 (Figure 3.11c), no upward flow was observed. However, upward flow from the deeper to the shallower CML was observed constantly at T4. As seen in Figure 3.11, downward flow dominated between the deeper OSLs and CMLs at T1, T2, and T3, and upward flow in the CML at T4, where the CMLs were perennially saturated.
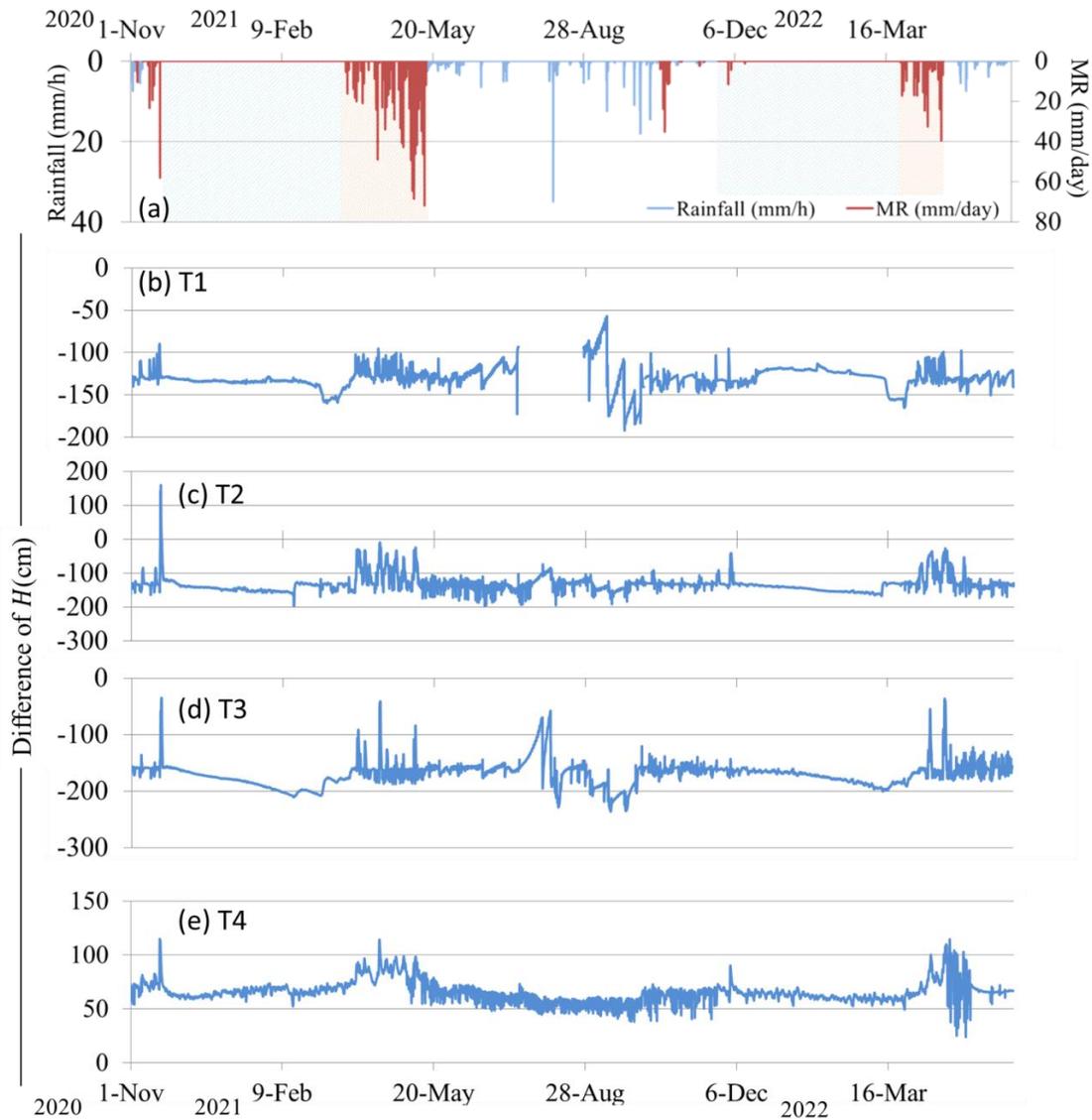
Figure 3.11. (a) Rainfall and MR, the differences in the total pressure head between the deeper OSL and the CML at (b) T1, (c) T2 and (d) T3, and the differences in total pressure head between shallower and deeper CMLs at T4. Blue and red shaded areas in (a) are the main snowfall and snowmelt periods, respectively.

3.3.1.3 Groundwater Level in OSLs and Bedrock and Specific Discharge

Figure 3.12 shows the hourly rainfall and groundwater levels in the OSLs at T2, T3, and T4, the bedrock groundwater levels at MB1 and MB2, and specific discharge through the OSLs at the catchment outlet. A groundwater level was not detected at T1.

65

Figure 3.12. (a) Rainfall and MR, the OSL groundwater level at (b) T2, (c) T3 and (d) T4, the bedrock groundwater level at boreholes (e) MB1 and (f) MB2, and (g) the rate of specific discharge of the spring. Blue and red shaded areas in (a) are the main snowfall and snowmelt periods, respectively. Dashed lines in (e) and (f) indicate the boundaries between CML and bedrock.
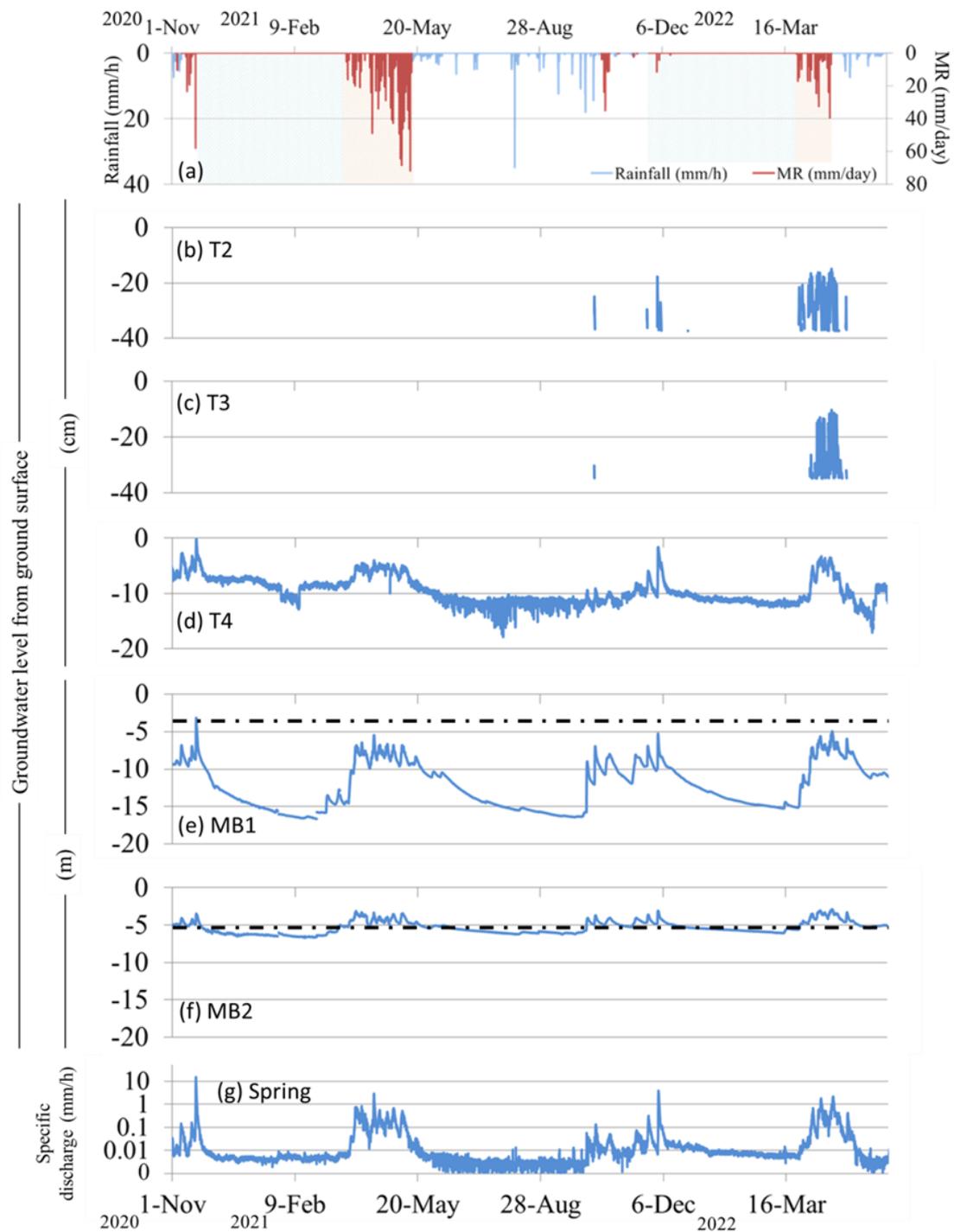
A groundwater level in the OSL at T2 (Figure 3.12b) was observed for 696 h during the observation period. In October and December 2021, the groundwater level occurred at −25 cm and −30 cm (i.e., 25 cm and 30 cm below the ground surface), respectively. While the saturation times measured by tensiometers did not necessarily correspond with the groundwater level, due to the differences in installation depths between the tensiometers and wells and to observation well plugging, the groundwater level formation times nonetheless corresponded to the saturation times measured for the shallower OSL ψ at T2. During the snowmelt period in 2022, a groundwater level formed at T2, with the maximum level reached at −15 cm on 22 April 2022. A groundwater level in the well was observed intermittently during the snowmelt period; it rose and fell daily, with a maximum difference between of ~2 cm. The daily rise during the snowmelt period usually occurred between 12:00 and 16:00. Snowmelt water was no longer supplied after 22 April 2022, according to calculated snowmelt water volume, and the groundwater level disappeared on 27 April 2022. After the end of the snowmelt period, a well-developed groundwater level in the OSL appeared temporarily, on 4 May 2022, in response to rainfall.

A groundwater level in the OSL at T3 (Figure 3.12c) developed for 512 h through the observation period, and thus for fewer hours than the groundwater level at T2. During the snowmelt period, a groundwater level formed intermittently from 4 April to 1 May 2022, at a maximum of −10 cm. Similar to the groundwater level at T2, the groundwater level at T3 formed intermittently in the well during the snowmelt period and underwent daily fluctuations. However, in contrast to T2, there was little response of the groundwater level to rainfall before the snowfall period.

At T4 (Figure 3.12d), a groundwater level was observed perennially in the OSL, with a minimum during the observation period at −18 cm. The maximum level was at –2 cm, occurring in early December 2021 and thus before the snowfall period. During the snowfall period, the groundwater level decreased slightly and slowly. While the groundwater levels in the OSLs at T2 and T3 were characterized by daily fluctuations during the snowmelt period in 2022, there were almost no daily fluctuations in the

groundwater level at T4. The groundwater level in the OSL at T4 also did not respond significantly to rainfall from the snowmelt periods in 2021, which in that year lasted until early October.

    In borehole MB1 (Figure 3.12e), a groundwater level within bedrock was observed perennially during the observation period. Although the borehole depth was deep (35 m), the groundwater level showed relatively rapid and large responses to rainfall and snowmelt water. The maximum groundwater level throughout the observation period was located at −3.1 m, occurring in response to snowmelt water on 20 November 2020. Thus, the groundwater level was higher than the CML depth at MB1, since the boundary between the CML and bedrock at MB1 was at −4.0 m. Except during this snowmelt period, the groundwater level never exceeded −5.0 m and thus never reached the interface between the CML and bedrock. The minimum groundwater level was at −16.6 m. A groundwater level of−5.5 m was reached during the snowmelt period in 2021, but it decreased slowly and gradually after that year's snowmelt period, finally reaching −16.4 m. A large, sharp rise of the groundwater level occurred in response to the rainfall event on October 2021 (4–5 October 2021, total rainfall: 84 mm). During the subsequent snowfall period in 2021–2022, the groundwater level dropped again, to −16.0 m. Large, sharp rises of the groundwater level were likewise recorded during the early snowmelt periods in both 2021 and 2022. The groundwater level increased stepwise during early snowmelt periods followed by fine daily fluctuations, with a maximum variation of ~1 m, as well as relatively large fluctuations, with a maximum variation of ~3 m, later in the snowmelt period. The bedrock groundwater level, however, fluctuated without fine fluctuations in response to rainfall.

    In borehole MB2 (Figure 3.12f), fluctuations of bedrock groundwater level were smaller and gentler than those in MB1. The maximum and minimum levels during the observation period were −2.9 m and −6.7 m, respectively. The boundary between the CML and bedrock at MB2 was −5.1 m, but the groundwater level was often higher. Although the borehole depth was as deep as 25 m and the groundwater level in MB2 consistently formed at shallower depths than in MB1, the groundwater level

in MB2 responded more slowly to rainfall and snowmelt water. Despite a few temporal and quantitative differences in the groundwater level between MB1 and MB2, the overall fluctuation characteristics were similar; for example, the groundwater level in MB2 also decreased slowly and gently during snowfall periods, with fine daily fluctuations during snowmelt periods. Figure 3.13 shows the relationships of MB1 and MB2 to bedrock groundwater levels. The strong correlation between MB1 and MB2 emphasizes the similarity of their fluctuation characteristics. *Kosugi et al.* [2011] reported localized bedrock aquifers with completely different fluctuations in their bedrock groundwater level, whereas, as can be inferred from Figure 3.13, the two groundwater levels in MB1 and MB2 were not localized and originated from the same aquifer.
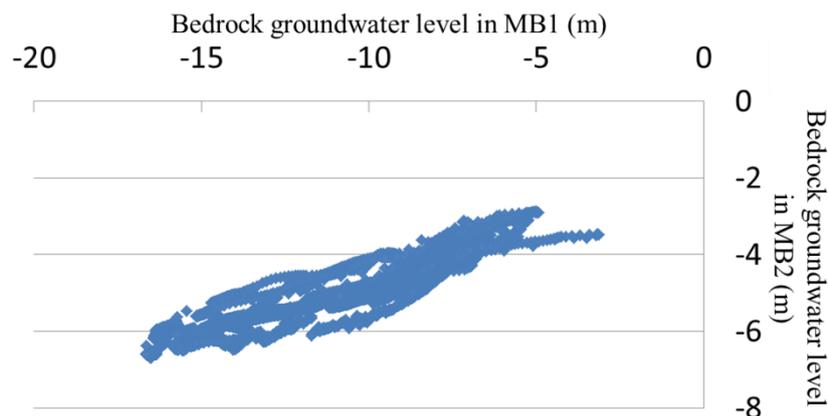
Figure 3.13. Relationships between MB1 and MB2 and the bedrock groundwater level.

The rate of specific discharge was calculated semi-perennially, and the maximum and minimum were determined to be 14.8 mm h^{-1} and 1.06×10^{-3} mm h^{-1}, respectively (Figure 3.12g). Total specific discharge during the observation periods and hydrological year were 837.6 and 472.3 mm, respectively. Of the total precipitation in the hydrological year, 24.6% was discharged from the Kanai catchment. Significant rate fluctuations were recorded before the snowfall period (from October to December) and during snowmelt periods. In response to some rainfall events, flash-like increases and decreases in the discharge rate were triggered; for example, in September 2021 and May 2022. Outside of these rainfall events, there was

significant increase in the discharge. The fluctuation characteristics of the specific discharge were similar to those of the groundwater level at T4 rather than those at T2 and T3 or MB1 and MB2.

3.3.1.4 Lag Time Analysis of Increase of Pressure Head and Groundwater Level in the CMLs and Bedrock in Response to Rainfall and Snowmelt Periods

The hydrological observations (Figures 3.10–12) showed the occurrence of water movement in the CMLs and bedrock despite the significantly low saturated hydraulic conductivity of the CMLs. *Tsukamoto* [1998] reported the characteristics of soil pipes formed in clay layers: pipe formation by washing with water took longer in clay layers than in sandy layers, but once the pipes had formed in the clay layers, they were supported by the hardness of the soil. Indeed, some studies have reported preferential flow in clay-rich soils [*Djodjic et al.*, 1999; *Glaesner et al.*, 2011]. In soil pipes formed in clay layers, rainwater can rapidly transit through them to flow out rapidly, despite the low saturated hydraulic conductivity of the clay layer matrix [*Feyen et al.*, 1996; *Tani*, 1997]. Thus, following rain events in the Kanai catchment, which is overlain by thick CMLs, the presence or absence of preferential flow should be noted.

The lag time between increases in ψ and the groundwater level provides information about the presence or absence of preferential flow, such as subsurface flow through pipes and its anomalies, especially in the longitudinal direction. *Lin and Zhou* [2008] described the occurrence of subsurface preferential flow, as a faster response of ψ, in deeper soil than in shallower soil. In this study, the route and form of water movement were assessed by determining the lag time following rainfall events in each layer, and in particular the lag time between the increase in ψ and that in the groundwater level at OSLs, CMLs, and bedrock. Specifically, the lag times of ψ in the OSLs and CMLs at T1, T2, T3, and T4, and the groundwater level in OSL at T4 and boreholes MB1 and MB2 were investigated. The lag time between the start of ψ and the rise in groundwater level was defined as: the time until a rise in $\psi \geq 1$ cm compared to ψ 1 h before the start of

the rainfall event (hereafter, initial ψ), the time until a ≥ 0.5 cm rise in the OSL groundwater level compared to the OSL groundwater level 1 h before the start of the rainfall event (hereafter, initial level), and the time until a rise in the bedrock groundwater level ≥ 10 cm from the initial level of bedrock groundwater. Rainfall events in which the strongest intensities were <2.0 mm h^{-1} and the total rainfall was <5.0 mm were excluded because the fluctuations in ψ and groundwater level were too small to allow an assessment of the lag times. Ten min interval datasets were used for the lag time analysis. Preferential flow was assumed to have occurred if the CML ψ or bedrock groundwater level responded to rainfall events > 10 min before both ψ and the groundwater level in the OSL responded.

During snowmelt periods, the lag time between when snowmelt water penetrates the snowpack and reaches the ground surface is difficult to determine. Indeed, two studies of rain-on-snow events showed that rainwater penetrates snowpack so quickly that rainwater flows laterally in snowpack [*Whitaker and Sugiyama*, 2005; *Ishii*, 2012]. MR, used to calculate snowmelt water volume in this study, is suitable for rough estimates of daily snowmelt water volume but provides little information on when the snowmelt water was supplied to the ground surface. Therefore, based on the presence or absence of MR, the two main snowmelt periods were divided into several snowmelt events. A snowmelt event was defined as the period from the day when the value of MR was positive to the day when it was 0. Assuming that the peak time for snowmelt is 14:00, we investigated the lag time in the rise of ψ and the groundwater level at 13:00 on the day when the snowmelt event began. The definitions of a rise in ψ and in the groundwater level and the occurrence of preferential flow were the same as for rainfall events.

Table 3.4b shows the snowmelt events and their total rate of snowmelt water. Table 3.6 shows the number of times the CML responded faster than OSL, and includes the number of total events as well as the geometric mean of the lag time for rainfall events and snowmelt events. The arithmetic means of the initial ψ and groundwater level and the peak ψ and groundwater level in each event are also shown in Table 3.6.

Table 3.6. Number of times the CML responded faster than the OSL, the number of total events, and the geometric mean lag time during (a) rainfall events and (b) snowmelt events. Arithmetic means of the initial ψ and level and of the peak ψ and groundwater level for each event are also shown.

(a)	T1 (MB1)			T2 (MB2)			T3			T4		
	Lag time (minute)	Initial ψ (cm) or level (m)	Peak ψ (cm) or level (m)	Lag time (minute)	Initial ψ (cm) or level (m)	Peak ψ (cm) or level (m)	Lag time (minute)	Initial ψ (cm)	Peak ψ (cm)	Lag time (minute)	Initial ψ (cm) or level (cm)	Peak ψ (cm) or level (cm)
Shallower OSL	225.4	-51.7	-2.4	130.4	-66.7	12.8	103.8	-13.2	19.3	192.3	-10.9	-9.3
Deeper OSL	234.9	-20.9	-3.8	245.7	-27.6	3.8	141.3	-19.0	11.4			
Shallower CML												
Deeper CML	435.8	-10.9	13.6	146.2	-22.9	19.1	244.9	-40.7	1.2	796.8	55.1	58.3
Bedrock Groundwater	1523.4	-12.7	-9.5	1988.2	-5.2	-3.1				340.4	259.2	269.2
Faster response/Total events	2/18			11/21			2/21			6/19		

(b)	T1 (MB1)			T2 (MB2)			T3			T4		
	Lag time (minute)	Initial ψ (cm) or level (m)	Peak ψ (cm) or level (m)	Lag time (minute)	Initial ψ (cm) or level (m)	Peak ψ (cm) or level (m)	Lag time (minute)	Initial ψ (cm)	Peak ψ (cm)	Lag time (minute)	Initial ψ (cm) or level (cm)	Peak ψ (cm) or level (cm)
Shallower OSL	134.8	-31.4	-11.0	65.0	-2.7	23.8	117.2	-9.2	17.5	627.8	-7.5	-5.1
Deeper OSL	238.7	-8.2	1.7	138.4	-4.1	20.2	187.5	1.2	17.9			
Shallower CML												
Deeper CML	324.2	1.4	27.5	125.8	1.8	100.3	805.9	-26.6	46.5	1280.9	54.7	58.7
Bedrock Groundwater	581.3	-10.3	-7.0	542.5	-4.6	-3.5				461.6	269.5	293.4
Faster response/Total events	3/12			4/12			1/12			4/12		

At T1 and T3, there were fewer faster responses in the ψ of the CML and little difference in the number of rainfall vs. snowmelt events. The average lag time at T1 and T3 also showed the order of ψ and groundwater level responses, with the shortest lag time at the shallower OSL and the longest at bedrock, indicating a nonsignificant contribution of preferential flow to rainwater infiltration. During rainfall events and to some extent snowmelt events, CML ψ responded faster than OSL ψ more often at T2 than at the other observation points. In Kanai catchment, vertical pipes and anomalies could not be ruled out during excavation of the trench adjacent to T2. Thus, it is possible that pipes and anomalies account for the rapid response in the CML at T2, similar to the pipes and anomalies formed in clay layers as described in previous studies [e.g., *Redding and Devito*, 2010; *Du et al.*, 2016]. Almost all faster responses of the CML at T1, T2, and T3 occurred under conditions in which all layers were unsaturated. This was also evidenced by the relatively large negative values (less than −10 cm) of the average initial ψ in the OSLs and CML. Rapid responses in unsaturated OSLs and CMLs in Kanai catchment are unlikely without preferential flow, due to the significantly low unsaturated hydraulic conductivities (ψ less than −10 cm) (Figure 3.7b). In addition, when faster responses in the CML were observed at T2, there was only one event (snowmelt event 1) in which the CML at T1 responded even faster. Therefore, the rapid responses of the CML at T2 can be attributed to vertical preferential flow through pipes and anomalies rather than to groundwater flow from T1. However, during rainfall events, the bedrock groundwater response was faster at MB1 than at MB2, although there was little preferential flow at T1, adjacent to MB1. Moreover, at MB2, bedrock groundwater responded more quickly to snowmelt events than to rainfall events, while the occurrence of preferential flow decreased significantly at T2 during snowmelt events. Taken together, these results suggest that preferential flow contributed to the development of a saturated zone in the CML of T2 but its contribution to increasing the bedrock groundwater level was small.

At T4, the significantly slower increase in ψ at the shallower CML revealed faster increases in ψ in the deeper CML. These rapid responses of

the deeper CML could be attributed to vertical preferential flow from the OSL to the deeper CML, bypassing the shallower CML. However, because all layers were perennially saturated at T4 (Figures 3.10 and 3.12), the water supply from the OSL to the deeper CML through pipes and anomalies was always accompanied by a rise in the OSL groundwater level. Moreover, if the OSL and deeper CML are connected by pipes and anomalies, any increase in ψ or the groundwater level in one should be promptly transmitted to the other. However, as the average lag time between the OSL and the deeper CML was at least 60 min, the rapid increase in the deeper CML ψ was more likely due to lateral subsurface flow in the deeper CML and to bedrock groundwater exfiltration into the deeper CML rather than to vertical preferential flow through pipes and anomalies. While a single groundwater zone was probable at T4, two different sources of water movement seemed to occur at this site, via the OSL and the CML.

3.3.1.5 Contribution of Extent of Saturated Zone in the OSLs and CMLs to Specific Discharge of Spring

In Kanai catchment, two separated but occasionally connected saturated zones were determined, in the OSLs and CMLs (Figure 3.10 and Table 3.5). The importance of the extent of the saturated zone on stream discharge is well documented [e.g., *McNamara et al.*, 2005; *Martínez-Carreras et al.*, 2016]. We therefore investigated how the extent of these two saturated zone affected the increase in the rate of specific discharge of the spring.

Figure 3.14 shows the relationship between the OSL groundwater and the specific discharge of the spring. Three conditions could be distinguished according to the extent of the saturated zones in the OSLs and CMLs at T2 and T3. In the first, only the shallower OSLs, not the CMLs, were saturated. Thus, the saturated zone in the OSLs extended above the unsaturated CMLs. In the second, only the CMLs were saturated, not the shallower OSLs. Thus, the saturated zone in the CMLs extended from T2 to T4 but that in the OSLs did not extend to T2. In the third, both the OSLs and CMLs were saturated. The number of hours of saturation under the first,

second, and third conditions was 971, 110, and 355, respectively. As seen in Figure 3.14, when the groundwater zones in the OSLs and CMLs were combined and extended (i.e., as in the third group), the OSL groundwater at T4 and the rate of specific discharge were noticeably higher. Although the first condition was the most frequently observed, the contributions of the extent of the saturated zone in the OSLs to OSL groundwater at T4 and to the specific discharge of the spring were small. However, the extent of the saturated zones in the CMLs, as described by the second condition, contributed more than those of the OSLs to the OSL groundwater at T4 and to the spring water during the fewest number of hours. These results suggest a greater contribution of the groundwater formed in the CMLs than within the OSLs to the OSL groundwater at T4 and to spring discharge fluctuations.
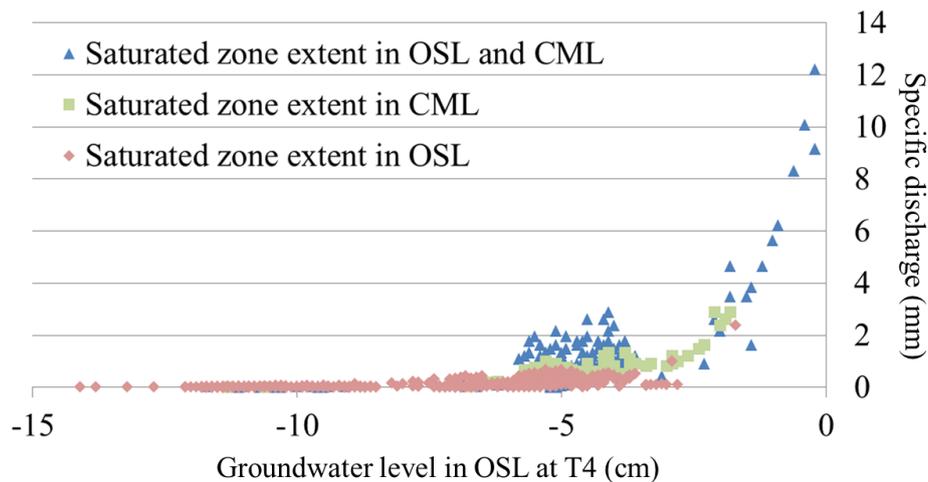

Table 3.14. Relationship between the OSL groundwater and the specific discharge of the spring. Extents of saturated zones in OSL and CML are also shown.

3.3.2 Results of Chemical Observations

Groundwater chemistry analyses can provide insights into the sources of groundwater and stream water. The concentrations of solutes (Al^{3+}, Ba^{2+}, Ca^{2+}, K^+, Li^+, Mg^{2+}, and Na^+) in the bedrock groundwater in MB1 and MB2, in the OSL and CML water at T2, in the OSL groundwater at T4, and in spring water are shown in Figure 3.15.
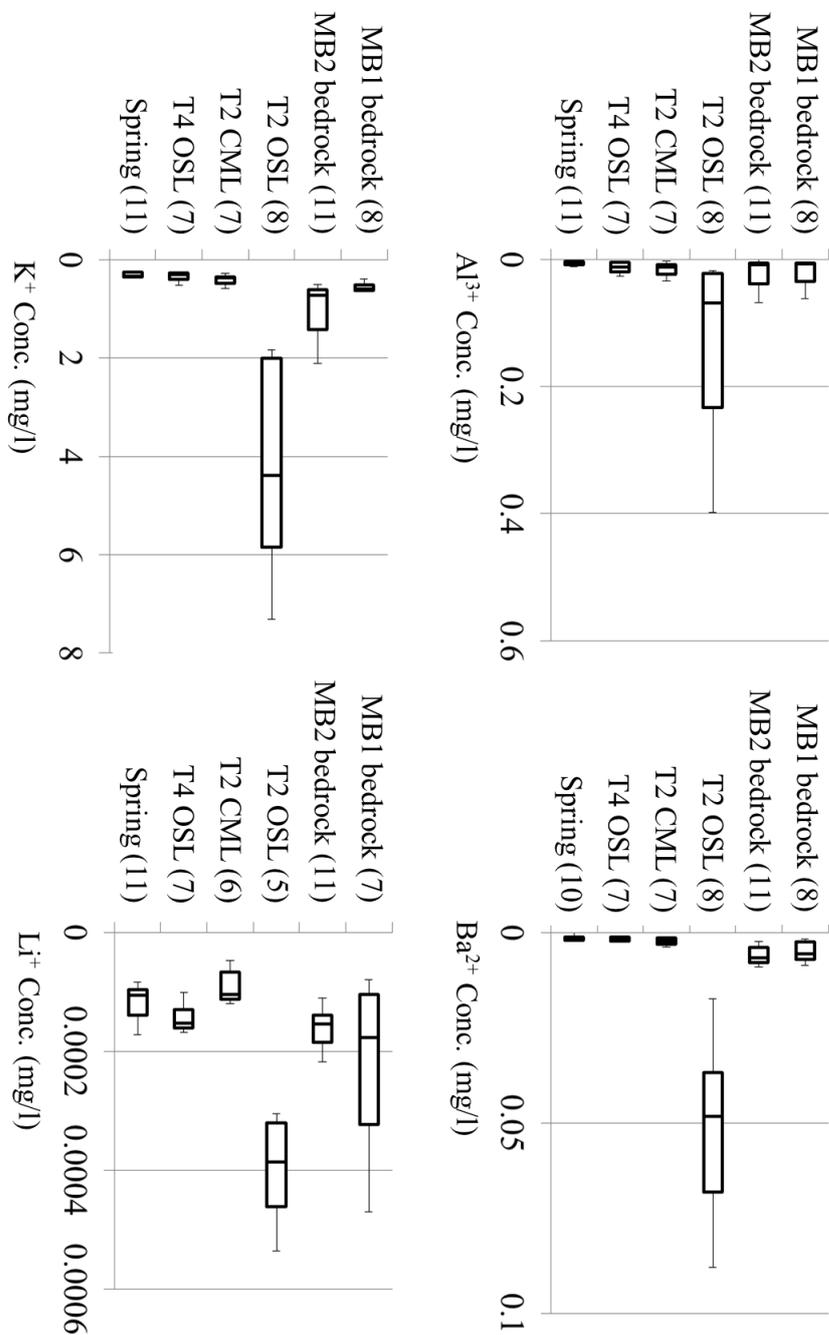
Figure 3.15. Solute concentrations of bedrock groundwater, water collected by applied suction, OSL groundwater, and spring water. The sides of the box closest to and fastest from zero indicate the 25th and 75th percentiles, respectively, and the line within the box denotes the median. The line to the left and right of the box respresent the 10th and 90th percentiles, repectively. The number of analyzed is given in parentheses.
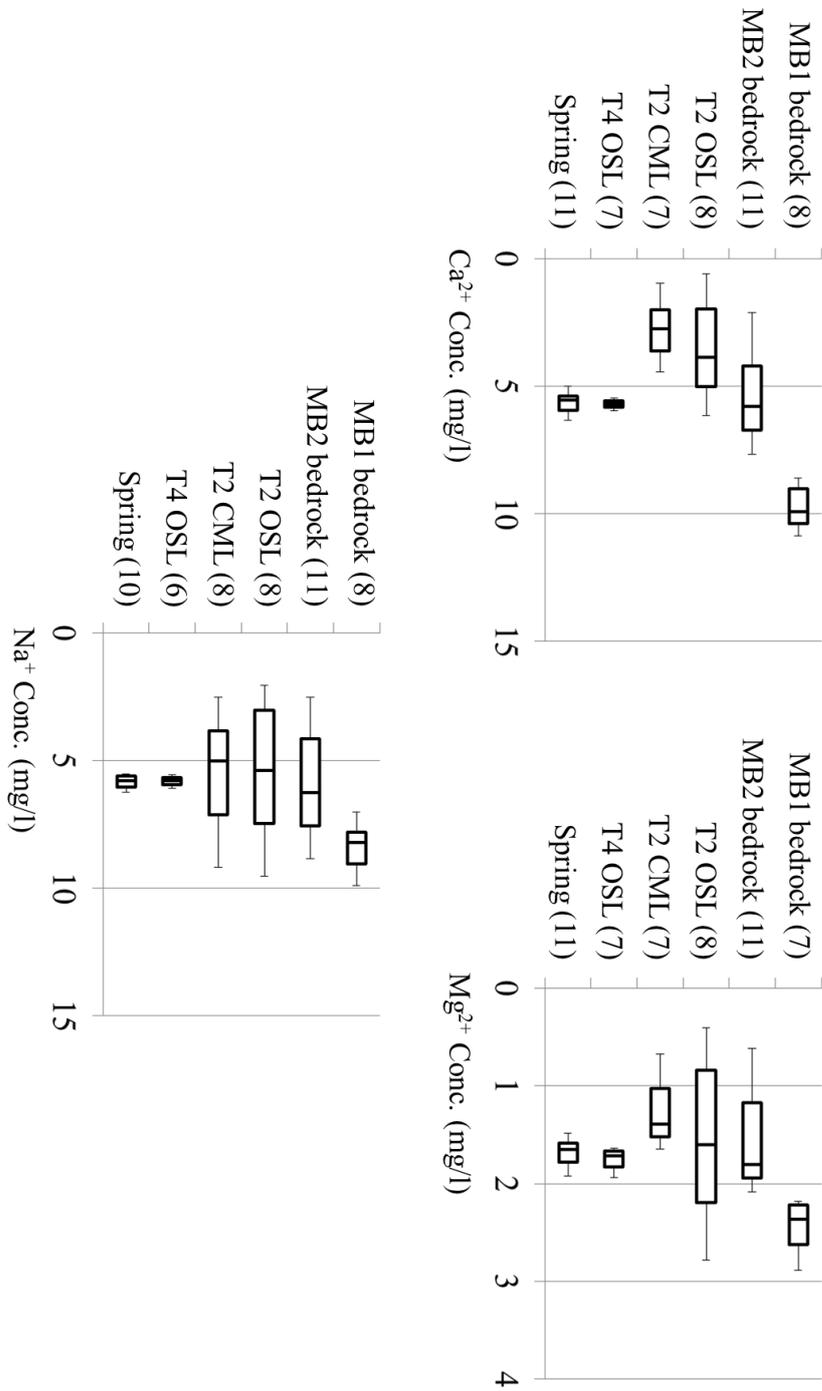
Figure 3.15. (Continued)

The solutes in Kanai catchment could be grouped according to two patterns. The concentrations in the first group (Al^{3+}, Ba^{2+}, K^+, Li^+) were higher in the OSL water collected by applying suction pressure at T2. Other water samples showed similar variation except for the Li+ concentration of MB1 bedrock groundwater. The concentrations of solutes in the second group (Ca^{2+}, Mg^{2+}, Na^+) were higher in MB1 bedrock groundwater. For this group, the variation in concentration was similar between MB2 bedrock groundwater and OSL and CML water at T2. *Asano et al.* [2004] chemically analyzed soil water, groundwater, springs, and streams in granitic catchments and found that Na^+ concentrations could be used to identify bedrock spring and bedrock groundwater. *Nakamura et al.* [1973] determined the chemical compositions of groundwater in a landslide area mainly underlain by tuff. They reported that contact with groundwater caused chemical weathering of the rock, resulting in the elution of Ca^{2+} and Mg^{2+} ions. Those results supported the higher concentrations of second-group ions in MB2 bedrock groundwater than in the other water samples. However, the concentrations of those ions in MB2 bedrock groundwater were lower than in MB1 bedrock groundwater and more similar to those in the OSL and CML water at T2. Considering the similarity of their concentrations of first-group ions, CML water and MB2 bedrock groundwater seemed to be of similar quality. Regardless of the group, there was little variability in ion concentrations in the OSL groundwater at T4 and in the spring water.

The potential contributing water sources and their chemistry were also considered. The OSL groundwater at T4 appeared to have contributed directly to the spring water in Kanai catchment. Although the depths at which OSL water samples were collected at T2 and T4 were almost the same, the respective concentrations of first-group ions deviated significantly. Specifically, the ion concentrations of OSL groundwater at T4 plotted roughly between those of CML water at T2 and bedrock groundwater in MB1 or MB2.

3.3.3 Results of Thermal Observations

3.3.3.1 Soil Temperature at Point E

Groundwater and soil temperature can provide insights into the sources of groundwater and spring water. Figure 3.16 shows the air and soil temperatures measured at Point E. In Kanai catchment during snowfall periods, however, the soil temperature was not influenced by the air temperature, since during snowfall and snowmelt periods the ground surface is covered with snowpack. The minimum soil temperature throughout the observation periods was −0.2℃, measured at a depth of −10 cm on April 2021, when snowmelt began and the snowpack decreased slightly despite minimum annual air temperatures below −30.7℃. The snowpack insulation influenced the temperature at −200 cm, the deepest thermal measurement in this study, at the outset of the snowfall period in 2020–2021. Although insulation by the snowpack was confirmed at all measurement depths, the soil temperature measured at Point E underwent sinusoidal seasonal variations, except during snowfall and snowmelt periods. The amplitude and phase of the temperature at each depth were damped and delayed as the measurement depth increased. The soil temperature at −200 cm exhibited the smallest variation, ranging from 2.7°C to 10.4℃, although there were many missing measurements due to equipment failure (Figure 3.16e).
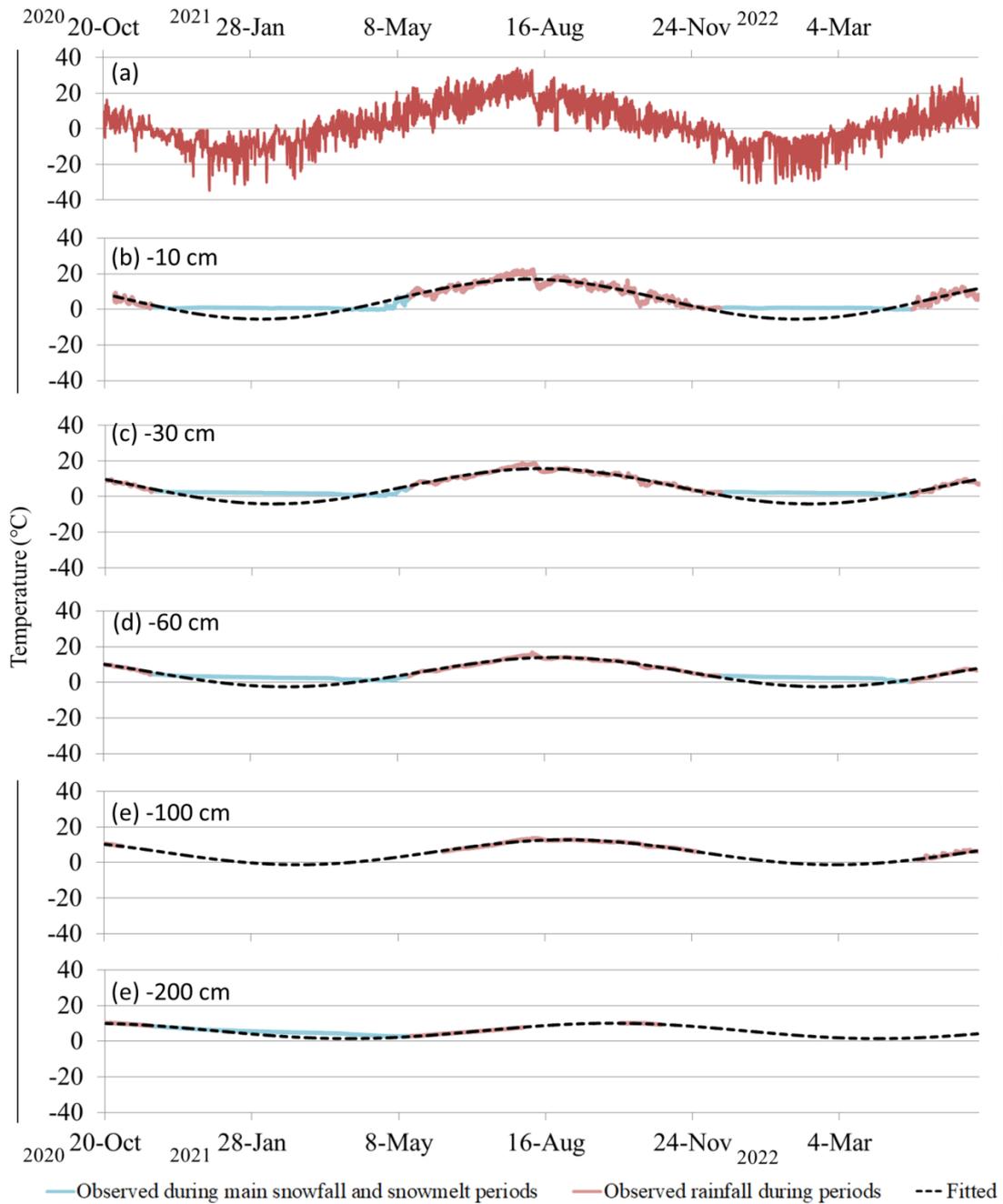
Figure 3.16. Variation in (a) air temperature and soil temperature measured at Point E. The sinusoidal curve fitted to the observed temperature is also shown. The temperature at (b–e) is shown for the main snowfall and snowmelt periods and rainfall periods.

3.3.3.2 Temperature in OSL Wells at T2−T4, Boreholes in MB1 and MB2, and Spring Water

Figure 3.17 shows the groundwater level and temperature in the OSL wells at T2−T4 and at boreholes MB1 and MB2.

At T2 (Figure 3.17c), the recorded temperature during the snowfall period in 2021−2022 was ~2℃, because snowpack on the ground surface insulated and stabilized the temperature, although the minimum air temperature during this period was −30℃. When the snowmelt period began and a groundwater level formed in the OSL well at T2, the recorded temperature in the well decreased gradually after 27 March 2022. The temperature in the OSL reached its lowest value, 0.3℃, on 10 April 2022, when 24.7 mm day^{-1} of snowmelt water was being supplied to Kanai catchment, based on the calculated snowmelt water volume. As the air temperature increased, so did the recorded temperature in the OSL well.

At T3 (Figure 3.17d), the recorded temperature in the OSL well dropped in response to the formation of a groundwater level, similar to the temperature dynamics at T2. Formation of a groundwater level and a decline in temperature began on 10 April 2022. The minimum value of 0.1℃ was recorded on 22 April 2022, when the volume of daily snowmelt water was 7.0 mm. After formation of a groundwater level had ceased, the temperature in the OSL well at T3 gradually increased.

At T4 (Figure 3.17e), the temperature in the OSL showed seasonal variation, with highest and lowest values of 8.1° C and 4.1℃, respectively. The maximum temperature was recorded on 7 August 2021, a week after the peak in seasonal air temperature dynamics at Kanai catchment. During snowfall periods, the temperature was stable (5.0−6.0℃) and remained higher than at T2 and T3. Notably, while the temperature in the OSL wells at T2 and T3 decreased at the same time as the formation of a groundwater level, the temperature in the OSL at T4 increased as the groundwater level rose. The maximum temperature during the snowmelt period in 2022 was 6.0℃, recorded on 14 April 2022. Throughout the observation periods, the temperature at T4 showed little seasonal variation with less variation than the air temperature.
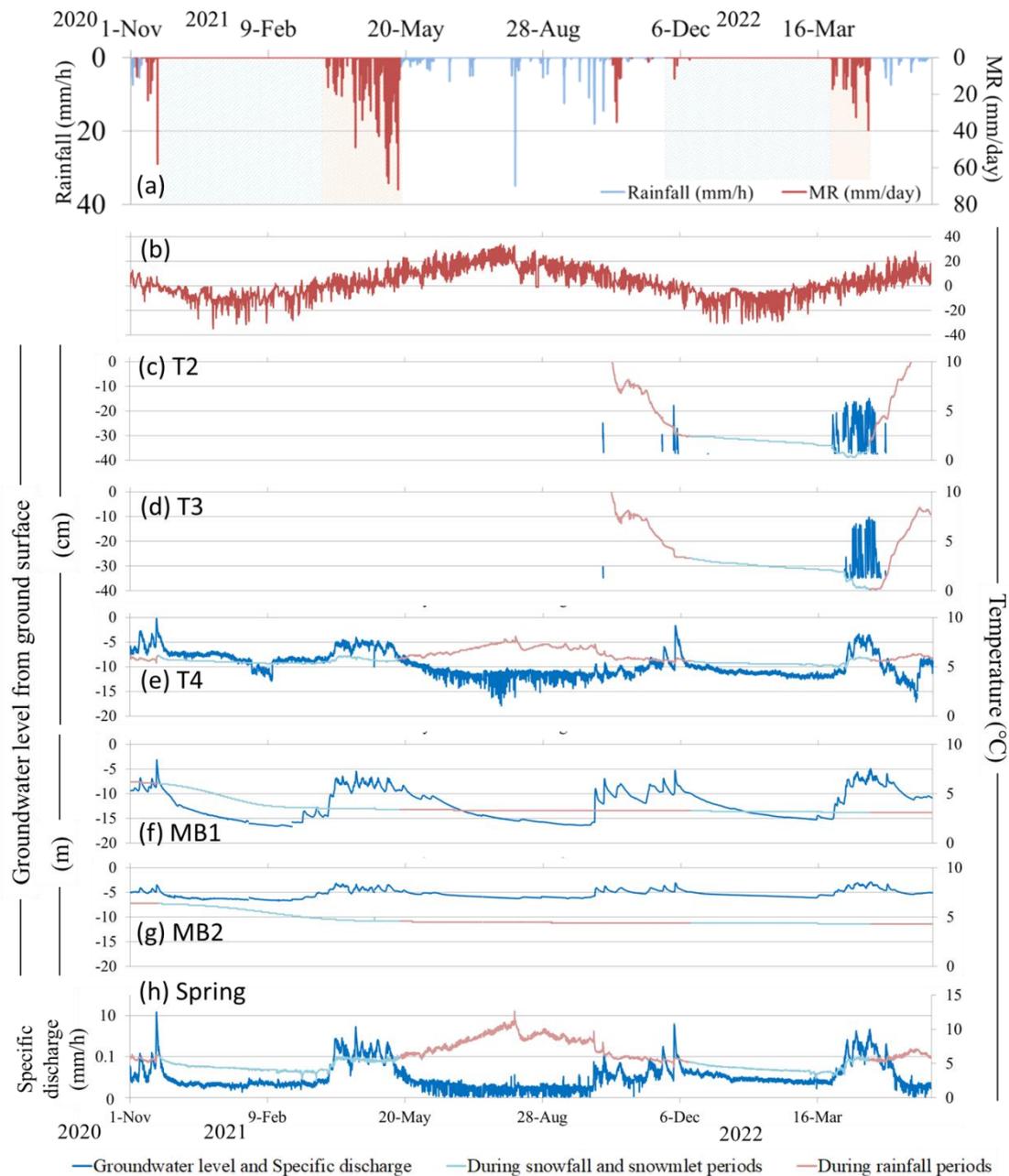
Figure 3.17. (a) Rainfall and MR, (b) air temperature, the OSL groundwater level, and the temperature at (c) T2, (d) T3, and (e) T4, the bedrock groundwater level and temperature at boreholes (f) MB1 and (g) MB2, and (h) the rate of specific discharge and the temperature of the spring. Blue and red shaded areas in (a) are the main snowfall and snowmelt periods, respectively. The temperature at (c–h) is shown for the main snowfall and snowmelt periods and rainfall periods.

82

At MB1 and MB2 (Figure 3.17f,g), the temperature in each borehole during the snowfall period of 2020-2021 dropped to 4.5°C and 3.5°C and then stabilized, with little variation during the observation period despite the increase in the bedrock groundwater level. The higher temperatures at MB1 and MB2, which occurred immediately after the observation began, reflected the drilling of the boreholes, which was conducted just prior to the observation period. Except for these higher temperatures, the temperature variation at MB1 and MB2 ranged from 3.5℃ to 3.1℃ and from 4.5℃ to 4.3℃, respectively.

The temperature of the spring water was influenced by the air temperature because the weir collecting the spring water was exposed to the open air, except during snowfall periods (Figure 3.17g), when the temperature dropped to ~4℃. However, with the start of the snowmelt period, the temperature suddenly began to rise, eventually reaching 6℃. Throughout the observation period, spring water temperature ranged from 2.4℃ to 12.6℃. Although the variation in temperature of spring water was slightly higher than that in the OSL well at T4 throughout the observation period, the temperature fluctuation patterns were similar.

In summary, the variation in temperature in OSL wells and boreholes can be described as follows: a rapid decrease during snowmelt periods, as observed in the OSL wells at T2 and T3; a smaller seasonal variations than that of the air temperature and increases during snowmelt periods, as observed in the OSL well at T4 and the weir; and no temperature variation, as observed at boreholes MB1 and MB2.

3.3.3.3 Application of Thermal Conduction Theory to Observed Temperature

The soil temperature at Point T showed nearly sinusoidal variation across the measurement depths, except during snowfall and snowmelt periods (Figure 3.16). When water movement does not affect the thermal response and the thermal diffusivity of the soil is vertically homogeneous, thermal diffusion can be described by Equation. 3.1:

$$\frac{\partial T(z,t)}{\partial t} = \kappa \frac{\partial^2 T(z,t)}{\partial z^2} \qquad (3\text{-}1)$$

where t is the time, z is the depth (positive upward), $T(z,t)$ is the temperature, and κ is the soil thermal diffusivity, defined as the thermal conductivity. If the amplitude of the annual thermal variation at the soil surface ($z = 0$) is represented by A_0, the amplitude of the annual soil temperature variation at depth z, $A(z)$, can be expressed as shown in Equation. 3.2:

$$A(z) = A_0 \exp\left(z\sqrt{\frac{\pi}{\tau\kappa}}\right) \qquad (3\text{-}2)$$

where τ is the period of one cycle (1 year) [*Jury et al.*, 1991], indicating that depth $A(z)$ decreases exponentially with increasing depth. The amplitude at each measurement depth at Point E was determined by fitting a sinusoidal curve to the observed temperature variation outside the snowfall and snowmelt periods (Figure 3.16). Figure 3.18 shows the relationship between the amplitude of the thermal responses and the measurement depth. The amplitude decreased exponentially with increasing depth. In addition, the value of κ at Point E, calculated from the slope of the regression line in Figure 3.18, was obtained ($\kappa = 4.2 \times 10^{-3}$ cm^2 s^{-1}) and was similar to that determined in previous studies, ranging from 2.5×10^{-3} to 6.0×10^{-3} cm^2 s^{-1} [*Tani et al.*, 1979]. These results suggest that the thermal responses at Point E were hardly influenced by water movement outside the snowfall and snowmelt periods.
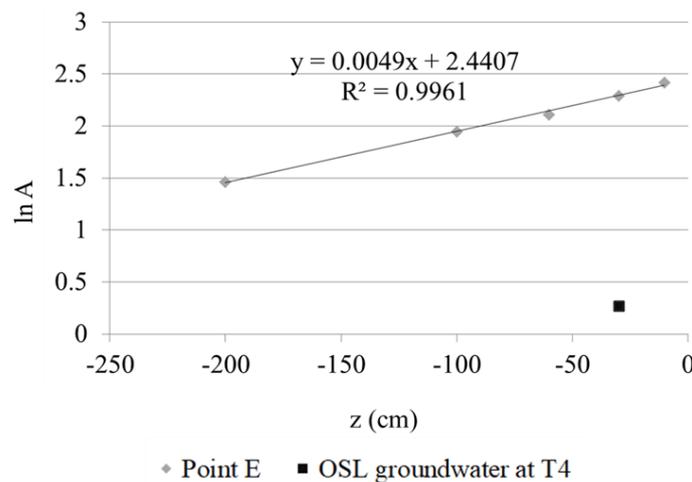

Figure 3.18. Relationship between ln A and depth z.

Figure 3.19 shows the sinusoidal curve fitted to the observed temperature at depths of −30 and −200 cm at Point E, and the temperature in the OSL well at T4. In terms of an increasing peak in temperature variation, the peak at −200 cm was significantly delayed, while the increasing peaks at −30 cm and the OSL well occurred around the same time, presumably because the depth of the OSL well at T4 was also −30 cm. However, the amplitude of the temperature variation in the OSL well was obviously smaller than that at −30 or −200 cm. The temperature at the bottom of the OSL well at T4 was also fitted to the sinusoidal curve using the method described above. The relationship between the amplitude of the thermal responses at the OSL well at T4 and the measurement depth is plotted in Figure 3.18. The amplitude at T4 was significantly different from that at −200 cm, which was the smallest amplitude determined in this study. Based on the regression line in Figure 3.18, the amplitude of the variation in temperature becomes progressively smaller with increasing depth, if the soil temperature changes without the influence of advection due to water movement. The smaller amplitude in the OSL well was disproportionate to the depth of the well and cannot be explained by the thermal conduction equation. These results suggest that the groundwater in the OSL well at T4 were not derived from groundwater flow through the OSLs.
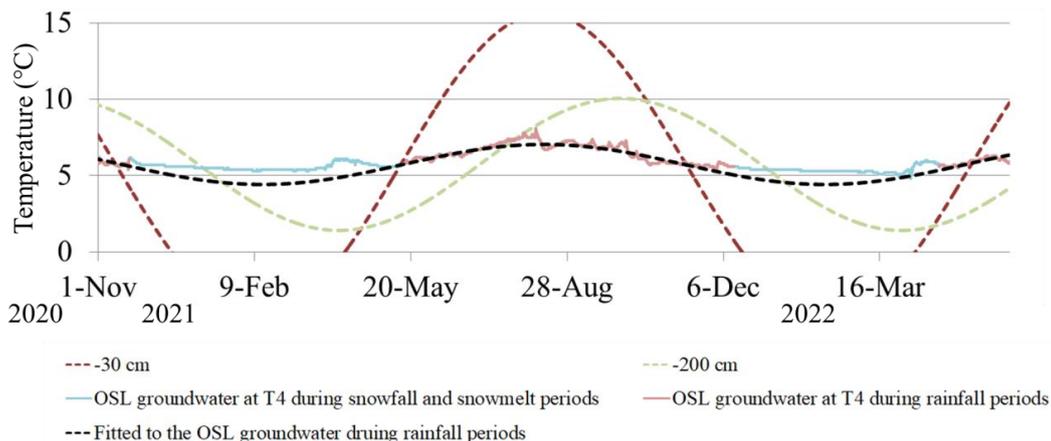

Figure 3.19. Variation in soil temperature fitted with sinusoidal curves at Point E at −30 and −200 cm, and in the OSL groundwater temperature at T4. Variation in temperature of the OSL groundwater is shown for the main snowfall and snowmelt periods and rainfall periods. The black dashed line is the sinusoidal curve fitted to the OSL groundwater temperature at T4.

3.4. Discussion

3.4.1 Hydrological Processes in Study Catchment

Figure 3.20 schematically depicts the hydrological processes in Kanai catchment, based on the results and discussion above. During rainfall and snowmelt periods, rainwater and snowmelt water infiltrated the OSLs. The OSLs were more likely to become saturated than the CMLs at a depth of 230 cm below the surface, except at T1 (Figure 3.10 and Table 3.5). Some water infiltrating the OSLs percolated to the CMLs as preferential flows through pipes and anomalies (Table 3.6), but without a noticeable effect on increases in bedrock groundwater. Instead, vertical unsaturated or saturated flow through the CML matrix likely contributed more to the increase in bedrock groundwater level in Kanai catchments. Although the saturated zones that formed in the OSLs and CMLs, sometimes combined, they were usually not connected, especially at T3. Saturated zones tended to form in the OSLs above unsaturated CMLs, but the extent of the saturated zones in the CMLs contributed more to the OSL groundwater at T4 and the spring than did saturated zones of the OSLs (Figure 3.14). These results imply that CMLs act as impeding layers and stimulate water movement within OSLs and that CMLs are an important source of OSL groundwater and spring water.

These inferences are supported by chemical and thermal analyses. Chemical analyses of the groundwater in the OSL at T4 and in spring water showed that the solute concentrations were between those of CML water and the bedrock groundwater in borehole MB1 or MB2 rather than similar to those of the water flowing through the OSLs (Figure 3.15). The chemical analyses indicated only a small contribution of the OSL water at T2 to the OSL groundwater at T4 and to the spring water, but the sources of the OSL groundwater and spring were not determined.

Based on the thermal analyses, the temperature amplitude of the OSL groundwater at T4 was smaller than that of the soil at -30 and -200 cm (Figure 3.19). In addition, during snowmelt periods, the temperature of the groundwater in the OSL wells at T2 and T3 decreased when groundwater levels were observed in the OSL wells. While the OSL groundwater
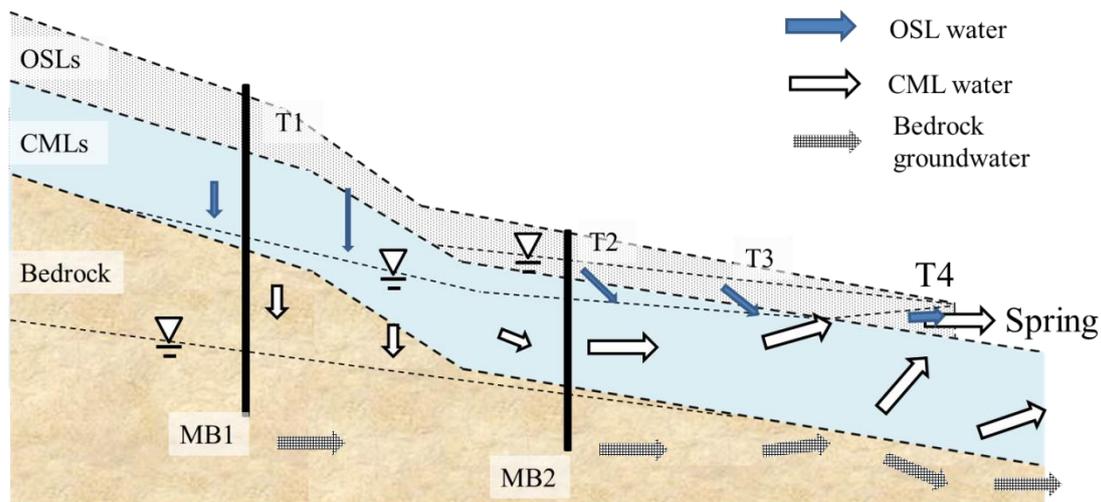
Figure 3.20. Schematic diagram of the hydrological processes at Kanai catchments.

temperature at T2 and T3 fell to nearly 0°C, the temperature of the OSL groundwater at T4 and of the spring water rose as both the groundwater level and the discharge rate increased (Figure 3.17). These results indicate that the formation of both groundwater at the OSL and spring water requires groundwater stored deeper than −200 cm. Because the variation in temperature of the OSL groundwater and spring water significantly differed from that of bedrock groundwater in MB1 and MB2, the OSL groundwater at T4 and the spring water could be attributed to CML water. Presumably, CML water drained to the OSL at T4 via the CML matrix or as preferential flow via the connection of the OSL with the CML through pipes, as inferred from a lag time analysis at T2.

3.4.2 Effects of CMLs on Hydrological Processes in the Study Catchment

3.4.2.1 Effects of CMLs on Bedrock Infiltration

As noted in Section **3.3.1.3**, ~25% of total precipitation in the hydrological year was collected at the weir installed at Kanai catchment. Because this weir only collected the water that flowed on the CML surface, the remaining ~75% of total precipitation infiltrated the CMLs. *Ishii et al.* [2004] noted that the rate of annual evapotranspiration during 1988–1998

ranged from 333 to 407 mm in the Moshiri Experimental Watershed, which includes Kanai catchment, a mountainous headwater catchment. Even assuming a larger evapotranspiration rate of 450 mm in Kanai catchment, approximately 50% of the total precipitation in the hydrological year infiltrated the CMLs. Given the relatively large fluctuations of bedrock groundwater levels (Figure 3.12), about half of the annual precipitation was stored in the CMLs and bedrock of Kanai catchment. Previous studies highlighted the importance of the bedrock infiltration rate in headwater catchments and calculated the rate of bedrock infiltration [e.g., *Katsuyama et al.*, 2010; *Oda et al.*, 2013; *Abe et al.*, 2020]. *Katsuyama et al.* [2010] calculated the annual bedrock infiltration in headwater catchments underlain by Cretaceous biotite granite. For an annual precipitation of 1521.1 mm, they reported annual bedrock infiltration rates of 89.9 and 112.0 mm at 5.99 ha and 1.75 ha catchments, respectively. *Oda et al.* [2013] reported an annual bedrock infiltration of 730 mm, equal to 23% of total precipitation, in a 7 ha catchment underlain by sedimentary rocks. In *Abe et al.* [2020], bedrock groundwater infiltration at 3.8 ha and 3.1 ha catchments underlain by granodiorite was 34% and 3% of total precipitation, respectively, a difference attributable to the significant spatial variability. Because it is difficult to calculate the rate of bedrock and CML infiltration separately at Kanai catchment, the infiltration rates could not be compared with those determined in previous studies. However, it is clear that a larger volume of rainwater infiltrated the CMLs and bedrock of Kanai catchment than in other studied areas.

Rainwater stored within CMLs is expected to infiltrate vertically and to finally form saturated zones in the CMLs above bedrock. The duration of the saturated zone above bedrock is an important factor controlling the rate of bedrock infiltration [e.g., *Bockgård and Niemi*, 2004; *Rodhe and Bockgård*, 2006]. *Bockgård and Niemi* [2004] described three situations of bedrock infiltration: the soil layers are unsaturated and the water table is located in the bedrock, the water table is located in the soil and the bedrock is saturated, erched groundwater in the soil overlays an unsaturated zone in the upper bedrock. *Kosugi et al.* [2006] noted the importance of the duration

of the saturated zone above bedrock for bedrock infiltration, based on hydrological observations and modeling. They demonstrated that, in highly weathered bedrock, where water flow through matrix is more important than flow through cracks, an increase in the bedrock infiltration rate can be expected when the saturated zone is sustained at a high level for a long time. *Langston et al.* [2015] examined water flow through cracks in bedrock as determined from hydrological observations and numerical simulations. They showed that the formation of a saturated zone in soil layers above bedrock increased the rate of bedrock infiltration through bedrock cracks. The presence of a saturated zone above bedrock for longer periods and at higher water tables is important in increasing the infiltration of bedrock through its matrixes and cracks. Figure 3.21 shows the relationship between the rise in bedrock groundwater levels at MB1 and MB2 and the durations of saturation (i.e., all tensiometers indicated positive values) in both the OSL and CML at T1 and T2 during each rainfall and snowmelt event. The longer the saturated zone exists in the OSLs and CMLs, the greater the amount of bedrock infiltration. These results provide further evidence of the importance of saturated zone duration to bedrock infiltration in Kanai catchment.

These findings together imply that the relatively large fluctuation in the groundwater level in the bedrock at Kanai catchment, which is covered by CMLs with low permeability, can be attributed to the durability of the saturated zone and the high groundwater level in the OSLs and CMLs. In Kanai catchment, half of the annual precipitation infiltrated was stored in the CMLs without subsequent discharge, which likely facilitated the formation of a saturated zone above bedrock. In addition, the deepest depth at which ψ was measured in this study was 228.5 cm (at T4), which was >2 m shallower than the soil thickness in Kanai catchment. The longest saturation period in the CMLs was 3656 h (at T1), but a saturated zone of even longer duration may have formed just above the boundary between the CMLs and bedrock, because water movement in the CMLs was slow due to low hydraulic conductivities in saturated systems. Moreover, the significantly high groundwater level above bedrock, which may have
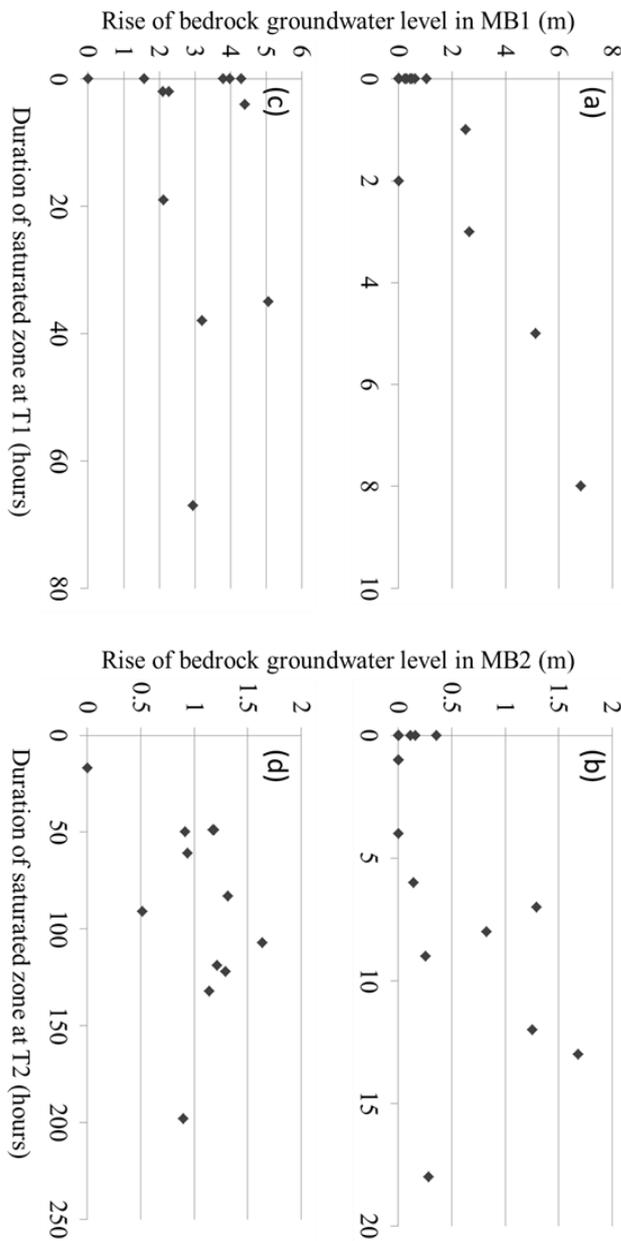
Figure 3.21. Relationship between the rise in the bedrock groundwater level at MB1 and MB2 and the duration of OSL and CML saturation at T1 and T2 in each (a, b) rainfall and (c, d) snowmelt event.

reached 5.5 m, also contributed to bedrock infiltration. Thus, in Kanai catchment, bedrock infiltration is enabled by the thick OSLs and CMLs, which maintain the saturated zone above bedrock for a relatively long period of time and facilitate an increase in the extent of the saturated zone.

3.4.2.2 Effects of CMLs on Exfiltration of Bedrock Groundwater

Bedrock groundwater contributes to the groundwater formed in soil layers and stream water, due to direct exfiltration through cracks or pipes into high-permeability soil layers and stream channels [e.g., *Miyata et al.*, 2003; *Gabrielli et al.*, 2012]. This effect is more pronounced during baseflow periods. In Kanai catchment, the groundwater level at borehole MB2 rose above the interface between the CMLs and bedrock during large rainfall events and snowmelt periods. The altitude of the minimum groundwater level at MB2 was 456 m. Thus, bedrock groundwater in MB2 had enough total potential to flow toward T4 (altitude of 440 m), but direct exfiltration to the OSL at T4 was hindered by the differences in the thermal dynamics of bedrock groundwater vs. OSL groundwater at T4. Indeed, previous studies have shown that, when bedrock groundwater exfiltrating into soil layers forms a groundwater zone in soil layers, the changes in temperature in the groundwater in soil layers are similar to those in bedrock groundwater [*Katsura et al.*, 2008].

However, upward flow occurred constantly in the CML within the groundwater zone at T4 (Figure 3.11), which indicated that the pressure on the deeper CML was strong enough to turn the flow direction upward. Possible sources of this strong pressure in the deeper CML were groundwater flow through the deeper CML and bedrock exfiltration into the CML. In previous studies, bedrock exfiltration occurred as saturated upward flux in association with the local exfiltration of bedrock groundwater into soil layers through fissures and cracks in the bedrock [e.g., *Montgomery et al.*, 1997; *Masaoka et al.*, 2016]. To detect the causes of the upward flow, the lag times of the increasing peak of the deeper CML ψ at T4 and the bedrock groundwater level in MB2 during rainfall and snowfall events were investigated. Figure 3.22 shows the relationship of the lag time from the time of event initiation to the peak of the deeper ψ and bedrock groundwater level in MB2 during the events. When the bedrock groundwater level did not exceed the boundary, the deeper CML ψ peaked faster than the bedrock groundwater level. In Kanai catchment, the initiation of a rise in the bedrock groundwater level in response to rainwater
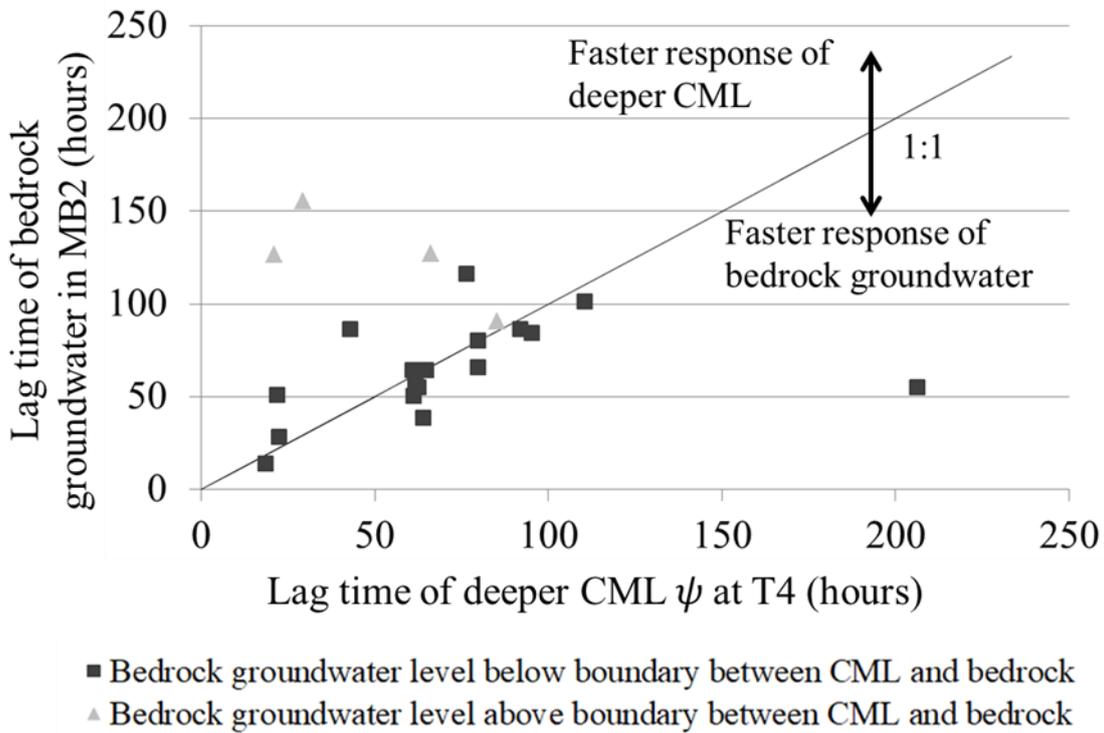
Figure 3.22. Relationship of the lag times from the time of event initiation to the peak of the deeper ψ and bedrock groundwater level in MB2 during the event. The plots are divided between the bedrock groundwater level below and above the boundary between the CML and bedrock.

and meltwater was slower than the rise in CML ψ, because the depth of bedrock groundwater formation at MB2 was deeper than the depth of the deeper CML at T4. Therefore, the difference in the start time of the rise in the CML ψ at T4 and the groundwater level at MB2 was directly reflected by the order of their peak appearances. When the bedrock groundwater level exceeded the boundary, it tended to peak faster. This suggests that the delayed peak in the deeper CML reflects propagation of the peak in the bedrock groundwater level at MB2. Bedrock groundwater in Kanai catchment did not exfiltrate into the OSLs, due to the low permeability of the CMLs, but it likely came in contact with CML groundwater and thus caused a pressure buildup in the deeper CMLs. Interference with bedrock exfiltration by clayey soil layers was reported by *Brönnimann et al.* [2013]. They also found that an increase in water pressure at the soil–bedrock

interface reduces the stability of soil layers, triggering the occurrence of shallow landslides. Because ψ at the boundary between CMLs and bedrock was not measured in this study, the boundary pressure was unknown. However, many landslides occur around the study area [*Kobayashi et al.*, 2020], which can perhaps be explained, at least in part, by the pressure increase resulting from the disturbance of bedrock groundwater exfiltration. The flow direction of disturbed bedrock groundwater in Kanai catchment is unclear. While the ratio of discharge to annual precipitation at Kanai catchment is approximately 25%, *Ishii et al.* [2004], in their study of Moshiri Experimental Watershed, reported a ratio of discharge to total precipitation of 80%. This difference indicates that water infiltrating the CML and bedrock in Kanai catchment eventually discharges in the Moshiri Experimental Watershed. Compared to the Kanai catchment, the Moshiri Experimental Watershed has a larger area, deeper and larger valleys, and exposed rock, all of which may allow bedrock groundwater to discharge directly into stream channels through fractures, without inhibition by the CMLs.

   In this study, chemical analyses did not allow identification of the source of the OSL groundwater at T4 and the spring, because the water quality of the bedrock groundwater in MB2 was similar to that of the CML water, despite the supposedly strong influence of bedrock weathering. As noted in Section **3.3.2**, the water quality of the bedrock groundwater at MB1 was consistent with inputs from bedrock weathering, while at MB2 those inputs were diluted. Previous studies have described the dilution system of bedrock groundwater [e.g., *Iwagami et al.*, 2010: *Iwasaki et al.*, 2015]. *Iwagami et al.* [2010] reported that a chemical mixture of soil layers and bedrock groundwater occurred when the bedrock groundwater level rose above the boundary between the soil layers and bedrock. *Iwasaki et al.* [2015] showed that the exfiltration of deeper bedrock groundwater, whose quality was strongly influenced by bedrock weathering, was not observed in a zero-order catchment, but was present in a larger-order catchment. They attributed this variation to the buffering and dilution of bedrock groundwater exfiltrating into riparian zones. In Kanai catchment, the

bedrock groundwater level at MB2 is only ~1 m below the boundary between the CMLs and bedrock. Information on the bedrock groundwater level between MB2 and T4 is lacking. Given the aforementioned pressure propagation from bedrock groundwater to the deeper CML, however, the bedrock groundwater level met the OSL and CML groundwater at least at T4, where both the OSL and CML were under perennial saturation. This suggests that, at least in the vicinity of T4, bedrock groundwater is in constant contact with CML groundwater. Then, by a dilution mechanism similar to that reported by *Iwagami et al.* [2010], CML groundwater and bedrock groundwater are likely to mix at the boundary. This would explain the similar ion concentrations of the bedrock groundwater at MB2 and the CML water at T2, because the MB2 groundwater level was often higher than the boundary between CML and bedrock, inducing the mixture of CML water and bedrock groundwater (Figure 3.15). The low hydraulic conductivity of the CMLs also promoted mixing, by increasing the contact times between saturated zones in the CMLs and bedrock groundwater. At MB1, however, bedrock groundwater was not mixed because the groundwater level was farther from the boundary. A sustained saturated zone that forms in the CML directly above bedrock would allow mixing with bedrock groundwater, resulting in a similar water quality.

3.5. Conclusion

This study investigated the effects of the CML on hydrological processes in headwater catchments underlain by permeable bedrock. Detailed hydrological, hydrochemical, and thermal observations were conducted in a forested tuff breccia headwater catchment containing mineral soil layers composed of thick clayey materials produced by the weathering of bedrock. The hydrological observations suggested the formation of two separate saturated zones above the bedrock, in OSLs and CMLs, indicating that the latter acted as an impeding layer. The OSL and CML located at the end of Kanai catchment (i.e., at T4) were saturated throughout the observation period. Broad fluctuations in the bedrock groundwater levels in Kanai catchment in response to rainfall and snowmelt

were observed. Although downward flow from the OSL to CML was the dominant subsurface flow direction at almost all observation points, upward flow in the CML occurred at T4. A lag time analysis indicated the presence of preferential flow, but its contribution to the subsurface flow system in Kanai catchment was small. Based on the extent of the saturated zones formed in the OSLs and CMLs, the contribution of the saturated zone in the CMLs to OSL groundwater at T4 and to the spring discharge was larger than that of the saturated zone in the OSLs. Chemical and thermal observations provided further evidence of the CML water as the source of the perennial groundwater zone in the OSL at T4 and of the spring water. Although fluctuations in bedrock groundwater levels indicated the occurrence of bedrock infiltration, bedrock groundwater did not contribute directly to the OSL groundwater at T4 and in the spring. These results indicate that while CMLs act as the impeding layers, water infiltration to bedrock occurred via the CMLs, with the latter also acting as an important source of spring water.

In Kanai catchment, about half of the annual precipitation infiltrates the CMLs and bedrock. The longer that saturated zones exist in the OSLs and CMLs, the greater the amount of bedrock infiltration. Therefore, both water infiltrating into the CMLs and the formation of relatively stable saturated zones in the OSLs and CMLs just above bedrock contribute to bedrock infiltration. The high groundwater level formed by thick OSLs and CMLs also contributes to bedrock infiltration. Exfiltration of bedrock groundwater was inhibited by the significantly low saturated hydraulic conductivity of the CMLs, resulting in a small contribution of bedrock groundwater to spring water quality. However, the inhibition of bedrock groundwater exfiltration increased the pressure head of the deeper CML at T4, causing upward flow to the shallower CML. In addition, the longer contact time between CML groundwater and bedrock groundwater as a result of the inhibition resulted in a dilution of bedrock groundwater quality at MB2.

Our findings have several important implications. First, the increase in bedrock infiltration and the inhibition of bedrock groundwater exfiltration can act as major triggers of landslides, which may shift the

boundary between CMLs and bedrock. In addition, a dilution of bedrock groundwater quality may occur even in bedrock, depending on the height of the bedrock groundwater level. Hydrologists should be aware of this local dilution when conducting component separation based on bedrock groundwater quality in catchments where bedrock is overlain by thick CMLs or bedrock groundwater is in prolonged contact with the saturated zone in soil layers above bedrock. Detailed studies of the boundary between CMLs and bedrock are needed to evaluate the pressure intensity due to flow inhibition.

Reference

Abe, Y., Y. Uchiyama, M. Saito, M. Ohira, and T. Yokoyama (2020), Effects of bedrock groundwater dynamics on runoff generation: a case study on granodiorite headwater catchments, western Tanzawa Mountains, Japan. *Hydrological Research Letters*, 14(1), 62–67.

Akitsu, T. K., T. Nakaji, T. Yoshida, R. Sakai, W. Mamiya, Terigele, K. Takagi., Y. Honda, K. Kajiwara, and K. N. Nasahara (2020), Field data for satellite validation and forest structure modeling in a pure and sparse forest of *Picea glehnii* in northern Hokkaido. *Ecological Research*, 35, 750–764.

Asano, Y., N. Ohte, and T. Uchida (2004), Sources of weathering-derived solutes in two granitic catchments with contrasting forest growth. *Hydrological Processes*, 18, 651–666.

Bockgård, N., and A. Niemi (2004), Role of rock heterogeneity on lateral diversion of water flow at the soil-rock interface. *Vadose Zone Journal*, 3, 786–795.

Brönnimann, C., M. Stähli, P. Schneider, L. Seward, and S. M. Springman (2013), Bedrock exfiltration as a triggering mechanism for shallow landslides. *Water Resources Research*, 49, 5155–5167.

Djodjic, F., L. Bergstrom, B. Ulen, and A. Shirmohammadi (1999), Mode of transport of surface-applied phosphorus-33 through a clay and sandy soil. *Journal of Environmental Quality*, 28(4), 1273–1282.

Feyen, H., J. Leuenberger, A. Papritz, M. Gysi, H. Flühler, and P. Schleppi (1996), Runoff processes in catchments with a small scale topography. *Physics and Chemistry of the Earth*, 21(3), 177–181.

Fukuzawa, K., F. Satoh, H. Shibata, T. Kamiura, C. Kozuka, T. Takanishi, S. Hayakashi, Y. Hirano, W. Mamiya, Y. Yabuhara, R. Sakai, H. Sugiyama, H. Matsumoto, N. Fukuzawa, J. Hassegawa, and T. Yoshida (2020), Stream water quality in relation to watershed-scale practical forest management in a cool-temperate natural forest in northern Japan. *Ecological Research*, 35, 742–749.

Gabrielli, C. P., J. J. McDonnell, and W. T. Jarvis (2012), The role of bedrock groundwater in rainfall-runoff response at hillslope and catchment scales. *Journal of Hydrology*, 450–451, 117–133.

Gannon, J. P., S. B. Bailey, and K. McGuire (2014), Organizing groundwater regimes and response thresholds by soils: A framework for understanding runoff generation in a headwater catchment. *Water Resources Research*, 50, 8403–8419.

Glaesner, N., C. Kjaergaard, G. H. Rubaek, and J. Magid (2011), Interactions between soil texture and placement of dairy slurry application: I. Flow characteristics and leaching of nonreactive components. *Journal of Environmental Quality*, 40(2), 337–343.

Ishii, Y., and D. Kobayashi (1995), Movement of subsurface water on a forested hillslope in the Moshiri experimental basin I; Observation of the pressure head using tensiometer nest (in Japanese with English abstract). *Low Temperature Science. Series A, Physical sciences*, 53, 23–24.

Ishii, Y., Y. Kodama, R. Nakamura, and N. Ishikawa (2004), Water balance of a snowy watershed in Hokkaido, Japan. In *Northern Research Basins Water Balance (Proceedings of a Workshop Held at Victoria, Canada, March 2004)*, IAHS Publication: Oxfordshire, UK, 2004, Volume 290, 13–27.

Ishii, Y. (2012), Hydrological study of snowmelt flooding during a rain-on-snow event (in Japanese with English abstract). *Journal of Japanese Association of Hydrological Science*, 42(3), 101–107.

Iwagami, S., M. Tsujimura, Y. Onda, J. Shimada, and T. Tanaka (2010), Role of bedrock groundwater in the rainfall-runoff process in a small headwater catchment underlain by volcanic rock. *Hydrological Processes*, 24, 2771–2783.

Iwasaki, K., M. Katsuyama, and M. Tani (2015), Contributions of bedrock groundwater to the upscaling of storm-runoff generation processes in weathered granitic headwater catchments. *Hydrological Processes*, 29, 1535–1548.

Iwasaki, K., Y. Nagasaka, and A. Nagasaka (2021), Geological effects on the scaling relationships of groundwater contributions in forested watersheds. *Water Resources Research*, 57, doi: 10.1029/2021WR029641.

Jury, W. A., W. R. Gardner and W. H. Gardner (1991), *Soil Physics*, 159–195, Wiley, New York.

Katsura, S., K. Kosugi, T. Mizutani, S. Okunaka, and T. Mizuyama (2008), Effects of bedrock groundwater on spatial and temporal variations in soil mantle groundwater in a steep granitic headwater catchment. *Water Resources Research*, 44, W09430, doi:10.1029/2007WR006610.

Katsuyama, M., M. Tani, and S. Nishimoto (2010), Connection between streamwater mean residence time and bedrock groundwater recharge/discharge dynamics in weathered granite catchments. *Hydrological Processes*, 24, 2287–2299.

Kobayashi, E., S. Taniguchi, H. Kikuta, R. Satoh, and T. Nitta (2020), Report on Geological Survey of the Moshiri Experimental Watershed (in Japanese*). *Asahikawa Boring Industry Cooperative*, Hokkaido, Japan.

Kosugi, K., S. Katsura, M. Katsuyama, and T. Mizuyama (2006), Water flow processes in weathered granitic bedrock and their effects on runoff generation in a small headwater catchment. *Water Resources Research*, 42, W02414, doi:10.1029/2005WR004275.

Kosugi, K., S. Katsura, T. Mizuyama, S. Okumura, and T. Mizutani (2008), Anomalous behavior of soil mantle groundwater demonstrates the major effects of bedrock groundwater on surface hydrological processes. *Water Resources Research*, 44, W01407, doi:10.1029/2006WR005859.

Kosugi, K., M. Fujimoto, S. Katsura, H. Kato, Y. Sando, and T. Mizuyama (2011), Localized bedrock aquifer distribution explains discharge from a headwater catchment. *Water Resources Research*, 47, W07530, doi:10.1029/2010WR009884.

Langston, A. L., G. E. Tucker, R. S. Anderson, and S. P. Anderson (2015), Evidence for climatic and hillslope-aspect controls on vadose zone hydrology and implications for saprolite weathering. *Earth Surface Processes and Landforms*, 40, 1254–1269.

Lin, H., and X. Zhou (2008), Evidence of subsurface preferential flow using soil hydrologic monitoring in the Shale Hills catchment. *European Journal of Soil Science*, 59, 34–49.

Martínez-Carreras, N., C. Hissler, L. Gourdol, J. Klaus, J. Juilleret, J. F. Iffly, and L. Pfister (2016), Storage controls on the generation of double peak hydrographs in a forested headwater catchment. *Journal of Hydrology*, 543, 255–269.

Masaoka, N., K. Kosugi, Y. Yamakawa, and D. Tsutsumi (2016), Processes of bedrock groundwater seepage and their effects on soil water fluxes in a foot slope area. *Journal of Hydrology*, 535, 160–172.

McGuire, K. J., and J. J. McDonnell (2010), Hydrological connectivity of hillslopes and streams: Characteristic time scales and nonlinearities. *Water Resources Research*, 46, W10543, doi:10.1029/2010WR009341.

McNamara, J. P., D. Chandler, M. Seyfried, and S. Achet (2005), Soil moisture states, lateral flow, and streamflow generation in a semi-arid, snowmelt-driven catchment. *Hydrological Processes*, 19, 4023–4038.

Miyata, S., T. Uchida, Y. Asano, H. Ando, and T. Mizuyama (2003), Effects of bedrock groundwater seepage on runoff generation at a granitic first order stream (in Japanese with English abstract). *Journal of the Japan Society of Erosion Control Engineering*, 56(1), 13–19.

Montgomery, D. R., W. E. Dietrich, R. Torres, S. P. Anderson, J. T. Heffner,

and K. Loague (1997), Hydrologic response of a steep, unchanneled valley to natural and applied rainfall.   *Water Resources Research*, 33(1), 91–109.

Nakamura, T., R. Yoshioka, and L. Joo (1991), Estimation of the presence of piton flow based on the quality of runoff water –For one test site within Rokko mountain– (in Japanese*).   *Journal of the Japan Society of Hydrology and Water Resources*, 4(1), 46–50.

Oda, T., M. Suzuki, T. Egusa, and Y. Uchiyama (2013), Effect of bedrock flow on catchment rainfall-runoff characteristics and the water balance in forested catchments in Tanzawa Mountains, Japan.   *Hydrological Processes*, 27, 3864–3872.

Redding, T., and K. Devito (2010), Mechanisms and pathways of lateral flow on aspen-forested, Luvisolic soils, Western Boreal Plains, Alberta, Canada.   *Hydrological Processes*, 24, 2995–3010.

Rodhe, A. and N. Bockgård (2006), Groundwater recharge in a hard rock aquifer: A conceptual model including surface-loading effects. *Journal of Hydrology*, 330, 389–401.

Suzuki, Y. (2022), Measurement of permeability and water retention of weathered bedrock in a tuff breccia headwater catchment (in Japanese*). *Graduation Thesis*, Hokkaido University, Hokkaido, Japan.

Tani, M., Y. Fukushima, and M. Suzuki (1979), Annual variation of soil temperature in a small mountain watershed (in Japanese with English abstract).   *Bulletin of Kyoto University Forest*, 51, 138–151.

Tani, M. (1997), Runoff generation processes estimated from hydrological observations on a steep forested hillslope with a thin soil layers. *Journal of Hydrology*, 200, 84–109.

Todd, A. K., J. M. Buttle, and C. H. Taylor (2006), Hydrologic dynamics and linkages in a wetland-dominated basin.   *Journal of Hydrology*, 319, 15–35.

Tsukamoto, Y. (1998), In *Conservation of Forest, Water and Soil* (in Japanese*).   Asakurashoten: Tokyo, Japan.

Whitaker, A. C., and H. Sugiyama (2005), Seasonal snowpack dynamics and runoff in a cool temperate forest: lysimeter experiment in Niigata, Japan.

Hydrological Processes, 19, 4179–4200.

Yamazaki, M., Y. Ishii, and N. Ishikawa (2007), Hydrochemical processes during snowmelt season in a nival mountainous watershed (in Japanese with English abstract. *Journal of Japanese Association of Hydrological Sciences*, 37(3), 123–135).

Yoshinaka, R. S. Sakurai, and K. Kikuchi (1989), *Bedrock Classification and its Application* (in Japanese*).   Doboku Kogakusha, Tokyo, Japan.

* The title or source is a tentative translation by the authors from the original.

Chapter 4
Summary and Conclusion

4.1. Introduction

Detailed hydrological, hydrochemical, and hydrothermal observations were conducted in two headwater catchments underlain by impermeable and permeable bedrock, respectively, to elucidate the effects of thick CMLs on hydrological processes in headwater catchments. This chapter summarizes the results presented in **Chapters 2** and **3** and discusses differences in the effects of CMLs between the two types of catchments; it also presents a general conclusion.

4.2. Effects of Thick Clay Layers on Hydrological Processes in a Headwater Catchment Underlain by Impermeable Bedrock

In **Chapter 2**, we described detailed hydrological, hydrochemical, and hydrothermal observations in a headwater catchment underlain by impermeable serpentinite bedrock, with a focus on quantitative and qualitative changes in water stored in OSLs and CMLs. We also described flux analyses of groundwater levels in OSLs; pressure head in OSLs and CMLs; and the hydrological properties of OSLs, CMLs, and boundaries between them. The results of these analyses can be summarized as follows:

1. In the study catchment, OSLs showed high saturated hydraulic conductivity and contained many pores of various sizes. In contrast, CMLs showed lower saturated hydraulic conductivity and had only a few large pores. Their boundaries had intermediate properties.

2. Distinct groundwater zones were observed within OSLs and CMLs.

3. Although rainwater rapidly discharged through OSLs because CMLs functioned as impeding layers during wet periods, groundwater zones were observed semi-perennially within the OSLs during dry periods despite the high permeability and thin

soil thickness of OSLs (maximum, 50 cm).

4. During dry periods, the electrical conductivity of groundwater within OSLs ranged from 175 to 279 μS cm^{-1}, approaching the electrical conductivity of groundwater within CMLs, which ranged from 221 to 426 μS cm^{-1}.

5. Upward flux from CMLs to OSLs frequently occurred for long intervals during dry periods, whereas downward flux from OSLs to CMLs mainly occurred during wet periods.

6. The rate of upward flux was sufficiently large to cultivate groundwater flux in the OSLs during dry periods, despite the effect of transpiration rate.

Based on these results, the following effects of CMLs on hydrological processes in the study catchment can be inferred. During rainfall, downward flow from OSLs to CMLs recharged the CML groundwater; during dry periods, water supplied from CMLs to OSLs as unsaturated upward flow accumulated in downslope hollows, which sustained groundwater zones in the OSLs during dry periods. Frequent long-term occurrence of upward flow may be attributed to differences in the hydraulic properties of OSLs and CMLs. This effect prevented OSLs in the hollows from drying, presumably causing volumetric and chemical changes in groundwater and streamflow.

4.3. Effects of Thick Clay Layers on Hydrological Processes in a Headwater Catchment Underlain by Permeable Bedrock

In **Chapter 3**, we described detailed hydrological, hydrochemical, and hydrothermal observations in a headwater catchment underlain by permeable tuff breccia bedrock (Kanai catchment), with a focus on quantitative and qualitative changes in water stored in OSLs, CMLs, and bedrock. Semi-perennial springs flowing over the CMLs were observed at the catchment outlet. The Kanai catchment had thick, highly permeable OSLs (~1 m), thick CMLs (4–5 m) with extremely low permeability, and bedrock with greater permeability than CMLs in previous studies. The results of these analyses can be summarized as follows:

1. In the Kanai catchment, three distinct groundwater zones that fluctuated in response to rainfall or snowmelt were observed in OSLs, CMLs, and bedrock.

2. Preferential flow such as bypass or pipe flow was not predominant, but vertical downward infiltration from OSLs to CMLs and from CMLs to bedrock was almost continually observed.

3. Upward flow (as described in Chapter 2) was not observed, whereas saturated upward flow was measured in the CML groundwater zone near the catchment outlet.

4. Bedrock groundwater collected from a downslope borehole had a lower concentration of ions derived from bedrock weathering, compared with bedrock groundwater collected from upslope boreholes.

5. CML groundwater contributed to the OSL groundwater zone near the catchment outlet and to spring water, whereas OSL groundwater upslope of the Kanai catchment and bedrock groundwater did not.

6. Bedrock groundwater contributed minimally to the OSL groundwater zone and spring water, although bedrock groundwater levels often reached and exceeded the CML– bedrock boundary downslope of the catchment.

7. Bedrock groundwater levels tended to peak faster than the pressure head in CMLs at the outlet when the bedrock groundwater level exceeded the boundary, although the increase in bedrock groundwater level was initiated later than the increase in the CML.

Based on these results, although CMLs functioned as impeding layers, rainwater and snowmelt also infiltrated into CMLs and bedrock. Additionally, CMLs inhibited bedrock groundwater exfiltration and stored water, which strongly contributed to OSL groundwater and streamflow at the catchment outlet. This study speculates that this inhibitory effect of CMLs induced upward flow in the CMLs, which diluted bedrock

groundwater quality. This effect increased the pressure head at the interface between the CML and bedrock. These effects of CMLs on hydrological processes have been suggested in previous studies; however, their importance has been obscured by commonly used research methods, such as chemical analysis and hydrograph separation.

4.4. General Conclusions

Our results demonstrate that in catchments with either impermeable and permeable bedrock, CMLs function both as impeding layers and as conduits for water movement. These effects influence hydrological processes such as groundwater level and pressure head fluctuations, as well as the quality of groundwater, spring water, and stream water. Figure 4.1 shows conceptual models that incorporate the effects of CMLs into two conventional conceptual models. In headwater catchments underlain by impermeable bedrock, CMLs function as impeding layers and groundwater zones form in OSLs above CMLs during rainfall (Figure 4.1a). A portion of the rainfall infiltrates into CMLs to form groundwater zones. After the cessation of rainfall and as catchments dry up, water stored in CMLs is supplied to OSLs via upward unsaturated flow (Figure 4.1b). This water quantitatively and qualitatively contributes to groundwater zones in OSLs. In headwater catchments underlain by permeable bedrock, CMLs function as impeding layers, such that groundwater zones form in OSLs. A portion of the rainwater infiltrates into CMLs, where it forms groundwater zones. Groundwater stored in CMLs infiltrates into bedrock, where it also forms groundwater zones. Although bedrock groundwater levels increase to reach the boundary between CMLs and bedrock, CMLs inhibit bedrock groundwater exfiltration. Because of this inhibition, bedrock groundwater has minimal effects on groundwater in OSLs and spring water at the headwater catchment outlet. This inhibition also increases pressure within CMLs and dilutes bedrock groundwater quality (Figure 4.1b).

The effects of CMLs differed between catchments; CMLs functioned as water suppliers through unsaturated upward flux in the impermeable bedrock catchment; they functioned as inhibiting layers for bedrock
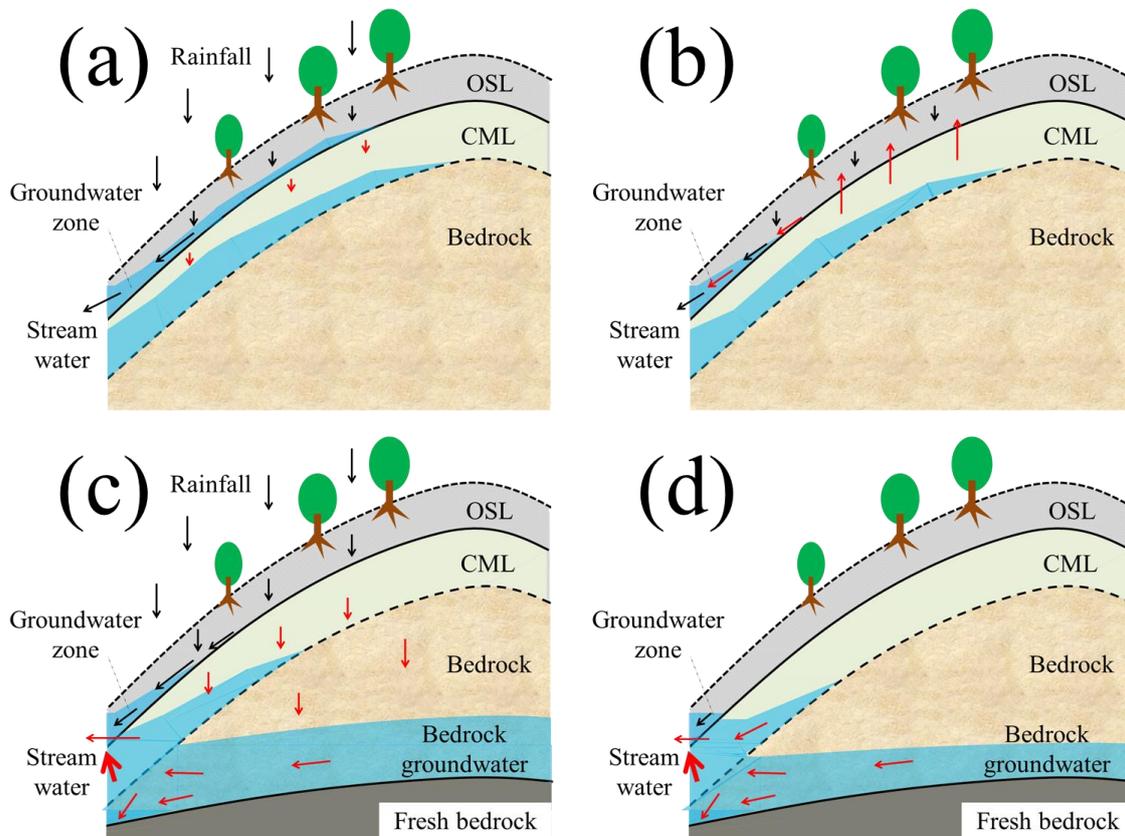
Figure 4.1. Effects of clay mineral layers incorporated into two conventional conceptual models: a headwater catchment underlain by impermeable bedrock (a) during and (b) after rainfall (dry periods), and a headwater catchment underlain by permeable bedrock (c) during and (d) after rainfall.

groundwater exfiltration in the permeable bedrock catchment. Bedrock permeability is regarded as the primary cause of these differences. CML saturated hydraulic conductivity measurements were higher in the headwater catchment underlain by serpentinite bedrock than in the headwater catchment underlain by tuff breccia bedrock (Tables 2.1 and 3.2). However, groundwater levels and pressure head observed in the CMLs tended to be higher in the serpentinite catchment than in the tuff breccia catchment, even after the catchment had dried up. For example, in the serpentinite catchment, when pressure head in the OSLs (depth, 30 cm) was approximately −150 cm, pressure head in the CMLs (depth, 50 cm) was

approximately −20 cm (Figure 2.5). In contrast, in the tuff breccia catchment, when pressure head in the OSLs (depth, ~35 cm) was approximately −150 cm, pressure head in the CMLs (depth, 227 cm) was lower, ranging approximately from −76 to −20 cm (Figure 3.10d, e). Considering the large influence of gravity on groundwater flow, water stored in CMLs was assumed to have vertically percolated to bedrock in the tuff breccia catchment. In contrast, in the serpentinite catchment, water stored in CMLs exhibited minimal vertical percolation because of impermeable bedrock; it remained within the CMLs for a longer period. Moreover, the thinner OSLs in the serpentinite catchment led to faster drying of the OSLs, resulting in a pressure head gap between OSLs and CMLs. Therefore, unsaturated upward flow was more likely to occur in the serpentinite catchment. No such gap occurred in the tuff breccia catchment because CMLs were likely to dry up as a result of bedrock percolation. Instead, the low permeability of these CMLs prevented bedrock groundwater exfiltration.

These results indicate the effects and importance of CMLs on hydrological processes in headwater catchments underlain by impermeable and permeable bedrock based on hydrological, hydrochemical, and hydrothermal observations. It is clear that CMLs function as impeding layers; however, water can also penetrate into CMLs and then interact with both OSLs and bedrock. These effects of CMLs on hydrological processes have been suggested in previous studies; however, their importance has been obscured by commonly used research methods, such as chemical analysis and hydrograph separation. Thus, our findings emphasized the importance of detailed observations in OSLs, CMLs, and bedrock to improve the methods used in this study, as well as the broader understanding of hydrological processes in headwater catchments with CMLs. In future research, detailed observations of other catchments underlain by other bedrock types with thick CMLs (e.g., slate and mudstone catchments) are needed to determine the generalizability of the observed effects. Additionally, the hydrological processes identified in this study may affect the quantity and quality of stream water, as well as the occurrence of

sediment disasters such as landslides, such that these aspects of headwater catchment hydrology should be further investigated.

Acknowledgement
謝辞

　研究室に配属されてから今日に至るまで，数多くの方々に支えられ，この学位論文の完成を見ることができました。研究室配属当初，研究室内にも斜面水文学に関する知見や観測機器が不足する中で，野外における観測手法や解析の方針，研究に取り組む基本姿勢から，発展的な解析の手法や英語論文の添削まで，様々な局面でご指導いただいた北海道大学大学院農学研究院 桂真也助教に深く感謝いたします。また，日常の研究生活からゼミ等の機会を通じて適切なご助言と激励を下さった北海道大学大学院農学研究院 山田孝教授，笠井美青准教授，北海道大学広域複合災害センター 山口真司特任教授，厚井高志准教授，そして本論文の副査を務めて下さった北海道大学大学院農学研究院　中村太士教授に深く感謝いたします。

　北海道大学大学院農学研究院　柏木淳一講師には水分特性の実測をする際に，測定機器を貸していただき，使い方も教示していただきました。また，水質分析の際には，北海道大学大学院農学研究院 渡部敏裕准教授に多大なるご助力を頂きました。調査地として利用させていただいた北海道大学中川研究林，雨龍研究林の技術職員の皆様には現地活動のみならず，素晴らしい宿泊環境を整えて頂き，充実した調査活動を行うことができました。特に，雨龍研究林の技術専門職員　坂井励さんには，冬期の調査において送迎から現地活動まで多大なるご助力を頂き，また渡来美香さんには美味しい食事を提供していただきました。

　本研究の研究対象となった家内流域の水分特性は，北海道大学農学部　鈴木優子さん（現ウェザーニュース）が中心となり実測してくださいました。また，研究室に所属して間もなく，稚拙だった私の発表スライドや論理構成に多くの助言を与えて下さった北海道大学農学院　溝口芽衣さん（現大地コンサルタント），梅谷涼太さん（現日本工営）らに感謝いたします。研究室の先輩・同期・後輩の皆様には，度重なる過酷な現地調査をお手伝いいただきました。特に，北海道大学農学院　青木稔弥さん（現ダイヤコンサルタント）には観測機器の設置，処理を大いに助けていただきました。また，同室の片山和紬さん（現日本工営），松永一慶さん（現日本工営），山口柊生さ

ん（現アジア航測），別室の松永隆正さん，岸本海笛さん（現砂防地すべりセンター）らの研究に取り組む姿勢から強い刺激を受け，本研究を継続し完成するまでの大きな原動力となりました。

　振り返れば，研究でうまくいかなかったことは数えきれないほどに多く，残せた業績も決して多いとは言えず，順風満帆な研究生活では無かったように思います。しかしそれでもなお研究生活を続け，こうして博士論文という形で成果を残すに至ったのは，多くの方々の支えがあったからこそだと感じています。今後も，我が国の未来の砂防を担う一研究者として精進してまいります。本当にありがとうございました。

2023 年

北海道大学農学院　流域砂防学研究室

吉野　孝彦